

Medium Range Unmanned Containerised Cargo Freighter

THINK GREEN AND LEAN

M. Boukema	1368389	R. Janssen	4147413
G.J. van Dam	4165799	U. Malik	4048679
L.K. Hassan	4165683	L.G.M. Meijboom	4202732
E. Hoogeboom	4215206	M.K. Sakyi-Gyniae	4047400
M.H. Jagtenberg	4081919	P.A. Scholten	4214099

Final Report
Design Synthesis Exercise

Preface

The concluding part of aerospace engineering bachelor's curriculum is the design synthesis exercise (DSE). The DSE gives students the opportunity to obtain design experience in a multidisciplinary design project. In the DSE, realistic and holistic design challenges are posed that require knowledge from multiple disciplines. These challenges are solved by ten students, working as a team. The aim of the project is not to attain a flawless final result, because the design can only be partially developed within the limited time-frame. The aim is to demonstrate skills and knowledge acquired during the bachelor's programme and accomplish a successful design of an aerospace system. The DSE can be divided into four phases: a planning phase, a requirements phase, a concept phase and a final design phase. This final report of the project is prepared by the DSE group 12 in accordance to the DSE regulations, which concludes the fourth and last phase.

This report is submitted to Paul Roling (Researcher/lecturer at Delft University of Technology), Giuseppe Caridi (PhD candidate at Delft University of Technology), Jaco Brandsen (PhD candidate at Delft University of Technology) and Hans Heerkens (Assistant professor at University of Twente). In this report the process of achieving the following objective is covered:

"Design an unmanned containerised cargo freighter that can reduce the cost of shipping by air and the time required for inter-modal transfers and transport on the ground".

We would like to mention our appreciation of the assistance and guidance given to us by the tutor, coaches and the staff of the faculty. We would also like to express our gratitude to Remco Onderdelinden (maintenance manager, KLM) for his valuable inputs and Platform Unmanned Cargo Aircraft (PUCA) for inviting us to the conference, which gave insight in the unmanned aircraft cargo industry. Finally we would like to thank faculty of Aerospace Engineering of Delft University of Technology for providing us with the opportunity to participate in this innovative project and provide us with work space and all the facilities.



Marijke Boukema



Geart van Dam



Lotfy Hassan



Emiel Hoogeboom



Michelle Jagtenberg



Richard Janssen



Usama Malik



Luuk Meijboom



Master Sakyi-Gyniae



Pepijn Scholten

Table of Contents

Preface	i
Executive summary	v
List of symbols	vii
List of abbreviations	xi
List of figures	xiii
List of tables	xvi
1 Introduction	1
2 Market analysis	2
2.1 Transportation market	2
2.2 Air transportation between regions	2
2.3 Products transported via air and their density	3
2.4 Boeing 747-400F information	4
2.5 ATLAS market volume and share	5
3 Mission analysis and concept design phase	6
3.1 Mission analysis	6
3.2 Functional flow diagram	6
3.3 Concept design phase	6
3.3.1 Concept generation	6
3.3.2 First trade-off	9
3.3.3 Second trade-off	10
4 Aircraft design methodologies and system characteristics	11
4.1 System engineering approach	11
4.2 Design driving characteristics	13
4.2.1 Inside-out method	13
4.2.2 Container layout	13
4.2.3 Pressurisation	13
4.2.4 Reference frame	14
4.3 Class I weight estimation	14
4.4 Wing loading and thrust loading	16
4.5 Subsystem design	19
4.5.1 Wing	20
4.5.2 Airfoil selection	20
4.5.3 Centre body	21
4.5.4 Empennage design	23
4.5.5 Control surfaces design	24
4.5.6 Landing gear positioning and sizing	27
4.5.7 Propulsion system	28
4.5.8 Environmental control	36
4.5.9 Fire protection system	36
4.5.10 Wing ice protection	37
4.5.11 Electrical power system	37
4.6 Class II weight estimation	38
4.7 Budget allocation	42

4.7.1	Weight budget allocation	42
4.7.2	Power budget allocation	42
4.8	Aircraft system characteristics	43
4.8.1	Key characteristics	43
4.8.2	Configuration layout	43
5	Design evaluation	45
5.1	Performance analysis	45
5.1.1	Payload range diagram	45
5.1.2	Climb performance	45
5.1.3	Descent performance	46
5.1.4	Stall performance	48
5.1.5	Manoeuvring performance	48
5.1.6	Turning performance	49
5.1.7	Take-off and landing performance	52
5.1.8	SEL noise contour	52
5.1.9	Fuel consumption	56
5.1.10	Emissions	56
5.2	Aerodynamic characteristics	56
5.2.1	Atmospheric conditions	56
5.2.2	Estimating C_{D_0}	57
5.2.3	Estimating C_{m_0} and $x_{a.c.}$	58
5.2.4	Analysis of aerodynamic performance	59
5.2.5	Aerodynamic parameters	59
5.2.6	Lift distribution	60
5.2.7	Winglet design	61
5.3	Structural analysis	63
5.4	Stability and control characteristics	75
5.4.1	Static longitudinal stability	76
5.4.2	Dynamic stability	76
5.5	Financial analysis	77
5.5.1	Development cost	79
5.5.2	Production cost	79
5.5.3	Maintenance cost	80
5.5.4	Operating cost	81
5.5.5	Aircraft unit price and cost	81
5.5.6	Return on investment	82
5.5.7	Break even point	82
5.5.8	Cost break-down structure	82
5.6	Sensitivity analysis	83
5.7	Verification & validation procedures	85
5.8	Technical risk assessment	85
5.9	Sustainability development strategy	87
6	Operations	89
6.1	Unmanned control	89
6.1.1	Regulations	89
6.1.2	Unmanned system design	91
6.1.3	Unmanned system safety	96
6.2	Operations and logistic concept	99
6.2.1	Cargo logistics	100
6.2.2	Container management & operations	103
6.2.3	Loading operations	104
6.3	Manufacturing, assembly, integration plan	105
6.3.1	Production plan	106
6.3.2	Impact on sustainability	107

6.3.3	Safety assurance	107
6.4	Reliability, availability, maintainability (RAM) characteristics	107
6.4.1	Expected availability	110
6.5	Data and electrical block diagrams	110
6.5.1	Data block diagram	111
6.5.2	Electrical block diagram	111
7	Requirement compliance matrix	113
8	Project design and future development strategy	118
8.1	Project design & development logic	118
8.2	Gantt chart post DSE	118
9	Conclusion	121
10	Recommendations	122
	Bibliography	127
	Appendix A Aircraft dimensions, planform details and characteristics	128

Executive summary

From the first cargo flight in 1911, cargo air transportation is recognised as one of the most time efficient means of transportation over long distances for over 100 years. However, for the past 100 years aircraft design has stagnated. New technology is already available and the markets are in need of a more time and cost efficient way to transport cargo. The substantially lower cost, due to both fuel savings and the reduction of crew cost, will make the air cargo transportation more attractive. Furthermore, using cross modality containers and unmanned, moderate capacity vehicles, the total transportation time and total operating cost can be significantly reduced. To offer a knowledge-based solution to this problem, the following project objective statement, to design an unmanned containerised cargo freighter that can reduce the cost of shipping by air and the time required for inter-modal transfers and transport on the ground, is set. Using a system engineering approach this resulted in an innovative design solution, named ATLAS.

The ATLAS is a blended wing body design, consisting of a composite structure and skin. The lift generating body of the design helps to make it more fuel-efficient compared to a conventional design. For each subsystem, a sustainability strategy is proposed.

The main purpose of ATLAS is to transport cargo. For that an inside-out approach is taken. This means that the design of ATLAS is based on the size of containers that have to fit in the cargo bay. New containers are designed to fit in the ATLAS, which are compatible with trucks and current airport operations. However, to be compatible with the current market, ULD's can also be used. It is chosen to fly at high altitudes due to aerodynamic efficiency. This means pressurisation becomes a concern when transporting goods at this altitude. It is chosen to pressurise the cargo bay instead of the whole fuselage. In order to design a cargo bay for a non-circular centre body, a multibubble design is applied.

To evaluate the design of ATLAS, the concurrent engineering approach is used. This approach focuses on the ability for simultaneous activities in the modules of performance analysis, aerodynamic characteristics, structural analysis, stability and control characteristics and financial analysis. A MATLAB computing environment was created to allow iterations through these modules in order to meet all the requirements. The individual modules have been verified and sensitivity analysis has been performed.

Through Roskam's first class weight estimation method, aerodynamic sizing via XFLR5 software and Torenbeek's second class weight estimation method a final design has been iterated. The final design includes an inherently stable blended wing body with a T-tail and two CFM International Leap 1A engines. The direct operation cost, fuel consumption and produced emissions compared to a Boeing 747-400 have been reduced with 75%, 50% and 46% respectively. Also, the noise production has been reduced with 78,5% compared to an Airbus A320. The carbon fibre composite structure of the ATLAS is able to cope with a maximum Von Mises stress of 625MPa and a maximum buckling load 85MN .

In order to let the unmanned design comply with the regulations from CS25, mitigation strategies for all possible failure modes have been provided. These failure modes are split in aviatational, navigational, communication and mitigation failures. Aircraft modes are designed to make sure that all these failures can be dealt with. The sensors and subsystems to control the aircraft are designed to be redundant to ensure safe flight.

Through Project Evaluation and Review Technique (PERT) and critical chain analysis the critical chain in the loading and unloading process has been improved. This resulted in a turn around time (TAT) of 24.4 minutes for unsimultaneous loading and 12.6 minutes for simultaneous loading, compared to an average of 30-50 minutes for current freighters.

Furthermore, while keeping an eye on sustainability, a reliability, availability and maintainability analysis has been performed, a data and electrical block diagram is sketched and a production plan has been proposed.

In summary, ATLAS satisfies almost all requirements and it also performs significantly better than any aircraft flying today. In the context of increasing fuel prices and high consideration for the environment, ATLAS is a sustainable choice due to its low fuel use and low noise contour. In order to satisfy with the fuel reduction requirement of 75% compared to a Boeing 747-400 it is recommended to investigate the possibility of flying even higher than the current cruising altitude of 12,500m. This would be beneficial for the fuel use and operating cost, but would make it harder to have stable eigenmotions. It is also recommended to use CFD to investigate the aerodynamic properties of the aircraft more accurately.

List of symbols

Table 1: List of symbols.

Symbol	Description	[Unit]
a	Temperature rate	$[K \cdot km^{-1}]$
a_{floor}	Cargo bay floor length	$[m]$
A	Aspect ratio	$[-]$
A	Cross sectional area	$[m^2]$
A_{fan}	Fan cross-sectional area	$[m^2]$
$A_{Highlight}$	Highlight area	$[m^2]$
$A_{V,eff}$	Effective vertical tail aspect ratio	$[-]$
b	Wing span	$[m]$
b_{floor}	Cargo bay floor width	$[m]$
b_{slats}	Span of slats	$[m]$
b_V	Vertical tail span	$[m]$
c	Vertical speed	$[m/s]$
C	Chord	$[m]$
\bar{C}	Mean aerodynamic chord	$[m]$
\bar{C}_{tail}	Mean aerodynamic chord of tail	$[m]$
\bar{C}_{wing}	Mean aerodynamic chord of wing	$[m]$
C_D	Drag coefficient	$[-]$
C_{D_0}	Zero lift drag coefficient	$[-]$
$C_{D_{ewm}}$	Engine windmilling drag coefficient	$[-]$
C_f	Friction coefficient	$[-]$
C_{m_α}	Moment coefficient change with angle of attack	$[-]$
C_l	2D lift coefficient	$[-]$
C_L	Lift coefficient	$[-]$
$C_{L_{max}}$	Maximum lift coefficient	$[-]$
$C_{L_{max,land}}$	Maximum lift coefficient in landing configuration	$[-]$
$C_{L_{max,tail}}$	Maximum lift coefficient of tail	$[-]$
$C_{L_{max,to}}$	Maximum lift coefficient in take-off configuration	$[-]$
C_{L_α}	Lift coefficient change with angle of attack	$[-]$
$C_{L_{\alpha,0}}$	Lift coefficient at 0 angle of attack	$[-]$
C_{m_0}	Moment coefficient at 0 lift	$[-]$
$C_{m_0,M}$	Moment coefficient at Mach number	$[-]$
$C_{m_0,M=0}$	Moment coefficient at Mach = 0	$[-]$
C_{m_α}	Moment coefficient rate	$[-]$
C_r	Root chord	$[m]$
C_{rr}	Rudder root chord	$[m]$
C_t	Tip chord	$[m]$
CG_{max}	Most aft centre of gravity position	$[m]$
d	Diameter	$[m]$
d_{floor}	Cargo bay support spacing	$[m]$
D	Drag	$[N]$
D_{data}	Engine diameter data	$[m]$
D_{ewm}	Engine windmilling drag	$[N]$
D_{req}	Engine diameter required	$[m]$
D_t	Highlight diameter	$[m]$

D_{th}	Throat diameter	[m]
e	Oswald factor	[-]
E	Material Young's modulus	[Pa]
f	Ratio between take-off and landing weight	[-]
g	Gravitational acceleration	9.81 [m/s ²]
h	Altitude	[m]
h_{Cruise}	Altitude cruise	[m]
i_{cl}	Inclination angle	[deg]
$I_{buckreq}$	Minimum required moment of inertia	[m ⁴]
$I_{xx} I_{yy} I_{zz} I_{xy} I_{yz} I_{zx}$	Moments of inertia	[m ⁴]
k	2D lift slope constant	[-]
k_a	Airfoil technology factor	[-]
l	Distance between tail and wing	[m]
l	Length	[m]
L	Lift	[N]
L_{beam}	Length of beam	[m]
L_{data}	Engine length data	[m]
L_{rear}	Rear length of fuselage	[m]
L_{req}	Engine length required	[m]
m	Mass	[kg]
\dot{m}	Mass flow rate	[kg/s]
M	Mach number	[-]
M_{Crit}	Critical Mach number	[-]
M_{Cruise}	Mach cruise	[-]
M_{DD}	Mach drag divergence	[-]
M_{res}	Reserve fuel fraction	[-]
M_{tfo}	Trapped fuel fraction	[-]
M_x, M_z	Bending moment	[Nm]
n	Load factor	[-]
n_{max}	Maximum load factor	[-]
p	Pressure	[Pa]
p_{floor}	Cargo bay floor loading	[N/m ²]
p_t	Total pressure	[Pa]
P	Power	[W]
P_{buck}	Buckling load	[N]
q	Shear flow	[N/m]
R	Air specific gas constant	287.058 [JK ⁻¹]
R_{ls}	Lifting surface correction factor	[-]
R_{turn}	Turn radius	[m]
R_{wf}	Wing fuselage interference factor	[-]
Re	Reynold's number	[-]
REV_{nmi}	Revenue generated per nautical mile flown	[USD]
s_L	Landing distance	[m]
S	Wing surface area	[m ²]
$S_{elevator}$	Elevator surface area	[m ²]
S_H	Horizontal tail surface area	[m ²]
$S_{segment}$	Segment surface area	[m ²]
S_V	Vertical tail surface area	[m ²]
S_w	High-lift devices surface area	[m ²]
S_{wet}	Wetted area	[m ²]
S_{wflap}	Surface area of flaps	[m ²]
S_{wslat}	Surface area of slats	[m ²]
S_x, S_z	Shear force	[N]
t	Thickness	[m]
tx_{inv}	Investment tax credit rate	[USD]

t_{xrev}	Revenue tax rate	[USD]
T	Thrust	[N]
T_{data}	Thrust data	[N]
t_{floor}	Cargo bay floor thickness	[m]
T_{req}	Thrust required	[N]
T_t	Total temperature	[K]
T_{turn}	Turn time	[s]
U_{annbl}	Annual block hours flown	[hrs]
ν	Material Poisson's ratio	[-]
V	Velocity	[m/s]
V_{bl}	Block speed	[m/s]
V_H	Horizontal tail volume coefficient	[m ³]
V_S	Stall speed	[m/s]
$V_{S,land}$	Stall speed in landing configuration	[m/s]
V_{true}	True airspeed	[m/s]
V_V	Vertical tail volume coefficient	[m ³]
w	Span of fuselage	[m]
w_{floor}	Cargo bay floor deflection	[m]
W	Weight	[N]
W_0	Gross Weight	[N]
W_{ai}	Air induction system weight	[N]
W_{api}	Air-conditioning, pressurisation, anti- and de-icing system weight	[N]
W_{apu}	Auxiliary power unit weight	[N]
W_{bc}	Baggage and cargo handling equipment weight	[N]
W_{crew}	Crew weight	[N]
W_e	Engines weight	[N]
W_{edata}	Engines weight data	[N]
W_{ereq}	Engines weight required	[N]
W_{els}	Electrical system weight	[N]
W_{emp}	Empennage weight	[N]
W_E	Empty weight	[N]
W_{iae}	Instrumentation, avionics and electronics weight	[N]
W_f	Fuselage weight	[N]
W_{fc}	Flight control system weight	[N]
W_{feq}	Fixed equipment weight	[N]
W_{fs}	Fuel system weight	[N]
W_F	Fuel weight	[N]
$W_{F_{used}}$	Used fuel weight	[N]
$W_{F_{res}}$	Reserve fuel weight	[N]
W_g	Landing gear weight	[N]
W_n	Nacelles weight	[N]
W_{OEW}	Operational empty weight	[N]
W_p	Propulsion system weight	[N]
W_{PL}	payload weight	[N]
W_{prop}	Propellers weight	[N]
W_{pt}	Paint weight	[N]
W_{pwr}	Powerplant weight	[N]
W_{struct}	Structure weight	[N]
W_{tfo}	Trapped fuel weight	[N]
W_{TO}	Take-off weight	[N]
W_w	Wing weight	[N]
x	X-coordinate	[m]
$x_{maingear}$	Longitudinal position of the main gear	[m]

y	Y-coordinate	[m]
Y	Von Mises stress	[Pa]
z	Z-coordinate	[m]
α	Angle of attack	[deg]
α_0	Zero lift angle of attack	[deg]
α_{stall}	Stall angle of attack	[deg]
α_{trim}	Trim angle of attack	[deg]
β	Prandtl-Meyer correction factor	[-]
γ	Isentropic expansion factor	1.41 [-]
δ	Rudder deflection angle	[deg]
ϵ_t	Wing twist	[deg]
η	Airfoil efficiency factor	[-]
η_V	Rudder angle of attack effectiveness	[-]
θ	Induced inlet angle	[deg]
λ	Taper ratio	[-]
λ_R	Rudder hinge angle	[-]
Λ	Sweep angle	[deg]
μ	Dynamic viscosity	[kg/s/m]
μ_0	Air reference dynamic viscosity	$1.716 \cdot 10^{-5}$ [kg/s/m]
π	Pressure recovery ratio	[-]
ρ	Density	[kg/m ³]
ρ_0	Density at sea level	[kg/m ³]
σ	Density ratio $\frac{\rho}{\rho_0}$	[-]
σ_{comp}	Ultimate compressive strength	[Pa]
σ_{ten}	Ultimate tensile strength	[Pa]
σ_y	Bending stress	[Pa]
τ	Shear stress	[N/m ²]
ϕ	Bank angle	[deg]
ω	Yaw rate	[rad/s]

List of abbreviations

Table 2: List of abbreviations.

Abbreviation	Description
a/c	Aircraft
AAS	Amsterdam Airport Schiphol
ACARS	Aircraft Communications Addressing and Reporting System
APU	Auxiliary Power Unit
ATC	Air Traffic Control
ATM	Available Ton Mile
BEP	Break Even Point
BPR	Bypass Ratio
bps	Bits per Second
BWB	Blended Wing Body
CBS	Cost Break-down Structure
CDA	Continuous Descent Approach
CFD	Computational Fluid Dynamics
CG	Centre of Gravity
Const	Constraint
CS	Certification Specifications
CSP	Communication Service Providers
DOC	Direct Operating Cost
DOT	Design Option Tree
DSE	Design Synthesis Exercise
Dsgn	Design
EASA	European Aviation and Safety Agency
ELM	Emergency Landing Mode
EMWET	Elham Modified Weight Estimation Technique
Envi	Environment
ERM	Emergency Recovery Mode
FAA	Federal Aviation Administration
FEM	Finite Element Method
FLM	Forced Landing Mode
FP	Flight Path
FPR	Fan Pressure Ratio
GDP	Gross Domestic Product
GHM	Ground Handling Mode
GPWS	Ground Proximity Warning System
HLD	High Lift Device
ICAO	International Civil Aviation Organisation
INM	Integrated Noise Model
INMTM	Integrated Noise Model / Management of Trajectory and Missions
IOC	Indirect Operating Cost
ISA	International Standard Atmosphere
ISO	International Organisation for Standardisation
LCR	Lip Contraction Ratio
LE	Leading Edge
LoitM	Loitering Mode
MAC	Mean Aerodynamic Chord
MAC	Mid-Air Collision
MMEL	Master Minimum Equipment List
MTOM	Maximum Take-Off Mass

MTOW	Maximum Take-Off Weight
NextGen	Next Generation Air Transportation System
OCB	Over-The-Centre-Body
OEI	One Engine Inoperative
OEW	Operational Empty Weight
Oper	Operations
OPR	Overall Pressure Ratio
Perf	Performance
PERT	Program Evaluation and Review Technique
Prop	Propulsion
PRR	Pressure Recovery Ratio
PUCA	Platform Unmanned Cargo Aircraft
RAM	Reliability, Availability, Maintainability
RAT	Ram Air Turbine
RDTE	Research, Development, Test and Evaluation
Regu	Regulations
ROC	Rate Of Climb
RoI	Return on Investment
RTM	Resin Transfer Molding
SEL	Sound Exposure Level
SFC	Specific Fuel Consumption
SIPOC	Supplier, Input, Process, Output and Customer
SRM	System Reboot Mode
Struct	Structures
Sust	Sustainability
Syst	Systems
TAT	Turn Around Time
TAWS	Terrain Awareness and Warning System
TCAS	Traffic Collision Avoidance System
Tech	Technical
Tkm	Tonne Kilometre
TOP	Take-Off Parameter
UAS	Unmanned Aircraft System
UAV	Unmanned Aerial Vehicle
UCCF	Unmanned Containerised Cargo Freighter
ULD	Unit Load Device
VHF	Very High Frequency
VLM	Vortex Lattice Method

List of Figures

2.1	Passenger and cargo growth in Europe compared to the GDP [1].	2
2.2	Air freight market share by route [2].	3
3.1	The mission profile showing all stages encountered in flight.	6
3.2	The functional flow diagram showing the cargo transportation process.	7
3.3	The functional breakdown structure showing the different elements of the cargo transportation process.	8
3.4	Concept 1: Formation flyer	10
3.5	Concept 2: Flying wing	10
3.6	Concept 3: Blended wing body	10
4.1	Scheme of the program showing the division in interconnected individual modules.	12
4.2	Reference frame used for designing ATLAS.	14
4.3	Statistical mass fuel fractions [3].	15
4.4	Wing loading versus thrust loading.	19
4.5	Whitcomb supercritical airfoil contour.	21
4.6	Describing a non-circular cross-section using circular elements.	22
4.7	Stress concentrations will be accounted for by local reinforcements.	22
4.8	The cargo bay dimensions (in meters).	22
4.9	Selected flap and slat.	25
4.10	Engine-out geometry.	26
4.11	Longitudinal tip-over criterion for tricycle gears [4].	27
4.12	Longitudinal ground clearance criterion [4].	27
4.13	Lateral tip-over criterion [4].	27
4.14	Lateral ground clearance criterion [4].	27
4.15	Side view of ATLAS including centre of gravity range.	29
4.16	Design process of the propulsion system.	29
4.17	CFM International's Leap 1A engine.	30
4.18	Shape of flow field at different stations.	32
4.19	Inlet separation trends [5]	33
4.20	Engine layout [5]	33
4.21	Rolls Royce's Ultrafan and GE open rotor [6].	35
4.22	BPR and FPR from simple flux turbojets to turboprops [7].	35
4.23	Final result of the first class weight estimation.	40
4.24	Final result of the second class weight estimation.	41
4.25	Configuration layout of ATLAS.	44
4.26	Front view of ATLAS.	44
5.1	Payload range diagram. Indicated with the dotted lines is the range (3000 nmi) for the typical payload weight (28000 kg).	46
5.2	Rate of climb at different altitudes versus true Mach number for MTOW.	47
5.3	Rate of climb at different altitudes versus true Mach number for OEW.	47
5.4	Continuous descent approach of the ATLAS versus a conventional approach.	47
5.5	Stall speeds for different weights without high lift devices.	48
5.6	Stall speeds for different weights with high lift devices.	48
5.7	Maximum achievable load factor for a given equivalent airspeed.	49
5.8	Drag as a function of airspeed and load factor.	50
5.9	Drag components versus airspeed.	50
5.10	Achievable load factor as a function of airspeed.	50
5.11	Minimum turn radius as a function of airspeed.	51
5.12	Minimum turn time as a function of airspeed.	51

5.13	Required bank angle for a rate one turn as function of airspeed.	51
5.14	Required bank angle for a rate two turn as function of airspeed.	51
5.15	Noise comparison between baseline and the ATLAS - Departure.	54
5.16	Noise comparison between baseline and the ATLAS - Approach.	55
5.17	Drag polar during cruise.	59
5.18	Lift distribution.	61
5.19	Comparison of NACA 63-412 airfoil with $Re = 9.0 \cdot 10^6$	62
5.20	Lift distribution XFLR5 vs Q3D.	63
5.21	Comparison of lift and weight loads between conventional aircraft (left) and blended wing body (right) [6, p. 19].	64
5.22	Front view of cross-section of wings and centre body showing integrated bulkhead and spar configuration.	64
5.23	Reference frame for the top view of the aircraft including the loads acting on the structure.	65
5.24	Reference frame for the front view of the aircraft including the loads acting on the structure.	65
5.25	Top view of the wing box indicating the different sections analysed.	66
5.26	Wing box cross-section view for centre body.	66
5.27	Wing box cross-section view for mid wing.	67
5.28	Wing box cross-section view for outer wing.	67
5.29	Bending moment in x direction.	68
5.30	Bending moment in z direction.	68
5.31	Torque distribution along the wing span.	69
5.32	Horizontal shear force distribution.	70
5.33	Vertical shear force distribution.	70
5.34	Von Mises stress.	70
5.35	Buckling loads.	71
5.36	Materials used for the ATLAS structure.	73
5.37	Loading diagram of the ATLAS.	75
5.38	X-plot of the ATLAS showing the stability and controllability range.	76
5.39	Short period: ATLAS' response to an input of -1 degree deflection on the elevator.	78
5.40	Phugoid: ATLAS' response to a step input of -1 degree deflection on the elevator.	78
5.41	Aperiodic roll: ATLAS' response to a step input of 3 degrees on the ailerons.	78
5.42	Dutch roll: ATLAS' response to step inputs of 10 and -5 degrees on the rudder.	78
5.43	Spiral: ATLAS' response to an initial roll angle of -10 degrees.	79
5.44	Research, development, test and evaluation cost for the ATLAS.	80
5.45	Production cost division for the ATLAS.	80
5.46	Direct operating cost of the ATLAS split in its main contributors.	81
5.47	Direct operating cost of the ATLAS split in all sub contributors.	82
5.48	Cost break-down structure for the post-preliminary design project activities	83
5.49	Response of key performance indicators to a change in major system parameters.	84
6.1	Communication flow diagram of the aircraft while preparing for flight.	92
6.2	Communication flow diagram of the aircraft during flight operations.	92
6.3	Communication flow diagram between ATC, the control room, the service provider, the UAV and other aircraft.	93
6.4	FANS ACARS datalink service provider networks.	94
6.5	SATCOM satellite coverage using the Inmarsat satellites [8].	94
6.6	Worldwide VHF ACARS coverage [8].	95
6.7	Cargo operations as sub-chain in the entire cargo transport chain.	100
6.8	Turn around time operations.	101
6.9	Turn around time PERT analysis.	102
6.10	ATLAS container.	104
6.11	Front nose loading.	104
6.12	Back loading.	105
6.13	Ball transfer units.	105

6.14	Graphic representation of the assembly line.	106
6.15	Lockheed C-130J Hercules maintenance platform.	109
6.16	Data handling block diagram.	111
6.17	Electrical block diagram.	112
8.1	Project design and development logic.	119
8.2	Gantt chart post DSE.	120

List of Tables

1	List of symbols.	vii
2	List of abbreviations.	xi
2.1	Belly share in freight transport between different regions [9].	3
2.2	Goods transported via air [9].	4
2.3	Large air freight shares with their corresponding mean densities.	4
2.4	Data on the Rolls-Royce engine for the Boeing 747-400F.	4
2.5	Boeing 747-400F operating data [10].	5
3.1	Design option trees categories.	9
3.2	First trade-off criteria and weights.	9
3.3	Second trade-off criteria and weights.	10
4.1	Centre body sizing constraints.	13
4.2	Required climb gradient as stipulated by CS25:25.121 [11].	18
4.3	Aerodynamic parameters.	19
4.4	Wing segment parameters.	20
4.5	Thicknesses for the pressure vessel.	23
4.6	Rudder sizing results.	27
4.7	Flow properties.	32
4.8	Inlet dimensions.	33
4.9	Final result of the first class weight estimation	40
4.10	Final result of the second class weight estimation.	40
4.11	Weight budget allocation.	42
4.12	Power budget allocation.	43
4.13	ATLAS key characteristics.	44
5.1	Input parameters for INMTM trajectory file.	53
5.2	Input parameters for INMTM grid file.	53
5.3	The origin of each parameter needed to define the INMTM input trajectory file for both the A320 and the ATLAS.	53
5.4	SEL comparison.	55
5.5	Values for physical constants.	57
5.6	C_{D_0} values for different components.	58
5.7	Aerodynamic parameters.	60
5.8	Stability coefficients.	62
5.9	Four wing sections used to model the wing.	66
5.10	Primary assumptions for the structural analysis approach.	67
5.11	Secondary assumptions for the structural analysis approach.	67
5.12	Discretisation errors for various n-values.	72
5.13	Material properties.	72
5.14	Selected composite characteristics explained.	73
5.15	The dimensions of the wing box cross-sections required to cope with the Von Mises stresses and buckling loads.	74
5.16	Eigenvalues of the eigenmotions of the ATLAS for different flight conditions.	77
5.17	Return on investment and the break even point given for different air cargo operators.	83
5.18	Risk map.	87
5.19	Mitigated risk map.	87
6.1	Unmanned control safety design.	97
6.2	Examples of subcontractors.	107
6.3	Master minimum equipment list for ATLAS.	108

6.4	Reliability of the subsystems divided in reliability groups.	109
6.5	Scheduled maintenance guideline.	110
7.1	Requirements compliance matrix.	113
A.1	Empennage details.	128
A.2	Rudder dimensions.	128
A.3	Container details.	128
A.4	Cargo bay details.	128
A.5	Main wing details.	129
A.6	Financial analysis summary.	129
A.7	Aircraft performance.	130

1 Introduction

From the first cargo flight in 1911, cargo air transportation is recognised as one of the most time efficient means of transportation over long distances for over 100 years. However, for the past 100 years aircraft design has stagnated. New technology is already available and the markets are in need of a more time and cost efficient way to transport cargo. Therefore, a team of 10 young engineers has been given the challenge to provide a knowledge-based solution for this technology-push and market-pull situation.

The project objective accompanying this challenge is to design an unmanned containerised cargo freighter that can reduce the cost of shipping by air and the time required for inter-modal transfers and transport on the ground. The design is a blended wing body which will be named ATLAS. The aim is to carry whole world cargo through ATLAS.

The purpose of this final report is to provide the reasoning and methodology used during the design and show the final results.

The following structure will be used to provide this purpose. In chapter 2 the results of the performed market will be presented. In chapter 3 it will be explained why and how ATLAS was chosen as the final concept. Following this, the three main chapters will be presented, which are the aircraft design methodologies and system characteristics in chapter 4, the design evaluation in chapter 5, and the operations in chapter 6. In more detail, chapter 4 will first explain the system engineering approach. Next, the design driving characteristics will be discussed. After that, the class I weight estimation will be explained, after which the wing loading and thrust loading can be computed. After the design point is chosen, the subsystems are designed and the class II weight estimation is executed. Now the budget allocation can be performed, and chapter 4 will end by describing the aircraft system characteristics. Chapter 5 will start by analysing the aircraft performance. Next, the aerodynamic characteristics will be explained, after which the winglets are designed. After that, the structural analysis is performed. Following this, the stability and control characteristics are evaluated and the financial analysis is done. Chapter 5 will end by explaining the sensitivity analysis, verification & validation procedures, technical risk assessment, and sustainability development strategy. Chapter 6 will start by evaluating the unmanned control. After that, the operations and logistic concept will be explained. Next, the manufacturing, assembly and integration plan will be stated. Following this, the reliability, availability and maintainability (RAM) characteristics will be explained. Chapter 6 will end by describing the data and electrical block diagrams. In chapter 7 it will be checked whether ATLAS complies with all requirements. In chapter 8 the project design and future development strategy will be explained. To end this report, the conclusion and recommendations are given in chapter 9 and chapter 10 respectively.

2 Market analysis

To place the project in a broader perspective, market research has been performed on the transportation market in the baseline report [12]. Firstly, the important results of this market analysis are summarised. Secondly, some research is done considering the market volume and market share of the ATLAS. This information is used during the financial analysis in section 5.5.

2.1 Transportation market

The transportation market is strongly dependent on the global economy. As can be seen in Figure 2.1, both the passenger and cargo transport growth in Europe are dependent on the growth of the Gross Domestic Product (GDP). Especially the cargo transport growth is closely related to the GDP. When the global financial crisis started in 2007, the cargo market collapsed as well. The cargo market has not recovered yet from the crisis and it is currently not back at the growth level of the GDP.

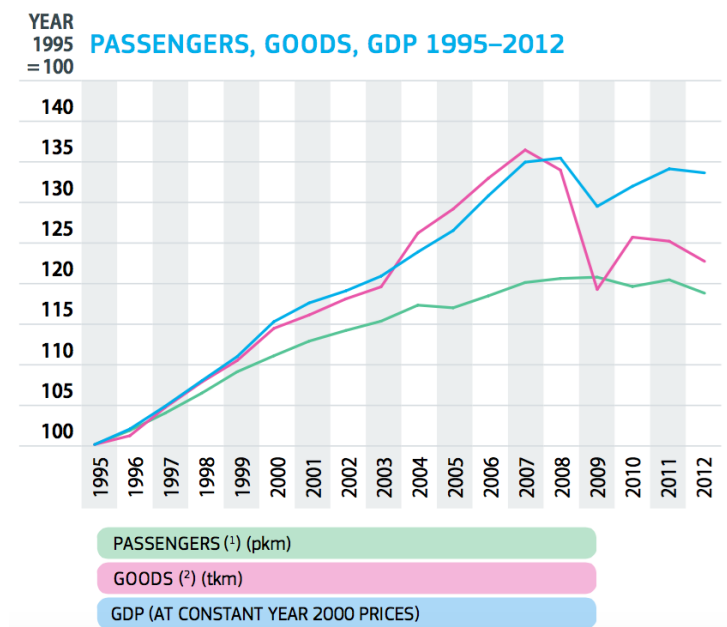


Figure 2.1: Passenger and cargo growth in Europe compared to the GDP [1].

2.2 Air transportation between regions

For the design of the medium range aircraft it is important to know between which regions most air freight transportation occurs. As can be seen in Figure 2.2, about 25% of the transportation is intra continental. However, inter continental transportation might be possible when the aircraft is flying over land making it possible to refuel at airports. The most challenging distances are flying from Europe to North America and vice versa and flying from North America to Asia and vice versa. This is because the aircraft cannot land to refuel when flying over the Pacific or the Atlantic Ocean. If these challenges can be met, the complete market can be covered with the medium range aircraft, while still being more efficient than the long range aircraft which has to take more fuel.

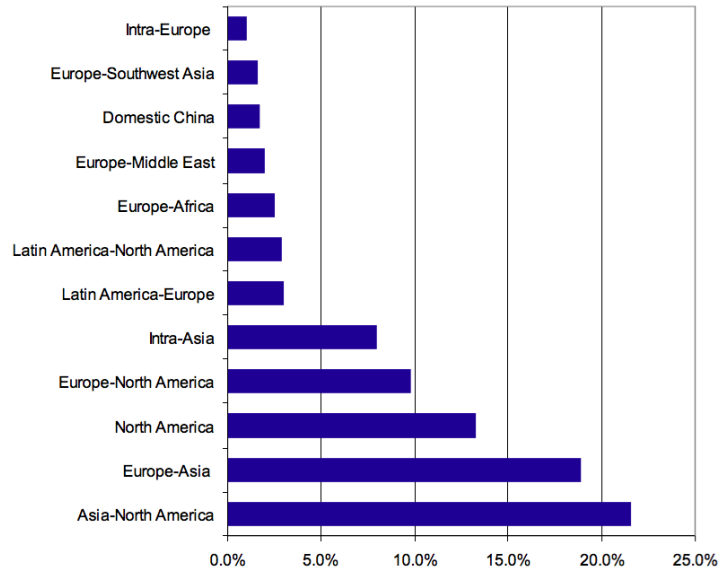


Figure 2.2: Air freight market share by route [2].

To finish the picture of the air freight market, the difference between belly share in freight transport and dedicated freight transport should be investigated. Belly share cargo transport is a hazard for the conventional cargo transport using dedicated cargo freighters. In belly share transport the cargo is carried in the 'belly' of a passenger aircraft. This is a lot cheaper than using dedicated cargo freighters since the aircraft are already flying for the passengers. The different belly shares in freight transport are given in Table 2.1. As can be seen in the table, the belly share is high for the challenging distances of Europe-North America and North America-Asia. This means that if the design for the cargo aircraft is not able to fly between these continents, relatively less market share is lost because 50% is already flying in belly share instead of a dedicated freight transport aircraft. It can also be seen that the intra continental belly share is relatively low, which means a big market will be intra continental flight. However, if the new aircraft design could be made favourable with respect to the belly share market, for example by improved operations or a faster turn around time, market share for dedicated freight transport can be improved.

Table 2.1: Belly share in freight transport between different regions [9].

Route	Belly Share
Europe-Europe	10%
Europe-Asia	50%
North America-North America	10%
North America-Asia	50%
Europe-North America	50%
Asia-Asia	30%

2.3 Products transported via air and their density

For some design choices like flying pressurised or unpressurised, it has to be known which types of goods are transported via air. The different goods transported and their corresponding shares are given in Table 2.2.

Table 2.2: Goods transported via air [9].

Air	
Goods	Share [%]
High tech	23
Capital goods	21
Fashion	14
Pharmaceutical	12
Perishables	8
Other, live, value	8
Automotive	7
Mail and Express	7

The current density standard in air freight transport is 1 ton per $6m^3$. This comes down to $166.67 \frac{kg}{m^3}$. To make sure most of the current cargo market can be transported, the densities of the largest shares are investigated in Table 2.3.[13] A more extensive airfreight density research has been done in the baseline report. From this research it became evident that the cargo density should be increased to $250 \frac{kg}{m^3}$. [12] This cargo density also ensures the ATLAS can transport all the goods currently transported.

Table 2.3: Large air freight shares with their corresponding mean densities.

Goods	Mean density [$\frac{kg}{m^3}$]
High tech	187.12
Capital goods	N.A.
Fashion	161.26
Pharmaceutical	174.82
Perishables	198.40
Other, live, value	199.12
Automotive	228.31
Mail and express	164.86

2.4 Boeing 747-400F information

Some top level requirements stated compare the ATLAS with the Boeing 747-400F. The 747-400F is an all freight version of the 747-400. While using the updated systems and wing design of the passenger versions, it features the original short upper deck found on the classic 747's in order to save weight. To verify these top level requirements, additional information on the fuel consumption and direct operational cost is required.

Fuel consumption

The fuel consumption heavily depends on the mission an aircraft is flying. It also depends on the engine choice for the aircraft. There is a choice of three different engine manufacturers for the Boeing 747-400F. The data on the Rolls-Royce engine is given in Table 2.4. [14]

Table 2.4: Data on the Rolls-Royce engine for the Boeing 747-400F.

Manufacturer	Rolls-Royce
Type	R.B.211-524G-T
M_{cr} [-]	0.85
h_{cr} [m]	10668
T_{cr} [N]	52547
SFC_{cr} [$\frac{kg}{s \cdot N}$]	$1.62 \cdot 10^{-5}$
Fuel Capacity of the aircraft [L]	203520

Cargolux has data available on the fuel consumption of their Boeing 747-400F's in real life conditions.¹ This shows a fuel consumption of 13.49 liter per 100 tonne-kilometer². These characteristics are from a 'typical' 5555 km trip with maximum payload in the aircraft.³

Another way to express fuel consumption is with the fuel / payload ratio. This ratio expresses the complete division between payload weight and fuel weight for the aircraft flying at maximum payload. The fuel weight then not only includes the fuel being burnt during cruise, as given above, but also the fuel taken as a reserve and fuel burnt during taxi, take-off, climb and descend. For the 747-400F this ratio was shown to be 0.72 for a 3000nmi trip, based on the payload range diagram provided by Boeing [15] [12].

Direct operational cost

Operating costs of air freight transportation can be split in direct and indirect operation cost. Since there is a top level requirement on the Direct Operating Cost (DOC), these have been investigated. The direct operating cost per Available Ton Mile (ATM) for a Boeing 747-400F is given in Table 2.5. The ATM is a unit used in the United States, but can be easily converted to tonne kilometers, since 1 ATM equals 1.46 tonne kilometers. [10]

Table 2.5: Boeing 747-400F operating data [10].

Parameter	1991	1992	1993	1994	1995	Compound annual % change
Stage length	2,210	2,218	2,212	2,241	2,265	0.62
ATM/departure	234,389	235,219	235,261	239,070	239,989	0.59
Aircraft years	7.99	8.02	7.99	7.99	8.60	1.83
ATM/gallon fuel	13.080	13.480	13.428	13.373	13.207	0.24
Total RTMs (000's)	1,070,121	1,128,354	1,172,575	1,224,797	1,316,289	5.31
Percent of airline total	13.06	10.90	10.23	9.04	8.47	-10.3
Load factor	69.04	70.30	73.08	76.81	76.89	2.73
Scheduled ATM/total ATM	96.54	99.35	99.67	99.30	96.49	-0.01
DOC/ATM	0.1468	0.1304	0.1244	0.1216	0.1668	3.35

2.5 ATLAS market volume and share

The market volume is an important parameter in estimating the cost of an aircraft. If it is possible to split the cost that are not dependant of how many aircraft that are produced over more aircraft, the production cost of the aircraft will be decreased. Airbus estimates the world freighter aircraft to reach almost 3000 aircraft in the next 20 years.⁴ Mid sized cargo aircraft are expected to have the greatest growth, with 1300 new aircraft necessary in 2032. The range of the ATLAS corresponds to this segment, however the cargo volume of the ATLAS is about half the size of the cargo volume of conventional cargo freighters. This means that an assumption can be made on around 2 ATLAS aircraft required for transport of the same cargo volume. This would mean that 2600 ATLAS aircraft could be sold if the market share would be 100%. However, a market share of 100% is of course not achievable. An assumption has been made that the market share possible is around 20%. This is based on the current market only, not considering the market share the aircraft could create because of its performance and innovation. Concluding, the ATLAS has a great opportunity in the market with a number of 500 aircraft to be sold.

¹<http://www.cargolux.com/images/Sustainability/comparison.swf> [accessed on 30/04/15]

²tonne payload

³<http://www.aviation-photography.lu/files/Cargolux%20747-8F%20Facts.pdf> [accessed on 30/04/15]

⁴<http://www.airbus.com/presscentre/pressreleases/press-release-detail/detail/world-freighter-fleet-to-reach-almost-3000-aircraft-in-next-20-years/> [accessed on 15/06/15]

3 Mission analysis and concept design phase

Preceding this final report a mission analysis has been conducted and the concept design phase has been done. In this chapter a summary of the previous phases of the design will be given: section 3.1 shows the mission profile, functional flow and functional breakdown diagrams that are specific to the mission. Section 3.3 explains how the design process was kept broad in the beginning in order to include all possible design options and how concepts were generated from this. It also elaborates on how the concepts have been traded-off against each other in order to find a sensible design.

3.1 Mission analysis

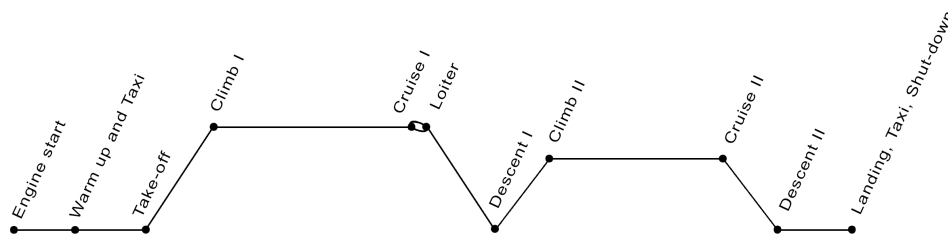


Figure 3.1: The mission profile showing all stages encountered in flight.

Every aircraft flies according to a specific flight profile that begins before take-off and ends after landing. The different phases of the mission are graphically shown in Figure 3.1. A more detailed explanation is given in [16].

3.2 Functional flow diagram

The functional flow diagram in Figure 3.2 shows an overview of the complete process a cargo package follows from the end-customer to its final destination. A typical airline however will not perform all steps in this process itself. Some process steps, marked in the flow with with dashed borders, will usually be performed by either the end-customer or a third party like FedEx or DHL. The other steps, with a solid border, will typically be performed by the airline. Therefore these are the steps this design project will focus on. The flow shows the logical order in which tasks must be performed, but offers no indication of the time required for a single step.

The functional breakdown structure in Figure 3.3 shows in more detail all the essential steps required to complete a total cargo transport for an airline. By doing so it gives insight in the functions the system should perform.

3.3 Concept design phase

The purpose of the concept phase is find a concept that suits the mission of this project most. This is done by concept generation (subsection 3.3.1) and by trading-off concepts (subsection 3.3.2 and subsection 3.3.3).

3.3.1 Concept generation

The concept generation consisted of two parts: creating design option trees (DOTs) for each subsystem and generating concepts using these DOTs. The purpose of a DOT is find and map

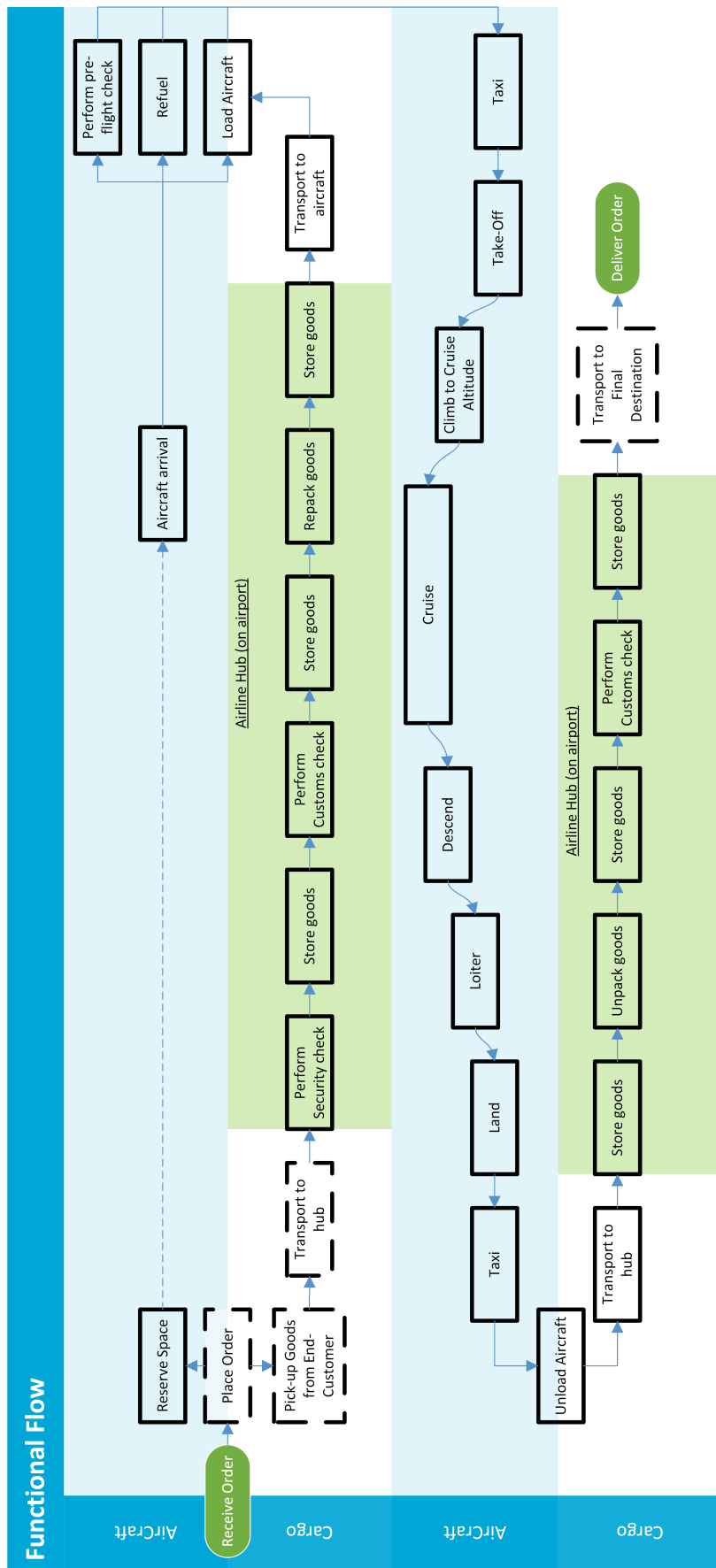


Figure 3.2: The functional flow diagram showing the cargo transportation process.

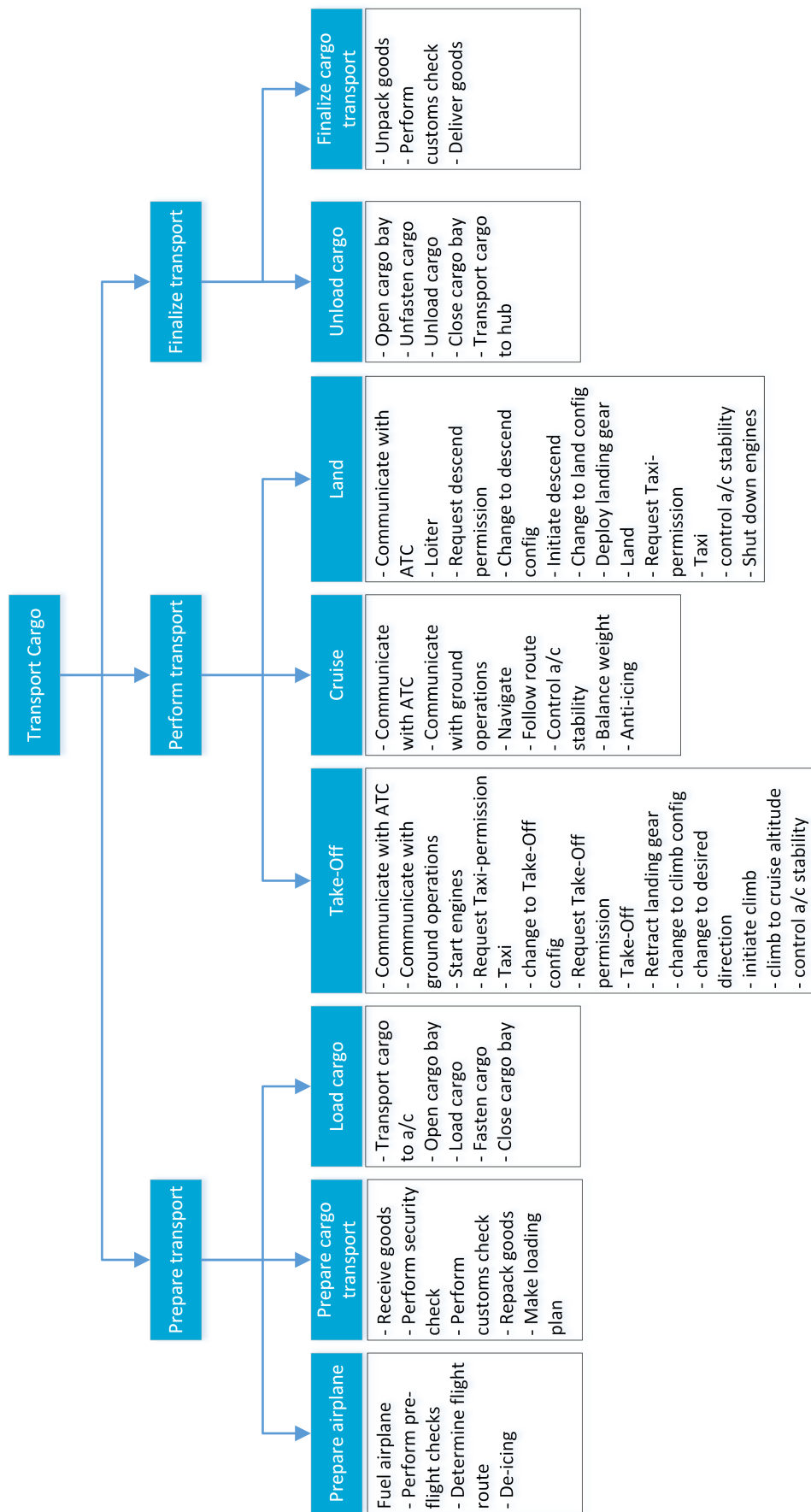


Figure 3.3: The functional breakdown structure showing the different elements of the cargo transportation process.

all possible design options for a certain design subsystem. It was assured that all options, also those considered exotic, silly and technically non-feasible, were included in the tree. The different systems that were explored using DOTs are shown in Table 3.1.

Table 3.1: Design option trees categories.

Categories	
Airport ground operations	Generate lift
Carry payload	Loading and unloading of cargo
Container design	Main control system
Manage payload system	Materials
Non airport ground operations	Power generation
Take-off and landing	Thrust
Failure management	Manoeuvrability
Longitudinal stability	Lateral stability

During a brainstorm session thirteen concepts were generated, based on the range of designs offered by the DOTs, that could suit the mission as defined in chapter 1. Included in the set of thirteen concepts were, amongst others, blended and hybrid wing bodies, flying wings, cargo centred concepts, a formation flying a/c, and a maritime aircraft. There was also variation in means of propulsion (i.e. jet or propeller), pressurisation options (i.e. the fuselage or the container), and lift generation (i.e. aerodynamically or vertically).

3.3.2 First trade-off

After the concept generation a reasoned selection of these concepts took place. Based on the weighted trade-criteria presented in Table 3.2 the top three aircraft were found. These were a formation flying concept (Figure 3.4), a flying wing concept (Figure 3.5), and a blended wing body design (Figure 3.6). The formation flying concepts is a conventional aircraft that is optimised for formation flying by using tail mounted engines on a t-tail, in order to minimise wing tail drag interference. It has a pressurised fuselage. The flying wing concept is a low flying propeller driven aircraft. Because it is flying at low altitudes, pressurisation of the cargo is not necessary. The BWB design resembles the flying wing concept at the front, in order to maximise aerodynamic efficiency, whereas the rear of the aircraft features a tail structure to accommodate improved operational compatibility and assure inherent stability. It features jet engines and is supposed to operate at high speed and at high altitudes.

Table 3.2: First trade-off criteria and weights.

Criterion	Weight	Criterion	Weight
Structural complexity	5.9	Production cost	5.4
Aerodynamic efficiency	10.2	Maintainability	10.2
Low fuel use	12.1	Cargo compatibility	11.1
Low emissions	9.3	Speed	5.1
Low noise	7.2	Airport operations compatibility	10.3
Proof of concept	6.7	Stability and controllability	6.5



Figure 3.4: Concept 1: For-
mation flyer **Figure 3.5:** Concept 2: Fly-
ing wing **Figure 3.6:** Concept 3:
Blended wing body

3.3.3 Second trade-off

For the three concepts that scored best on the first trade-off preliminary designs were made. Each concepts was researched to come up with initial weight, aerodynamic, flight performance, and operational characteristics. Also a cost analysis was done for all concepts. Based on the preliminary designs a second trade-off was conducted to find the best concept to be developed. The used criteria and their respective weights are shown in Table 3.3. The best concept turned out to be the BWB concept, which was therefore selected for further development.

Table 3.3: Second trade-off criteria and weights.

Criterion	Weight
Production cost	11.70
Operating cost	27.45
Noise contour	14.88
Safety (proof of concept)	20.87
Sustainability (fuel and emissions)	25.10

4 Aircraft design methodologies and system characteristics

In this chapter the design decisions for the final design will be explained in detail. This chapter will first explain the system engineering approach. Secondly, the design driving characteristics will be discussed. After that, the class I weight estimation will be explained, after which the wing loading and thrust loading can be computed. After the design point is chosen, the subsystems (for example the wing or the propulsion system) are designed. Next, the class II weight estimation is executed. Following this, the budget allocation is shown, and to conclude this chapter the aircraft system characteristics will be described.

4.1 System engineering approach

In order to ensure a time-efficient process leading to an high quality design, a good engineering approach can be of the utmost importance. The design process is based on the concurrent engineering process as defined by the International Council on Systems Engineering and described by [17]. The definition according the International Council on Systems Engineering is: "Concurrent Engineering is the concurrent running of separate phases during the product definition trajectory". It focuses on the ability for simultaneous activities and involvement performed by a multi-disciplinary team. In this design process this is implemented in a number of ways. The design team consists of different disciplinary work groups, thereby creating a multi-disciplinary team: Structures & Materials, Control & Operations, Systems Engineering, Aerodynamics and Flight Performance & Propulsion. This team then first defines the actions needed to be performed and the design strategy. Already taking into account all aspects of the product life cycle, from concept to disposal, including cost, quality, planning and requirements. Based on this a work-flow diagram and work-breakdown structure are created. The next important step in implementing the concurrent engineering strategy is the integrated use of information technology. For this MATLAB 2015a is chosen as the computing environment and in there a complete programming framework is created. This framework is depicted in Figure 4.1 and consists of several individual interconnected modules. Each module has a clearly identifiable purpose, input and output values. The main file (in Figure 4.1 shown as "Run.m") executes the different modules and manages all required iterations. This approach enables the different disciplinary work groups to work simultaneous on there modules, thereby eliminating the need for a work group to wait for a result of another work group before they can get started.

This does however create the need for a single integrated source of product information. In the framework this is implemented using a single hierarchical dataset, containing all aircraft characteristics, assumptions and parameters. The different modules use this integrated product model to load input variables and store output variables. If some input variables are not known yet, the module can still be tested and developed using assumed reference variables. This increases the ability for simultaneous engineering and decreases the total development time. Simultaneous to the module development, the aircraft performance is constantly monitored. Weight optimisation is performed based on the results of the fully automated sensitivity analysis and known aircraft design principles. It must be noted that apart from MATLAB, three other programs are used in the design: Q3D, EMWET and XFLR5. These programs will be explained in this chapter. Also all the developed modules will be explained in the following sections. At the end of these sections, it is mentioned what sustainable decisions are made for that particular system. Additionally it is explained what the implication of being unmanned is on that system. It can be seen that after the initial concept design is finished, the wing characteristics and stability and eigenmotions are analysed separately. This is done since it is not possible to fully implement the full 3D aerodynamic analysis, done in XFLR5, in the code. If these two final checks are okay, the initial concept design is finished.

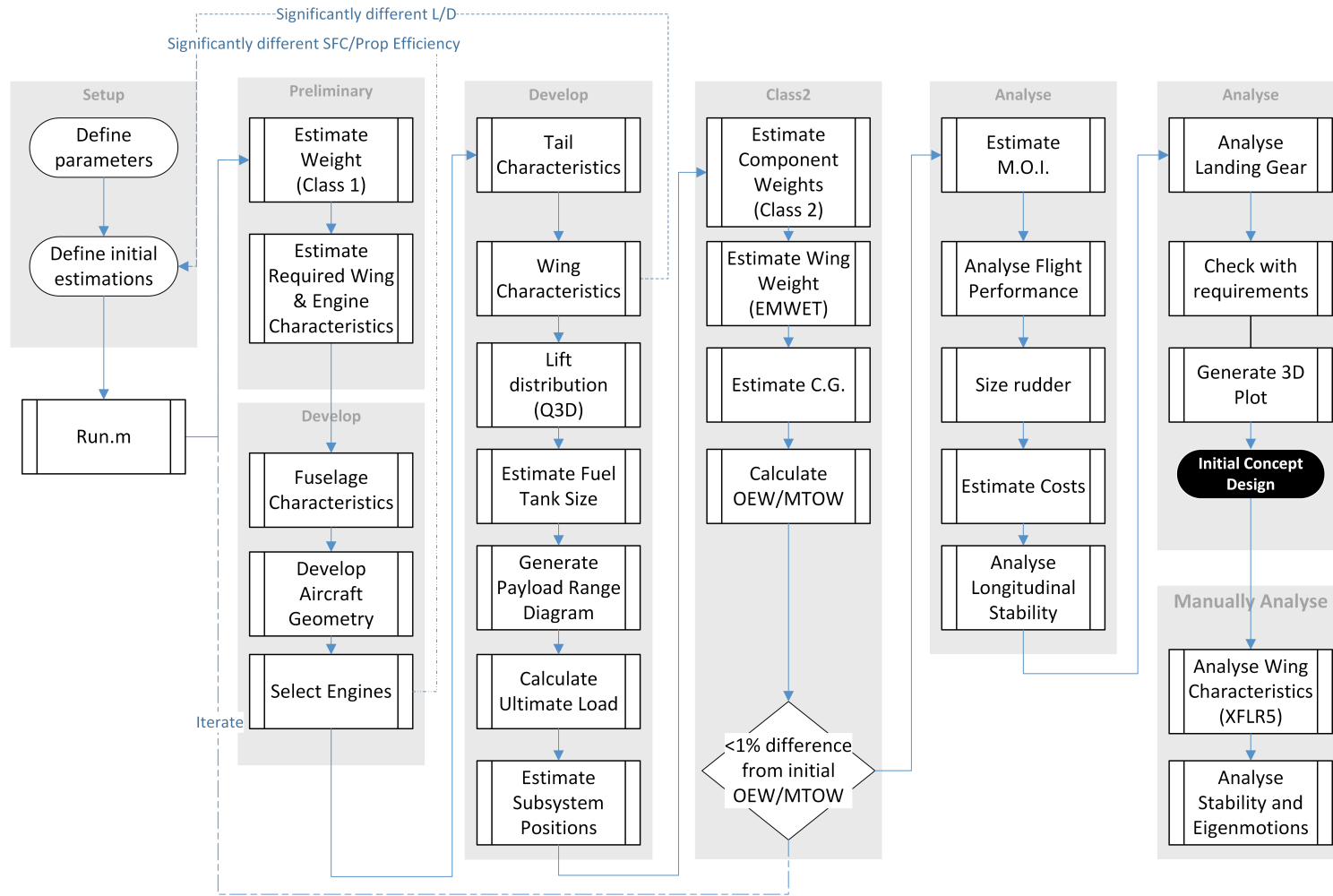


Figure 4.1: Scheme of the program showing the division in interconnected individual modules.

4.2 Design driving characteristics

This section emphasises on the process used to set a basis for the design of the aircraft. It starts with explaining how the aircraft size is constrained by the container size preferred. The sizing and the amount of the containers is elaborated on. Furthermore, a decision on whether to pressurise the container or aircraft is explained. As a last part of this section, a reference frame for the aircraft final design is provided.

4.2.1 Inside-out method

The ATLAS is designed starting from the inside, working to the outside. This means that the design is based on the size of the containers that have to fit in the cargo bay. Preferably, these containers are truck compatible in order to ease the loading and unloading of the aircraft. Also, it is preferable that humans are able to walk inside the aircraft. Lastly, the aim is to design an aircraft that is compatible with current airport operations (i.e. using ULDs that are currently used). The reason for this is that future operators of ATLAS do not necessarily have to buy new containers, but still have the possibility to use ULDs that are currently used.

4.2.2 Container layout

It is chosen to transport four containers: two next to each other and two behind each other. This is done since this enables ATLAS to meet the required minimum payload volume of $50m^3$. Besides that, this configuration makes good use of the shape of a blended wing body aircraft, by limiting the length of the centre body and instead being wider. Additionally this configuration is shown to still make stabilisation of the aircraft possible. The size of the container is based on two preferences. The first preference is that the container should be truck compatible. The second preference is that the container can fit in a shipping container, which enables the container to transfer quickly between transport by airplane and ship. To comply with these preferences, the inner floor width and length of a shipping container are used for the container. The height is affected by the preference that a person should be able to walk inside the centre body. To comply with this preference, the height of the container is set to 1.95m. In Table 4.1 the values of these constraints are summarised.

Transporting four containers as described in Table 4.1 provides customer flexibility: in one ATLAS flight each container can be used by a different customer. However, if the customer wishes, the ATLAS also offers the flexibility of transporting two 11.4 meter long containers, or even one large container that takes up the entire cargo bay space. This introduces increased compatibility with cargo featuring extraordinary dimensions.

Table 4.1: Centre body sizing constraints.

Constraint	Value [m]	Based on
Container height max	1.95	Able to walk inside aircraft
Container height min	1.64	Compatible with current airport operations
Container width	2.35	Truck compatible
Container length	5.7	Truck compatible

4.2.3 Pressurisation

In order to be aerodynamically efficient, it is chosen to fly at a high altitude: preferably an altitude above 40,000ft to make sure the ATLAS flies in segregated airspace. For various types of cargo (e.g. perishables), pressurisation is required at this altitude. Since the shape of a blended wing body is structurally inefficient to pressurise and thus very heavy, it is decided to design a separate pressure vessel within the fuselage. The detailed design of the pressure vessel is depicted in subsection 4.5.3. The pressure vessel enforces a weight penalty, but this is deemed acceptable due to the increased range of cargo that can be transported and the fact that part of the pressure vessel will double function as the horizontal cargo bay floor.

4.2.4 Reference frame

The reference frame that will be used in this design can be seen in Figure 4.2. As can be seen, a right-handed coordinate system is used, with the origin at the nose of the aircraft. Later in this report, when the position of systems and subsystems will be determined, Figure 4.2 should be taken in mind.

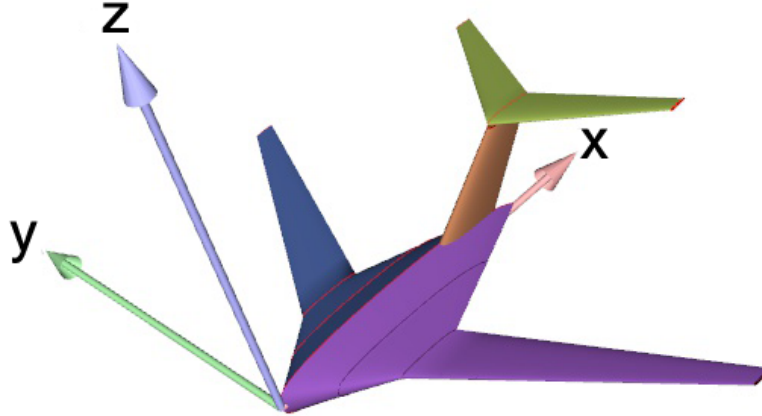


Figure 4.2: Reference frame used for designing ATLAS.

4.3 Class I weight estimation

A first class weight estimation is performed in order to get a first estimations of the fuel weight, operational empty weight (OEW) and maximum take-off weight (MTOW). These values are required for a first estimation of the engines, required surface area, performance, noise and costs. In this section the take-off weight is first expressed as a general equation. After that the individual variables in these expressions are defined.

General equation

The take-off weight (W_{TO}) of an aircraft consists the operational empty weight (W_{OEW}), fuel weight (W_F), and payload weight (W_{PL}). This can be seen in Equation 4.1.

$$W_{TO} = W_{OEW} + W_F + W_{PL} \quad (4.1)$$

This equation can be further analysed by splitting the terms up. Firstly, W_{OEW} can be divided into the aircraft empty weight (W_E), the trapped fuel weight (W_{tfo}), and the crew weight (W_{crew}). Since the aircraft is an unmanned freighter, W_{crew} is equal to 0 and is left out of further equations. Often there exists a empirical relationship between W_E and W_{TO} . This can be linear, but also logarithmic. For now this relationship will be called Rel_{W_{TO}, W_E} . W_{tfo} is usually expressed as a fraction of W_{TO} . Secondly, W_F can be divided into reserve fuel weight ($W_{F_{res}}$) and the used fuel weight ($W_{F_{used}}$). The weight of the used fuel can be expressed as the fraction of the mass used times W_{TO} . Next, this fraction of the mass can be expressed as one minus the mass fuel fractions (M_{ff}). $W_{F_{res}}$ can be expressed as a fraction of $W_{F_{used}}$. This results in a new expression for W_{TO} as can be seen in Equation 4.2.

$$W_{TO} = Rel_{W_{TO}, W_E}(W_{TO}) + M_{tfo} \cdot W_{TO} + M_{res} \cdot (1 - M_{ff}) \cdot W_{TO} + (1 - M_{ff}) \cdot W_{TO} + W_{PL} \quad (4.2)$$

Variables calculation

In this section, all variables of Equation 4.2 will be either defined or calculated, such that the only unknown in Equation 4.2 will be W_{TO} .

Payload weight

The aircraft will be designed to transport a typical payload weight over the required 3000nmi. The typical payload weight is defined as the cargo hold volume multiplied by the typical payload density. This typical payload density is determined by looking at the average density of goods transported via air. It is chosen to set this typical payload density at $250kg/m^3$. This is slightly higher than all of the mean densities of goods transported via air (see Table 2.3). This enables the aircraft to carry all goods currently being transported by air. It is assumed that the container weight is part of the payload weight. The cargo volume is based on the container layout as described in subsection 4.2.2 including some margin, and is set to $102m^3$. Multiplying the typical payload density with the cargo volume gives a typical payload mass of $28000kg$ (or $274680N$).

Relationship between empty weight and take-off weight

An empirical relationship between the empty weight and take-off weight is usually found by looking at similar reference aircraft. However, not many reference aircraft exist for blended wing bodies (BWB). However, some studies have been performed on concepts like these, and the results can be used to get a first estimation of the relationship between empty weight and take-off weight of BWBs [18] [19]. This relationship is assumed to be linear.

Mass fuel fractions

The mass fuel fractions (M_{ff}) describe the change in total weight of the aircraft due to fuel being burnt during the complete mission profile. The fractions for the cruise and loiter phases are calculated based on the fuel consumption by the engine. First, estimations for the other fractions are gained from statistical data (see Figure 4.3). For this jet engined aircraft the data of the transport jets is used.

aircraft type	engine start and warm-up	taxi	take-off	Climb and acceleration to cruise	descent	landing, taxi and shut-down
transport jets	0.990	0.990	0.995	0.980	0.990	0.992

Figure 4.3: Statistical mass fuel fractions [3].

Further in the design stage it turned out that the chosen mass fuel fractions of Figure 4.3 were not completely applicable. Since the fuel consumption for this design is lower than for regular aircraft, the change in total weight of the aircraft is less significant. Therefore these fractions were updated to reflect this.

As mentioned before, the three phases of the flight that have to be analysed separately are the two cruise phases and the loiter phase. These mass fuel fractions are calculated using the Breguet's range and endurance equations [20]. Fixed inputs in these equations are the range of 3000nmi, loiter endurance of 1800s and a cruising altitude of 12500m. Based on reference aircraft, estimations have to be made on the cruising Mach number, the $\frac{L}{D}$ value and the specific fuel consumption of the engine. During the design, more accurate and specified values for this specific design are found, and these updated values will be used in the iterations.

Reserve fuel fraction

In the mission profile, a $100km$ safety range and a by CS25 stated 30 minute loiter [11] is already included. This was already incorporated when calculating the mass fuel fractions (M_{ff}). Therefore it is chosen to set the reserve fuel fraction (M_{res}) equal to 0. The already included

extra range and extra loiter time will give the aircraft sufficient freedom of movement in case of unforeseen situations.

Trapped fuel fraction

Typical values for the trapped fuel fraction lay between 0.001 and 0.0045 [20]. This means that between 0.1% and 0.45% of the take-off weight consists of trapped fuel. Trapped fuel consists for example of fuel under the pump-intake or fuel in lines between the tanks and the engines. The trapped fuel fraction M_{tfo} is set to an average value of 0.00225.

Verification

The verification of the model made used to do the first class weight estimation is done by using examples from [20]. After changing the input values to the ones of the examples in the slides, the model gets exactly the same answers as the answers provided in the slides. This is a confirmation that the model is working as intended.

4.4 Wing loading and thrust loading

Due to constraints, either by regulations, customer requirements, or design decisions, the maximum wing loading (W/S) and minimum thrust loading (T/W) are limited. In this section, the limiting requirements affecting the wing loading or thrust loading are explained. Each of these requirements results in a relation between W/S and T/W . Using these relationships a graph is constructed showing the limits and the remaining design space. In this remaining design space a design point will be chosen. Based on this point, a required surface area and thrust will then be found. Next the results are shown, and finally the verification procedure is explained.

Sizing to requirements

This section will explain for which requirements are designed, and what their effect will be on the outcome. These requirements will size for stall, take-off, landing, cruise, climb and manoeuvring.

Sizing to stall performances

In order to size for the stall requirement, Equation 4.3 [21] is used. This requirement limits the maximum allowable wing loading in order to meet the stall requirement. In Equation 4.3, ρ was taken equal to the density at sea level on a hot and humid day [22], which is equal to $1.100\text{kg}/\text{m}^3$. At higher altitude, landing would be possible with a higher approach speed. For the maximum lift coefficient $C_{L_{max}}$ (in landing configuration), three different values were chosen in order to see the effect of $C_{L_{max,land}}$ on the requirement. This will result in three vertical lines in the wing loading graph. At the end, when the decision has to be made for which $C_{L_{max,land}}$ will be designed for, it has to be taken into account that increasing the value for $C_{L_{max,land}}$ leads to more required high lift devices which [21]:

- Weigh more
- Cost more
- Are more sensitive to failure
- Require more maintenance

According to [21], the stall speed V_S for civil aircraft is usually 1.2 times lower than the approach speed. Looking at reference aircraft, it can be seen that the approach speed does not differ a lot between different aircraft.¹ Therefore the same approach speed was assumed as reference aircraft have, being equal to 130kts ($67\text{m}/\text{s}$).

$$\frac{W}{S} = \frac{1}{2} \cdot \rho \cdot V_s^2 \cdot C_{L_{max,land}} \quad (4.3)$$

¹<http://www.boeing.com/assets/pdf/commercial/airports/faqs/arcandapproachspeeds.pdf> [accessed on 13/05/15]

Sizing to take-off distance

In order to size for the take-off distance requirement, Equation 4.4 is used [21]. In this equation, three different values for $C_{L_{max,to}}$ (in take-off configuration) are chosen in order to see the effect of $C_{L_{max,to}}$ on the maximum wing loading. σ in these equations is equal to the density ratio $\frac{\rho}{\rho_0}$. Again, ρ is based on the value on a hot and humid day ($1.100kg/m^3$), and ρ_0 is the density at sea level ($1.225kg/m^3$). The take-off parameter (TOP) is based on a statistical graph [23]. The decision has been made to be able to take-off at a runway 1500m, instead of the maximum required take-off length of 3000m. This enables ATLAS to land at smaller airports as well, since its take-off and landing distances are smaller than reference aircraft, even smaller than the Airbus A319.² Using this and the type and number of engines (which differs per concept) a value for the TOP can be found. After converting the value that was read off from the x-axis to SI-units, it could be inserted into Equation 4.4. Substituting these values in the equation result in a relation between the wing loading and the thrust loading.

$$\frac{T}{W} = \frac{W}{S} \cdot \frac{1}{C_{L_{max,to}}} \cdot \frac{1}{\sigma} \cdot \frac{1}{TOP_{jet}} \quad (4.4)$$

Sizing to landing distance

In CS-25 [11] Equation 4.5 is provided, relating the required landing distance to the stall speed in landing condition. This equation can be used to come to an expression that limits the wing loading, as can be seen in Equation 4.6. [21] According to the requirements, the maximum landing distance is equal to 2000m. However, preferably the aircraft can land at the same runway length as which it takes off from. Therefore the maximum landing distance is taken equal to 1500m. Again, ρ is based on the value on a hot and humid day ($1.1kg/m^3$). f is the ratio between the take-off and landing weight. In this case, this value was assumed to be equal to 1. In this way the aircraft is able to land at the same weight as it took off (useful for example in an emergency situation). For $C_{L_{max,land}}$, a range of values was taken in order to see the effect of $C_{L_{max,land}}$ on the maximum wing loading. The landing distance requirement results in a vertical line in the graph.

$$S_L = 0.5847 \cdot V_{S_{land}}^2 \quad (4.5)$$

$$\frac{W}{S} = \frac{C_{L_{max,land}} \cdot \rho \cdot \frac{S_{land}}{0.547}}{2 \cdot f} \quad (4.6)$$

Sizing to cruise performance

This requirement makes sure the aircraft is able to fly at the desired cruise speed. For this requirement, Equation 4.7 is used [21]. In this equation, V is equal to the cruise speed. ρ is equal to the density at cruise altitude. The variable e is the Oswald factor, which is estimated in section 5.2. For the Aspect Ratio A a range of values was taken in order to see the effect it has. The value of C_{D_0} during cruise was first taken from reference aircraft. After the graphs are completed, an airfoil is selected (this process will be explained in section 5.2), an updated value of C_{D_0} is used in the iterations. It should be noted that the value 0.9 appears in both equations. This is done so the aircraft is able to cruise at 90% thrust setting. This time, different possible values were taken for the aspect ratio A , each resulting in a different limit.

$$\frac{T}{W} = \frac{1}{0.9} \left(\frac{\rho_0}{\rho} \right)^{3/4} \left(\frac{C_{D_0} \frac{1}{2} V^2}{\frac{W}{S}} + \frac{W}{S} \frac{1}{\pi A e \frac{1}{2} \rho V^2} \right) \quad (4.7)$$

²<http://jetadvisors.com/airbus-a319-performance/> [accessed on 22/06/15]

Sizing to climb requirement

Since CS-25 has no requirement on the climb rate [11], the only climb requirement that has to be designed for is the required climb gradient. CS-25 specifies the required climb gradients shown in Table 4.2, all with one engine inoperative.

Table 4.2: Required climb gradient as stipulated by CS25:25.121 [11].

Number of Engines:	4	3	2
First Take-Off Segment	0.50%	0.30%	0.00%
Second Take-Off Segment	3.00%	2.70%	2.40%
Final Take-Off Segment	1.70%	1.50%	1.20%
Enroute Climb	1.60%	1.40%	1.10%
Approach Segment	2.70%	2.40%	2.10%
Landing Segment	3.20%	3.20%	3.20%

For this phase only the two most critical segments are evaluated, the ones most likely to limit the design space. These are the second take-off segment, which should be met in take-off configuration, and the landing segment, which should be met in landing configuration.

The relation between the wing loading and the thrust loading to meet this climb gradient can be seen in Equation 4.8 [21]. This equation has to be evaluated for both segments. In this equation, $\frac{c}{V}$ is the minimum required climb gradient, which can be found in Table 4.2. In this equation, C_{D_0} is taken for either the landing or the take-off configuration. Both are first estimated based on reference aircraft and then updated with the values found in section 5.2. The Oswald factor e is taken the same as before, and ρ was taken equal to the density on a hot and humid day ($1.1kg/m^3$). Again a range of values was used for A . Substituting all values gives a minimum thrust loading.

$$\frac{T}{W} = \frac{c}{V} + 2\sqrt{\frac{C_{D_0}}{\pi A e}} \quad (4.8)$$

No requirement exists for climbing at cruising altitude, but it is highly preferable to have an aircraft that can still increase its altitude a bit when flying at cruising altitude. In this way it has more freedom in changing flight path if necessary, instead of having only the possibility to decrease altitude. This turns out to be the most limiting factor compared to the climb and landing segment, since the thrust at this point is less than at take-off or landing. The reasons for this are that the thrust decreases with altitude, as well with increasing Mach number.

Sizing to manoeuvring requirement

The aircraft must be able to handle a certain load factor in order to make a sustained turn. From regulations [11], the aircraft has to be able to withstand a maximum load factor of 2.5g. For this limit, the equation can be seen in Equation 4.9 [21]. All parameters in this equation are evaluated during cruise conditions (C_{D_0} , ρ , V , e). Again, this requirement is plotted for different aspect ratios A .

$$\frac{T}{W} = \frac{C_{D_0} \frac{1}{2} \rho V^2}{\frac{W}{S}} + \frac{W}{S} \frac{n_{max}^2}{\pi A e \frac{1}{2} \rho V^2} \quad (4.9)$$

Results

Using all limits found in section 4.4, a wing loading versus thrust loading diagram can be made. Firstly, it is favourable to have an as high wing loading as possible, since then smaller surface area is sufficient for the same maximum take-off weight. Secondly, it is favourable to have a low thrust loading, since then a lower thrust is sufficient for the same maximum take-off weight.

From the wing loading versus thrust loading diagram, the values found in Table 4.3 are then selected for $C_{L_{max,land}}$, $C_{L_{max,to}}$, $C_{L_{max,land}}$ or A . The wing loading versus thrust loading diagram can be seen in Figure 4.4, with only showing the lines with the C_L and aspect ratio values that are used for this design. As can be seen, the limiting requirements for this design are the climb during cruise and the take-off distance. This results in a wing loading of 2579 N/m^2 and a thrust loading of 0.39 (see black circle in Figure 4.4). Comparing these values to reference aircraft, it can be seen that the wing loading is relatively low, and the thrust loading relatively high. This can be explained by the strict take-off requirement of 1500m, and the high cruising altitude of 12500m.

Table 4.3: Aerodynamic parameters.

	$C_{L_{max,land}}$	$C_{L_{max,to}}$	A
Value [-]	1.8	1.6	11.3

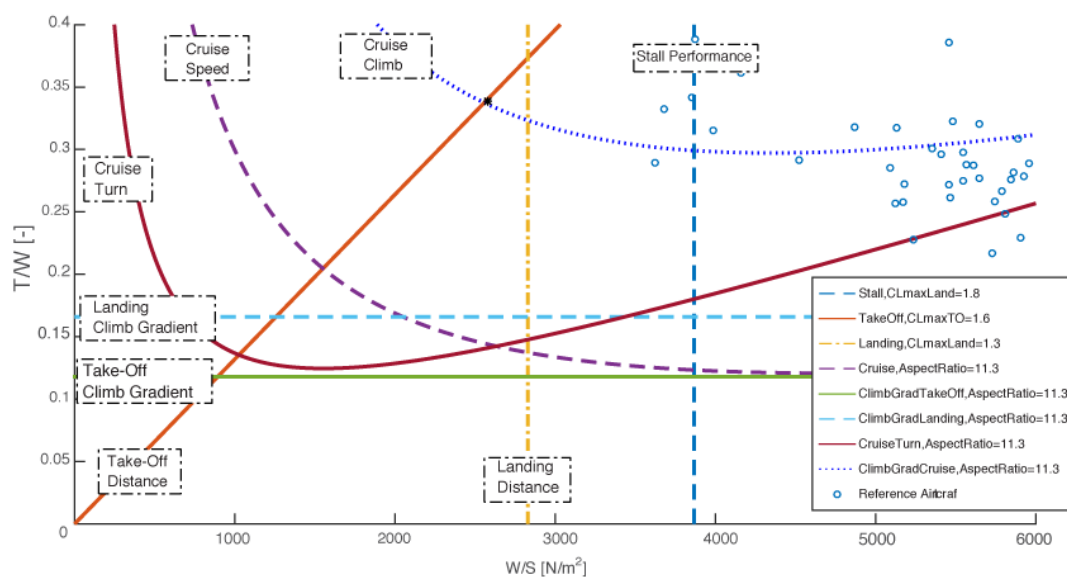


Figure 4.4: Wing loading versus thrust loading.

Verification

For verifying the model used to create the wing loading versus thrust loading diagram, the examples in the lecture slides of the "Aerospace Design and Systems Engineering Elements I" course are used [21]. After inserting the input values from the slides into the model, plots can be created. These are compared to the resultant plot provided in the slides. All lines have been verified individually, so at the end the program is verified.

4.5 Subsystem design

In this section the subsystems are designed in more detail. Firstly the wing, centre body and empennage are designed. Following this the control surfaces, landing gear and the propulsion system are investigated. Finally the environmental control, fire protection, ice on wing protection and the electrical system are researched.

Table 4.4: Wing segment parameters.

(a) Aircraft parameters.

Parameter	Value [Unit]
b	49.9 [m]
S	221 [m ²]
A	11.3 [-]
C_{root}	24.5 [m]
C_{tip}	1.49 [m]
λ	0.0608 [-]
Λ_{LE}	- [°]
\bar{c}	4.71 [m]
Γ	- [°]

(c) Body parameters.

Parameter	Value [Unit]
b	10.5 [m]
S	158 [m ²]
C_{root}	24.5 [m]
C_{tip}	5.68 [m]
λ	0.232 [-]
Λ_{LE}	51.0 [°]
\bar{c}	17.1 [m]
Γ	1.00 [°]

(b) Trapezoidal wing parameters.

Parameter	Value [Unit]
b	49.9 [m]
S	207 [m ²]
C_{root}	6.80 [m]
C_{tip}	1.49 [m]
λ	0.219 [-]
Λ_{LE}	31.0 [°]
\bar{c}	4.71 [m]
Γ	8.50 [°]

(d) Outer wing parameters.

Parameter	Value [Unit]
b	39.4 [m]
S	141 [m ²]
C_{root}	5.68 [m]
C_{tip}	1.49 [m]
λ	0.262 [-]
Λ_{LE}	31.0 [°]
\bar{c}	4.00 [m]
Γ	8.50 [°]

4.5.1 Wing

The wing geometry is defined by variables and parameters. Together these influence the shape and size of the wing segment. For the aerodynamic analysis a particular distinction between the segments has been made. The tailless aircraft consists of the body and the outer wing. The main wing of the aircraft is divided in these segments for aerodynamic analysis. Alternatively for certain analyses the trapezoidal wing approximation is used [24]. This wing has been defined has the projection of the outer wing on the body. For the trapezoidal wing and the entire aircraft the surface area and therefore the aspect ratio are different. The values for different sections are shown in Table 4.4.

To increase the internal space of the body segment, the thickness over chord (t/c) ratio is increased from 0.11 to 0.17 by scaling the airfoil. To minimise the increase in wave drag, the sweep angles were increased. This makes the body segment less effective at generating lift. It is assumed that the body is 50% effective at generating lift. This assumption is supported by the lift pressure distribution discussed in subsection 5.2.6 and the fact that the body also has a fuselage part at its rear end which is less lift generating.

The wing span for the aircraft is calculated since the aspect ratio and the surface area is known. The taper ratio and the mean aerodynamic chord can also be calculated. The division of surface area for the body and the outer wing is largely based on interior space required for the cargo bay. The parameters of the wing segments are shown in Table 4.4.

4.5.2 Airfoil selection

The airfoil affects a lot of the parameters during all phases of flight such as cruise speed, take-off and landing distances, stall speed, handling qualities and overall aerodynamic efficiency [23]. For all these reasons a correct choice of an airfoil is important. A supercritical airfoil has been selected for the design. Supercritical airfoil are designed to increase the Mach drag divergence number and delay the transonic drag rise. These airfoils increase the aerodynamic efficiency by reducing the intensity of the shock waves. It is flatter on the top, rounded on the bottom and the upper trailing edge is accented with a downward curve to restore lift lost by the flattening

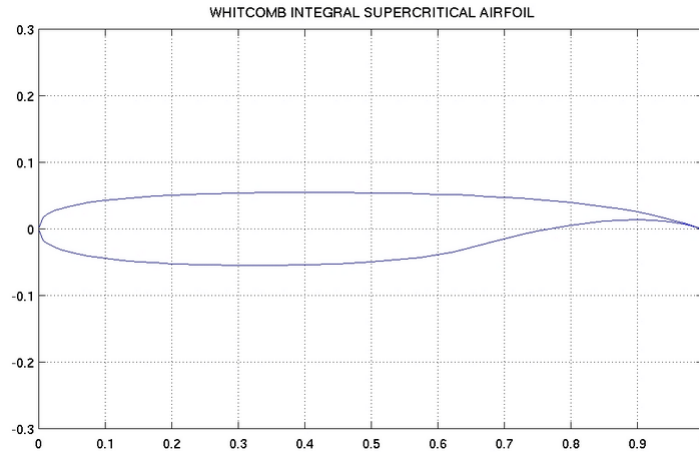


Figure 4.5: Whitcomb supercritical airfoil contour.

the upper surface.³ At speeds in the transonic range, a supercritical airfoil delays the formation of the supersonic shock wave on the upper wing surface and reduces its strength, allowing the aircraft to fly faster with less effort. For this design the Whitcomb integral supercritical airfoil is selected. The body uses the airfoil scaled with 17% thickness and the outer-wing uses the standard airfoil with 11% of thickness. For the 2D analysis of the airfoil, XFLR5 software is used. The airfoil is shown in Figure 4.5⁴.

4.5.3 Centre body

As mentioned in section 4.2 an inside-out method is used to finalise the design. The constraints on the container dimensions can be seen in Table 4.1. Another constraint for the size and shape of the centre body is the decision to pressurise the centre body. Since it is difficult to pressurise a non-circular object, the cargo bay shape is defined using the concept of a multibubble. [25][26] The next section will explain more about this solution.

Pressure vessel

The main difference between the pressurisation of circular and non-circular cross sections is the occurrence of bending stresses in any non-circular cross section, whereas circular cross sections carry only in-plane loads. To cope with extra bending stresses extra material is required, resulting in a severe weight penalty. The multibubble concept defines non-circular cross-sections by building them with circular arcs, as illustrated in Figure 4.6. Using this concept, the pressure vessel can be designed to fit into the space limitations of the system induced by the aerodynamic department and still carry solely in-plane stresses. At the intersection between each two circles a wall has to be designed, which will assure force equilibrium at these locations. [25][26] In this design the bottom wall will function as the cargo bay floor as well. At each point where two arcs and a wall meet, local stress concentrations will exist. These have not been analysed in this phase of the design. However, they can be accounted for by locally adding more material, as shown in Figure 4.7.

The radius of the vertical arcs is derived from the cargo bay dimensions. The cargo bay space is used most efficiently when the distance of the cargo bay area centroid to each of the cargo bay corners is equal. Using the container dimensions, the radius for the vertical arcs is found to be 2.5 meters. The difference between the maximum container height and the maximum centre body height is 0.42 meters, which implied that the height of the top and bottom circular arc must fit within this constraint resulting in the radii of these arcs being 22.5 meters. With

³https://www.nasa.gov/pdf/89232main_TF-2004-13-DFRC.pdf [accessed on 03/06/15]

⁴<http://m-selig.ae.illinois.edu/ads/afplots/whitcomb.gif> [accessed on 03/06/15]

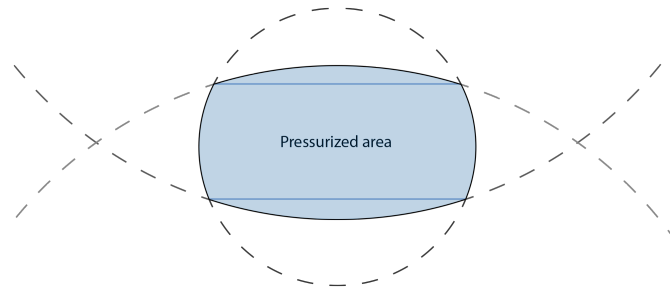


Figure 4.6: Describing a non-circular cross-section using circular elements.



Figure 4.7: Stress concentrations will be accounted for by local reinforcements.

these radii and the container dimensions, the cargo bay cross-section looks as shown in Figure 4.8.

The thicknesses of the arcs and walls are calculated using the equations as in [25], where a pressure differential of $102,700 \text{ N/m}^2$ was accounted for, which is comparable to current aircraft⁵. The results are presented in Table 4.5. Note that a minimum production thickness of 1 mm is accounted for. The caps closing the pressure vessel on either end are designed using analogous methods from [25]. With the cargo bay length of 11.4 meters the total pressure vessel mass is 2,591 kilograms.

Besides the pressure loads, the cargo bay floor must also be able to handle the stresses induced by the payload weight. For this additional vertical supports will be mounted under the floor. These are not designed in detail in this report, but their horizontal spacing is determined using plate theory equations 4.10 and 4.11 [27]^{6 7}. Equation 4.10 computes the required spacing to satisfy the bending moment, using the material compressive strength (with a 0.2 safety factor) and dividing the max payload weight by the cargo bay area to compute the floor loading. Equation 4.11 computes the required spacing to satisfy the floor deflection, which is set at a maximum allowable deflection of 0.03 meters. Solving both equations gives spacings of 2 meters and 0.95 meters, the

⁵<http://boeing.mediaroom.com/2008-09-27-Boeing-Completes-787-Dreamliner-High-Blow-Test> [accessed on 08/06/15]

⁶http://m-5.eng.uml.edu/22.311/S2015/22311--Chapter13-v2015_v2.pdf [accessed on 12/06/15]

⁷http://www.efunda.com/formulae/solid_mechanics/plates/theory.cfm [accessed on 12/06/15]

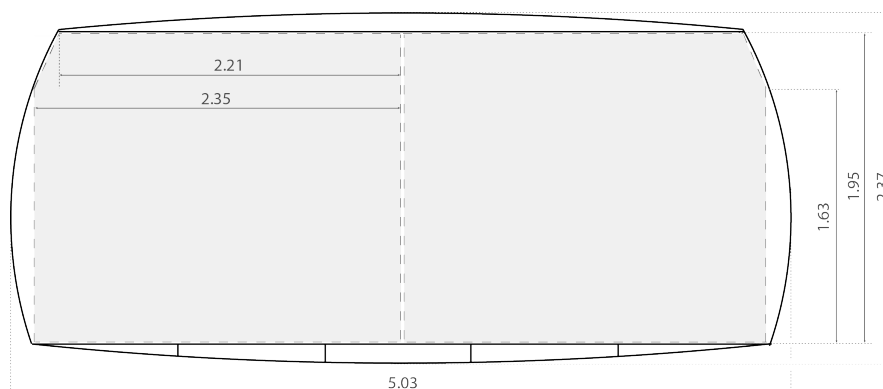


Figure 4.8: The cargo bay dimensions (in meters).

Table 4.5: Thicknesses for the pressure vessel.

Member	Thickness [m]
Top arc	0.0043
Bottom arc	0.0043
Vertical arcs	0.001
Top wall	0.004
Bottom wall	0.0041

latter of these will be used as a preliminary value.

$$\frac{\sigma_{comp} t_{floor}^2}{1.2 \cdot 6} = \frac{p_{floor} d_{floor}^2}{12(1 + (\frac{b_{floor}}{a_{floor}})^4)} \quad (4.10)$$

$$w_{floor} = \frac{0.032(1 - v^2) p_{floor} d_{floor}}{1 + \frac{b_{floor}^4}{a_{floor}^4}} \frac{p_{floor} d_{floor}}{Et_{floor}^3} \quad (4.11)$$

It should be mentioned that the pressure vessel is analysed to only carry the pressurisation loads. In section 5.3 the load carrying structure into which the pressure vessel will be integrated is designed.

4.5.4 Empennage design

This section explains the design method that is followed for the empennage. Here a general outline of the method followed is stated, a more detailed description can be found in [28]. It should be stated that empennage design is an iterative process, like most design processes of an aircraft. The results of the empennage design can be found in Table A.1 in Appendix A.

Horizontal tailplane

1. Select empennage configuration. For the ATLAS the engine location limited the configurations option to the T-tail, since it is the only configuration where the horizontal tailplane is out of the airflow of the engine.
2. Determine the tailplane location. In general the horizontal tailplane should be located as more aft as possible. This increases the horizontal moment arm for longitudinal stability and decreases the surface area of the tailplane and therefore the parasitic drag.
3. Calculate the surface area using the horizontal tail volume coefficient V_H . For a first estimate the volume coefficient is determined from statistical data.
4. Select an airfoil and calculate the lift coefficient. For the horizontal tailplane the airfoil lift curve slope must be as large as possible along a wide range of angles of attack. Since the aircraft centre of gravity moves during cruising flight, the airfoil must be able to create both positive and negative lift. For this reason, a symmetric airfoil is the most suitable candidate.
5. Select a Taper ratio, Aspect ratio and Sweep angle. For a first estimate the Taper ratio and Aspect ratio were determined from statistical data. The Sweep angle of should be larger than that of the main wing in order to increase the drag divergence Mach number.
6. Determine the incidence angle. The primary requirement of the incidence angle is to nullify the pitching moment about the centre of gravity at cruise. Tail incidence is determined to satisfy the trim design requirement when no control surface (i.e. elevator) is deflected.
7. Calculate the Span, Root chord, Tip Chord and Mean Aerodynamic Chord. These unknown are determined by solving the equations on [28, p. 326] simultaneously.
8. Check if aircraft is longitudinally stable. The static longitudinal stability is examined through the sign of the longitudinal stability derivative C_{m_α} or the location of the aircraft neutral point. The reader is encouraged to read section 5.4 on stability and control.
9. Modify and optimise the tailplane. If the aircraft is unstable the empennage planform should be modified. This is an iterative process. Profound knowledge of longitudinal, di-

rectional and lateral stability ensures that these iterations can be done swiftly.

Vertical tailplane

For the vertical tailplane the same design methodology was followed as for the horizontal tailplane. For a T-tail the location of the vertical tailplane is directly influenced by the location of the horizontal tailplane. The horizontal and vertical tailplane location is an iterative process since the horizontal tailplane is on the tip of the vertical tailplane. Iterations are necessary to ensure an optimal result, where the weight and size of the overall empennage is kept as low as possible. For the vertical tailplane surface area the MAC (\bar{C}) is replaced by the Span of the main wing (b) and the horizontal volume coefficient is replaced by the vertical volume coefficient. The vertical volume coefficient is determined from statistical data.

Implication of being unmanned

The fact that the ATLAS flies unmanned does not have a direct influence on the empennage design. However, since there is no pilot to correct the aircraft it is necessary that the aircraft is stable in all modes. This will be investigated in section 5.4. The requirement on spiral stability did have an influence on the tail geometry.

4.5.5 Control surfaces design

In this section the control surfaces are designed which behaviour is necessary to meet some requirements. Firstly the high lift devices are designed and secondly the rudder design is given.

High lift devices

High lift devices (HLD) are used to extend the flight envelope during individual phases of flight. They can be retracted during cruise and deployed during take-off and landing to increase the lift and drag respectively. There are two types of high lift devices (HLDs), namely flaps and slats. Flaps are placed on the trailing edge and slats are placed on the leading edge of the wing. The selected HLDs can be seen in Figure 4.9.⁸

Flaps

There are different kind of flaps, the most common ones are plain, split, slotted and fowler flaps. For the design, single slotted flaps have been selected for their simplicity, easy maintenance as well as them taking lesser space in the wing structure. They increase the wing camber and when extended they open a slot between the wing and the flap. Because of this slot, high pressure air from the bottom of the wing flows through the slot into the upper side. This adds energy to the wing's boundary layer, delays airflow separation and produces less drag. Figure 4.9a shows the single slotted flap. The lift increment is caused by three main factors. The first is the effective change of camber produced by lowering the flap. The second is due to the flow through the slot re-energising the boundary layer and thus delaying flow separation from the flap. The third is the increase of effective lifting surface due to the rearward movement of the flap [29, p. 5].

Slats

Slats allow the wing to operate at higher angles of attack. Slats let the aircraft take-off and land at shorter distances. At higher angle of attack, the slats change the airflow at the front of the wing, making it flow more smoothly over the upper surface. This allows the wing to be operated effectively at higher angles to produce more lift. Krueger flaps have been selected for the design because of its simple architecture and low complexity. It can be seen in Figure 4.9b. Unlike other leading edge devices the main upper surface area of the wing and its nose have not changed. Instead, from the lower part of the wing, a portion is rotated out in front of the main wing.

⁸[https://en.wikipedia.org/wiki/Flap_\(aeronautics\)](https://en.wikipedia.org/wiki/Flap_(aeronautics)) [accessed on 12/06/15]



Figure 4.9: Selected flap and slat.

Dimensioning the HLDs

After selecting the HLDs, their dimensions have to be determined. To determine the surface area of the flaps and slats, the required ΔC_L is determined for takeoff and landing conditions. The lift distribution between the HLDs is divided in such a way that the slats are wider than the flaps. Highly efficient slotted flap systems take up to 35% or even 40% of the wing chord. The flaps for the design are assumed to be placed at 35% of the chord from the trailing edge. The slats are assumed to be at 10% of the chord from the leading edge. Equation 4.12 has been used to calculate the required wetted surface area (S_w) for both flaps and slats. The sweep at the hinge line is calculated by Equation 4.13. The dimensions for flaps and slats can be seen in Table A.5. Single slotted flaps typically have a $C_{l_{max}}$ value of 1.3, Krueger flaps typically have a $C_{l_{max}}$ value of 0.3. [30]

$$S_w = \frac{C_{L_{max}} \cdot S}{0.9 \cdot C_{l_{max}} \cdot \cos \Lambda_{hingeline}} \quad (4.12)$$

$$\tan \Lambda_{hingeline} = \tan \Lambda_{LE} - \frac{x}{c} \cdot \frac{2 \cdot c_r}{b} \cdot (1 - \lambda) \quad (4.13)$$

Rudder sizing

One of the movable control surface on conventional aircraft is the rudder. This surface, located at the trailing edge of the vertical tail, is responsible for the aircrafts directional control and trim. When the rudder is rotated with a deflection angle δ_R , a lift force L_V is generated by the components of the vertical tail. As a result a yawing moment about the centre of gravity is provided by the rudder, making it the primary means for directional control and trim. In a multi-engine aircraft when an engine fails, as depicted in Figure 4.10 [31], the thrust generated by the operating engine creates a yawing moment and rotates the aircraft in the direction of the critical engine. This yawing moment has to be counteracted by the rudder. The critical engine failure is the most critical mode of power plant failure w.r.t controllability during flight. Since ATLAS is flying transatlantic tracks, it is required to keep its controllability during the whole phase of the flight as stipulated by ICAO. Hence the rudder sizing is based on the asymmetric thrust requirement[28].

When assuming the aileron is not deflected and there is no sideslip angle, the rudder deflection angle in order to trim the aircraft in asymmetric thrust is given by Equation 4.14 [31]. T the maximum available take-off thrust as specified by CS 25.149. The minimum control speed V_{MC} is used to obtain the dynamic pressure in this equation which is defined as 1.13 of the stall speed in CS 25.149.

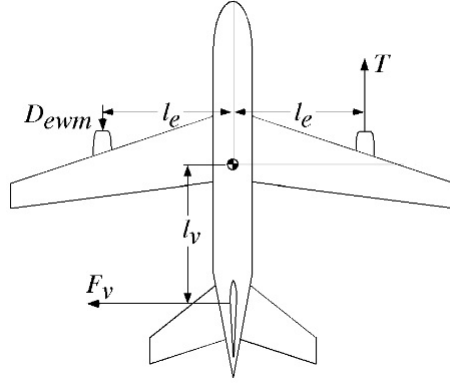


Figure 4.10: Engine-out geometry.

$$\delta_R = \frac{(T_L + D_{ewm})l_e}{-qSbC_{n_{\delta R}}} \quad (4.14)$$

D_{ewm} is the windmilling drag that the fan of the inoperative engine produce as can be seen in Figure 4.10. This value is obtained by computing Equation 4.15, where the windmilling drag coefficient is given by Equation 4.16 [32]. In Equation 4.16; d_i is the diameter of the engine inlet, A_{Inlet} is the inlet area and $\frac{V_n}{V}$ is the windmilling mean flow velocity in the nozzle over the aircraft velocity [32].

$$D_{ewm} = qSC_{D_{ewm}} \quad (4.15)$$

$$C_{D_{ewm}} = \frac{0.0785d_i^2 + \frac{2}{1+0.16M^2}A_{Inlet}\frac{V_n}{V}(1 - \frac{V_n}{V})}{S} \quad (4.16)$$

$$C_{n_{\delta R}} = -C_{L_{\alpha V}}V_V\eta_V\tau_r\frac{b_R}{b_V} \quad (4.17)$$

The next important variable is $C_{n_{\delta R}}$ which is the directional control stability derivative. This derivative is highly dependent on the vertical tail size in relation to the wing. Conventional aircraft generally have a vertical tail surface to wing surface ratio with typical values ranging from 0.1 - 0.3 [4]. For the ATLAS this is 0.15, which is well within the range. This ratio affects the effectiveness of the control stability derivative, in Table A.2. A low $C_{n_{\delta R}}$ means that a bigger deflection angle will be needed for the same yawing moment. To estimate $C_{n_{\delta R}}$, Equation 4.17 is used, where V_V is the volume coefficient of the vertical tail and η_V the rudder angle of attack effectiveness. The value is obtained from statistical data [33]. Because of the large sweep angle of the vertical tail of the ATLAS, more surface area for the rudder will be required. In this case a rudder-chord to vertical tail ratio of 0.4 is assumed. $C_{L_{\alpha V}}$ is lift slope angle of the vertical tail and is estimated with Equation 4.18, where AR_{eff} is the aerodynamic aspect ratio; the aspect ratio on which aerodynamic properties are based such as the lift curve slope. The dimensions of the rudder can be found in Table A.2.

$$C_{L_{\alpha V}} = \frac{2\pi A_V}{2 + \sqrt{\frac{A_{V,eff}^2(1-M^2)}{k^2}}(1 + \frac{\tan^2\Lambda_{\frac{\sigma}{2}}}{(1-M^2)}) + 4} \quad (4.18)$$

$$A_{eff} = 1.55\frac{b_V^2}{S_V} \quad (4.19)$$

$$K = \frac{2\pi}{C_{l_{\alpha}}} \quad (4.20)$$

Table 4.6: Rudder sizing results.

Desing parameters	Values	Units
Aerodynamic Aspect Ratio ($A_{V,eff}$)	1.86	[/]
Rudder angle of attack effectiveness (η_V)	0.6	[/]
2D lift slope C_{l_α}	6.27	$[\frac{1}{rad}]$
Maximum available thrust (T)	954	[N]
Engine windmilling drag coefficient ($C_{D_{ewn}}$)	0.0011	[/]
Engine windmilling drag (D_{ewn})	1786	[N]
3D Lift slope of Naca0015 C_{L_α}	1.5454	$[\frac{1}{rad}]$
2D lift slope constant (k)	1	[/]
Directional stability derivative ($C_{n_{\delta R}}$)	-0.0118	[/]
Maximum rudder deflection angle(δ_R)	30.5	[deg]
Rudder root chord (C_{rR})	1.89	[m]
Rudder span (b_R)	4.77	[m]
Rudder Hinge Angle (λ_R)	50	[deg]

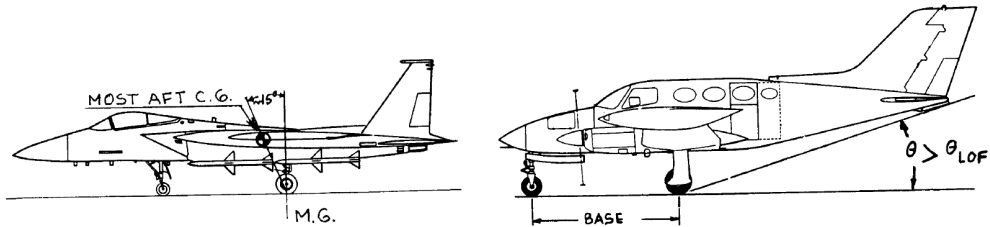


Figure 4.11: Longitudinal tip-over criterion for tricycle gears [4]. **Figure 4.12:** Longitudinal ground clearance criterion [4].

4.5.6 Landing gear positioning and sizing

After all dimensions and weights are determined, the position of the landing gear as well as its length can be determined based on [4] and [34].

The position of the landing is related to its length. This is because the aircraft has certain tip over and ground clearance criteria it has to fulfil, as is depicted in Figure 4.11, Figure 4.12, Figure 4.13 and Figure 4.14.

Firstly, the length and longitudinal position of the main landing gear is determined by using Figure 4.11 and Figure 4.12. For the longitudinal tip over criterion, a 15° angle is taken, as explained in [4]. The take-off angle is assumed to be 9.5° , which is similar (but still conservative) compared to Boeing aircraft.⁹ Choosing this conservative 9.5° take-off angle results in making

⁹<http://www.bangaloreaviation.com/2009/05/typical-takeoff-and-climb-angles-of-all.html> [accessed on 11/06/15]

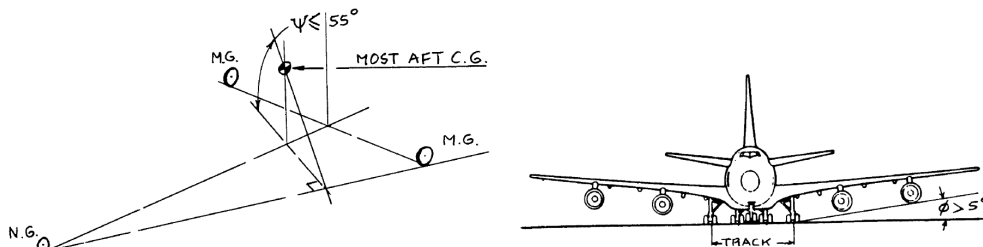


Figure 4.13: Lateral tip-over criterion [4]. **Figure 4.14:** Lateral ground clearance criterion [4].

it easier designing the high-lift devices. Including a 0.5° safety margin results in a 10° angle. These criterion and the dimensions of the aircraft results in a length of 1.39m (measured from the bottom of the centre body to the ground) and longitudinal position of the main landing gear (12.94m measured from the nose of the aircraft).

The next step is to determine the position of the nose gear. For this, the requirement is used that the nose gear should at least support 8% of the maximum take-off weight, in order to have sufficient steering capabilities. Using this criteria, the position of the main landing gear and the position of the centre of gravity position of the empty aircraft results in the position of the nose landing gear. The centre of gravity position of the empty aircraft is used because when loading the aircraft, the centre of gravity will move forward (except when all cargo would be put in the back of the aircraft) as can be seen in section 5.4, which will increase the load on the nose gear.

Following this, the lateral position of the main landing gear is determined. This is done based on the aircraft geometry and the longitudinal position of the main landing gear. Since the centre body does not provide any space for the landing gear, it has to be placed in the mid-wing. The lateral position of the main landing gear is manually chosen looking at the top view of the aircraft (see Figure 4.25). This results in a lateral distance of 3m measured from the centre. The implication of this is that the main landing gear is folding in flight direction.

Next, the criteria showed in Figure 4.13 and Figure 4.14 are tested. It turns out that these criteria are met without making adjustments to the earlier defined length and positions of the landing gears.

Preferably, the nose landing gear supports maximum 15% of the maximum take-off weight in order to provide sufficient braking capabilities to the main landing gear. Calculations show that this configuration exceeds the 15% limit. Therefore the nose landing gear of this aircraft needs to have braking capabilities as well.

The final step is to determine the type of wheels and the shock absorber size. Determining the type of wheels is done manually by using the tables provided in [34]. It is assumed that the nose landing gear consists of a single strut which has two wheels, and the main landing gear consists of two struts with two wheels each. If no proper tires can be found for this, the assumption will be reconsidered and changed. Using the loads per wheel calculated and the maximum operating speed during take-off or landing, a tire is selected from the tables in [34], taking also the weight of the wheel into account. This maximum load per wheel is evaluated at all centre of gravity positions with their corresponding weights. Tires from Goodrich are selected for both the nose and the main landing gear. The wheels of the main landing gear have the dimensions 91x28 cm (diameter x width) and can support a load of 140 kN each. The wheels of the nose landing gear have the dimensions 86x28 cm (diameter x width) and can support a load of 72 kN each. These tires have a higher maximum load than required, with a safety factor included. Using the equation for sizing the shock absorber length and thickness [34] shows that for the main gear a shock absorber length of 9.2 cm is required, and for the nose gear a shock absorber length of 3 cm. This small value can be explained by the fact that the chosen tires already absorb a significant part of the loads.

The result of the landing gear sizing and positioning can be seen in Figure 4.15. Here, the centre of gravity range of ATLAS is indicated as well. This centre of gravity range comes from section 5.4.

4.5.7 Propulsion system

To fulfil requirement UCCF-Tech-Syst-Prop-01, which states that the aircraft shall be able to provide 95429 N thrust, a propulsion system has to be chosen. This value is a system constraint given by the flight performance department. It is dictated by the maximum thrust needed to climb to cruise altitude. Not only does the propulsion system provide thrust during the flight

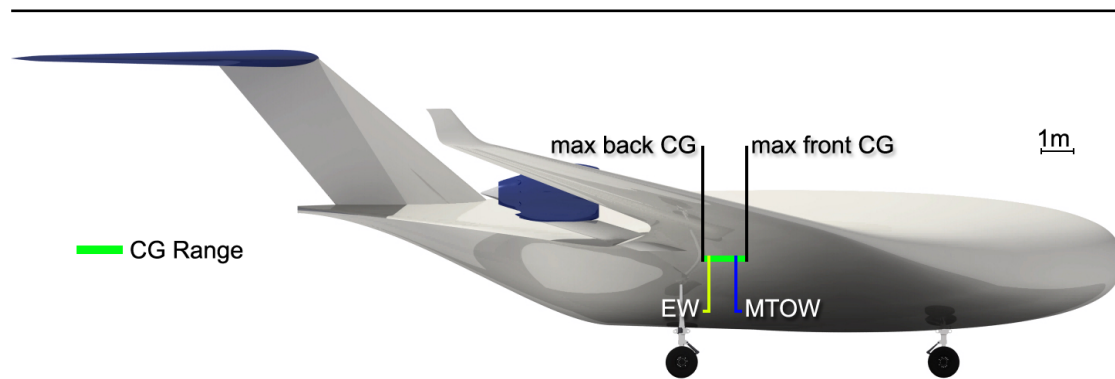


Figure 4.15: Side view of ATLAS including centre of gravity range.

profiles, it also has a considerable influence on the design. The efficiency, weight and cost have a large effect on operational cost, aircraft weight and aircraft unit production cost, respectively. Therefore, special attention must be given to the design process of the propulsion system, which is presented in Figure 4.16. In the midterm report a high bypass turbofan was selected by means of systems engineering. To power the ATLAS two of these are needed. The leading requirement of the number of engines was one engine inoperative (OEI) requirement. Two engines are needed to complete international flights in case of an engine failure as stipulated by ICAO¹⁰. In this section the final concept design phase is presented as shown in Figure 4.16. It starts off with the selected engine and its performance characters. In the following subsections the design of the engine inlet and the engine integration are presented. At the end of this section the implications of being unmanned w.r.t. the propulsion system and the sustainability aspects of the design are provided.

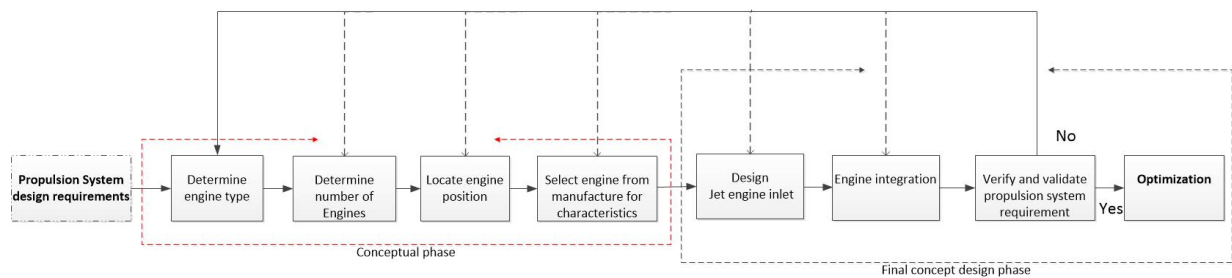


Figure 4.16: Design process of the propulsion system.

Engine selection

The engine selected for ATLAS is the Leap 1A of CFM International. This engine as shown in Figure 4.17 is a high bypass turbofan.¹¹ It is a state of the art engine based on two engine families; CFM56 and GE90/GENx. It has a high efficient core architecture, consisting of a eight-stage compressor and single-stage turbine, thanks to the design contribution of the GE90/GENx pro. This efficient core helps in reducing the fuel consumption of the engine. The design contributions of the CFM56 makes the Leap engine reliable and able to maintain. The leap engine is said to reduce fuel burn by 15% compared to the CFM56-7E.¹² Furthermore, thanks to its incorporated three-dimensional, woven resin transfer molding (3-DW RTM) technology, the engine weight is expected to be reduced by 181 kg.¹³

¹⁰<http://www.icao.int/sustainability/Pages/economic-policy.aspx> [accessed on 1-05-2015]

¹¹<http://www.cfmaeroengines.com/engines/leap> [accessed on 11 May 2015]

¹²<http://www.cfmaeroengines.com/engines/leap> [accessed on 11/05/15]

¹³http://www.deagel.com/Turbofan-Engines/LEAP-1A_a002224001.aspx [accessed on 05/05/15]



Figure 4.17: CFM International's Leap 1A engine.

Engine scaling

During the design of a new aircraft it is frequently not possible to use an already existing engine. This is because the engine manufacturers promise improved performance for future engines when the designed aircraft will be flying. Other times an engine might have good properties but does not meet the required thrust. In such cases, engines can be scaled to the required thrust in the process called rubberising. For the design, the thrust provided by Leap 1A, as stated by CFM International, is higher than the thrust required. However, since Leap 1A meets the rest of the propulsive requirements, its power is scaled down to the thrust level needed for the ATLAS without changing the major thermodynamics properties such as specific fuel consumption (SFC) and overall pressure ratio (OPR). This is only possible when the power differences are well within a 10-20% margin range [32]. For the size and the weight there are noticeable changes when performing rubberising. The scaling laws proposed by [35] presented in Equation 4.21 to Equation 4.24 are used size the engine for its design purposes. This yields new weight and size characteristics which are implemented in the design.

$$S.F. = \frac{T_{req}}{T_{data}} \quad (4.21)$$

$$L_{req} = L_{data}(S.F.)^{0.4} \quad (4.22)$$

$$D_{req} = D_{data}(S.F.)^{0.5} \quad (4.23)$$

$$W_{e_{req}} = W_{e_{data}}(S.F.)^{1.1} \quad (4.24)$$

Engine properties

Since the Leap 1A is still in production there is not a lot of information published about it, especially concerning thermodynamic properties. Some of the properties are estimated using several equations, such as the mass flow rate in Equation 4.25 and news presented by CFM international. Some performance comparisons with the predecessor, CFM56-7E, are made by CFM International.

$$\dot{m} \frac{A_{fan} P_t}{\sqrt{T_t}} = M \sqrt{\frac{\gamma}{R}} \left(1 + \frac{\gamma - 1}{R} M^2\right)^{\frac{\gamma+1}{2(1-\gamma)}} \quad (4.25)$$

Engine inlet design

Generally the inlet design is best performed together with the engine manufacture. However, some basic preliminary sizing can be done to obtain basic diffuser dimensions of the engine. The steps take to size the inlet will be presented in this section.

The purpose of the inlet is to slow down the incoming air to a specified Mach number and to bring the air smoothly to the compressor fan. There are two main reasons why turbofan inlets are generally designed as a diffuser. Firstly, by slowing down the air, the airspeed at the tip of the fan blades decreases and shock-wave formation is prevented on the blades. As a result, propulsive efficiency is increased. Secondly, with a good inlet design, pressure recovery over an extended range of angle of attacks can be realised. It is important that the pressure losses are minimal because of the effect on the pressure due to compressor. This leads to an increase in thrust, thermal efficiency and hence the overall efficiency of the engine.

To accomplish a smooth flow transport, flow separation on the inside walls of the inlet must be avoided. Separation occurs when there are unfavourable pressure gradients in the inlet. The first negative effect is that the flow no longer slows down isentropically and henceforth decreasing the pressure inside the inlet. Furthermore the effective cross-sectional area of the inlet decreases whereby the desired airspeed at the fan face increases.

Inlet sizing

For this inlet design the stations depicted in Figure 4.18 are of interest. Here the geometric parameters and the flow conditions at each station have to be known. Point 0 represents the area of the free stream at far-field. At rest this area is infinite in size and the local Mach number of the flow zero. Also for this station the flow conditions such as temperature and pressure are known. During cruise these parameters change as can be seen in Figure 4.18. The far-field area decreases and deforms into a stream tube. The area of this stream tube is smaller than the area at the inlet lip. Only air within this stream tube is ingested by the engine. It might seem like the engine is not ingesting enough air. However this is not the case. In contrast to air suction at static operation more air than required by the engine will be available due to the cruise speed. Using the process described in [5], in order to start sizing the geometry at these different stations, the limiting factors must be identified. These limiting factors are the maximum mass flow rate required and the Mach number in front of the fan face. These values are usually obtained from the engine manufacturer. For this design however they are estimated. With Equation 4.25 the maximum required mass flow rate is found. The maximum air flow rate is dictated by the engine performance at static T-O thrust. The airspeed in front of the fan face of the CFM56-3 is 0.4 Mach[36]. This value will also be used for the Leap 1A.

Flow at different engine stations

Despite the conditions of static thrust at sea level and zero airspeed velocity at far-field, the air can still accelerate to high velocity at the inlet lip when operating statically. However, for high subsonic speeds, engine manufacturers size the inlet area such that the air velocity at the inlet lip will not exceed a certain Mach number, usually 0.8. For this design the Mach number during cruise speed is chosen. The isentropic flow relations, in [5] on page 226, are used to obtain the flow conditions at station 1.

As already mentioned, the flow velocity in front of the fan face is 0.4, so the conditions at station two can also be estimated. This is done by substituting 0.4 Mach in the isentropic relations.

With this information the pressure recovery ratio (PRR) can be calculated for this inlet. However, this is done disregarding contributions of the inlet geometry. In Table 4.7 the pressure recovery ratio of 0.9 can be seen. For perfect inlets the PRR is 1, yielding the maximum thrust for a given flight condition. For podded jet engines holds that the shorter the inlets, the closer the PRR will be to the value of 1. Integrated inlets usually have a PRR well below one.

$$\pi_2 = \frac{P_{T2}}{P_0} \quad (4.26)$$

Inlet geometric parameters

As mentioned the length of the inlet is imperative to the design of the engine nacelle. Together with the induced angle θ , the geometric dimension can be determined such that there is no flow

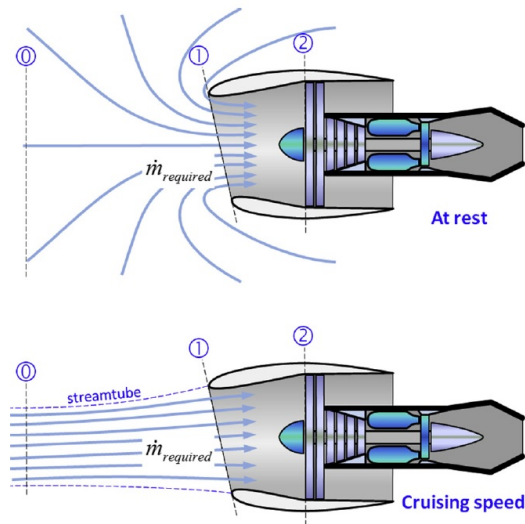


Figure 4.18: Shape of flow field at different stations.

Table 4.7: Flow properties.

Flow Condition	Station 0.	Station 1.	Station 2.
Area [m^2]	∞	1.9	2.7
Mach number [/]	0	0.72	0.4
Total pressure [Pa]	101325	71741	90748
Temperature [K]	288	261	279
Density [$\frac{kg}{m^3}$]	1.225	0.9574	1.13
Pressure Recovery Ratio [/]	-	-	0.9

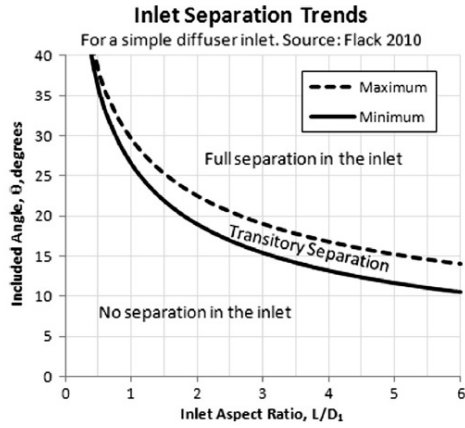


Figure 4.19: Inlet separation trends [5]

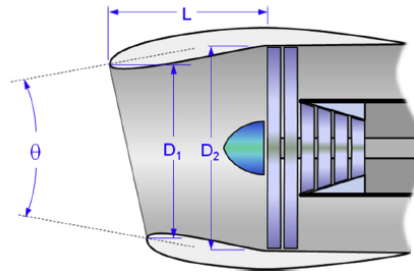


Figure 4.20: Engine layout [5]

Table 4.8: Inlet dimensions.

Parameter	Value
Highlight diameter (D_l) [m]	1.6
Throat Diameter (D_{th}) [m]	1.5
Lip Contraction Ratio [m]	1.1
Forebody Length (L) [m]	1.2
Inlet Aspect Ratio ($\frac{L}{D_1}$) [/]	0.8
Induced inlet angle (θ) [deg]	30

separation on the walls of the inlet using empirical data. For a certain inlet aspect ratio, which is defined as the diffuser length [L] over the highlight diameter [D_1] the induced angle is too large and the flow in the diffuser will expand too fast. As a result, flow separation on the walls of inlet will start to form. So for the design it is important to find an angle which is large enough for air flow at different angles of attacks, but also small enough to counteract flow separation. Using the maximum mass flow rate, the highlight area can be calculated with Equation 4.27 and with Equation 4.28 the diameter is found. Furthermore the throat is sized using the lip contraction ratio (LCR) which is given in equation Equation 4.29 [37]. For turbofans, LCRs range from 1 to 1.2, with 1 representing sharp lip edges and 1.2 a well-rounded lip. With an inlet aspect ratio of 0.8 of a forebody length of 65% of the fan diameter, an induced angle of 30 degrees is found, which is well below the separation curve as depicted in Figure 4.19. In Table 4.8 the dimension of the inlet can be seen.

$$A_{Highlight} = \frac{\dot{m}_{required}}{M_1} \sqrt{\left(\frac{1}{P_0 \gamma}\right) \left(\frac{\rho_0}{\rho_1}\right)} \quad (4.27)$$

$$D_1 = 2 \sqrt{\frac{A_{Highlight}}{2}} \quad (4.28)$$

$$LCR = \frac{D_1^2}{D_{th}^2} \quad (4.29)$$

Engine integration

In this section the engine location and integration are defined. According to [6], based on CFD analysis, the best location of the propulsion system for a hybrid wing body is an over-the-centre-body (OCB) podded engine placement. There are several benefits in placing the engines on top of the centre body. The first is that the centre body acts like a shield to acoustic vibrations. Secondly a high placement engine has a higher ground clearance and is not likely to suffer

from foreign object damage during take-off and landing. The third benefit is the specific fuel consumption of the engine. According to [19] an OCB podded engine placement exhibits lower specific fuel consumption compared to an rear centre body buried and under-the-wing engine configuration. Also, [6] proposes engine placement at the trailing edge of the centre body of the aircraft. The interference drag experienced by the engine is the lowest at this location. It must be noted that the interference drag due to the pylons are not taken into account in the analysis. The location of the trailing edge is chosen such that the engine is placed in a low pressure region in order to create leading edge thrust. The description of the location of the engines is given in the subsections below. These are based on the reference frame shown in subsection 4.2.4.

Location of the centre of gravity of the engines

x-direction

The x-location of the centre of gravity of the engine is constraint by inherent longitudinal stability requirements. However, the engine is still placed on the trailing edge on the intersection of the mid wing and the outer wing.

y-direction

In order not to disturb the flow over the inboard wing section with the engine's jet flow, the root of the outboard wing section is a reasonable location for the centre of gravity in the y-direction. It is also advisable not to place the engine too far from the fuselage. In doing so, the bigger rudder control surface will be needed to control the aircraft in case of one engine inoperative. Based on the studies presented in [6] and the assumptions made, the best location in the x and y directions is the intersection of the mid wing and the outer wing.

z-direction

For an over-the-wing podded engine, the engine should be placed above the boundary layer over the wing [19]. This has to be analysed for using CFD for the worst case scenario during flight. In order to continue with the preliminary design, it is assumed that the wing is a flat plat and the boundary layer thickness is estimated to be 13 cm. In Figure 4.25 the location of the engine can be viewed.

Future engines

One benefit the propulsion system integration has is that it is podded, making it easier to relocate or even replace the engines. For this reason it is advisable to consider future advanced engine promised by manufacturers, regardless of the availability of the Leap 1A. If a more sustainable engine is available in the future, which meets the design requirements, then the logical choice would be to use it on the ATLAS. The PW1124G is the first a suitable replacement engine, which is also available in the present. It is an advanced high bypass geared turbofan, meaning that the gearbox reduces the rotational speed of the fan in order to operate at more beneficial RPM. However when the SFC (-12% in fuel burn) was estimated by evaluating its predecessor, the V2500-A5¹⁴, it showed a higher value than the leap 1A. However, it is said that the PW1124G will target a lower maintenance cost of up to 20 %. So an operational cost evaluation on these two engines would be interesting to the costumer.

Rolls Royce states that the new ultrafan engine, in Figure 4.21, is able to maximise transonic propulsive efficiency while benefiting from the acoustic attenuation improvements the nacelle offers. In this design the nacelle based cascade thrust reverser is removed and hence relocated. As a result, the bypass ratio constraints posed by the thrust reverser are uplifted. The engine can have a BPR exceeding 30, hence improving propulsive efficiency.

¹⁴<http://www.tes-uk.com/en/content/cms/media-centre/articles/leap-pw1000g-engine/> [accessed on 20/06/15]

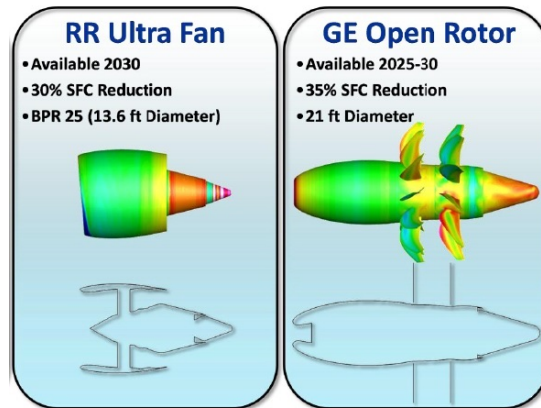


Figure 4.21: Rolls Royce's Ultrafan and GE open rotor [6].

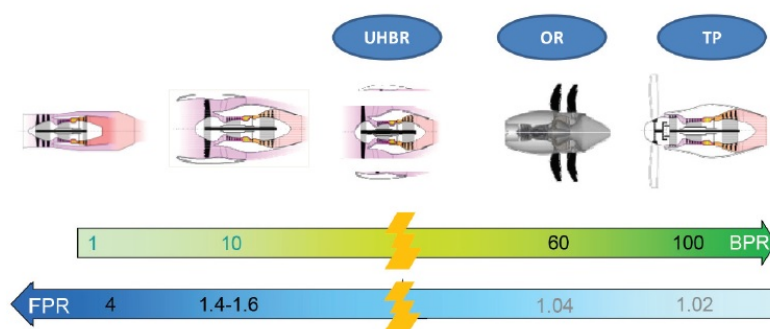


Figure 4.22: BPR and FPR from simple flux turbojets to turboprops [7].

The SFC is primarily controlled by thermal efficiency, high OPR, loss minimisation, low fan pressure ratio (FPR) and unducted fans and propellers. The last aspect makes unducted fans appealing, since it can have a BPR of 60 as can be seen in Figure 4.22. In the trade-off between the engine types, the unducted fan scored the second best. Since the engine has counter rotating propellers (in Figure 4.21), and a gearbox to decrease the tip velocities, it makes it much harder to maintain. However, it is still a suitable option to look at if there is a promising 35% SFC reduction to be gained as predicted by General Electric engines, if acoustic limitations can be dealt with. The counter rotating propeller diameter might also be a problem, but an engine relocation or an engine scaling can be performed to solve this problem.

Impact on safety

The most critical mode of power plant failure during flight, which has a big impact on safety, is the critical engine failure. If an engine fails, the lateral stability of the aircraft is lost due to asymmetric thrust. Not only the safety of the aircraft but also the safety of people on ground in populated areas become jeopardised. To mitigate this technical risk, the rudder control surface of the aircraft is designed for the asymmetric thrust requirement subsection 4.5.5.

Implications of being unmanned

During flight profiles, the throttle percentage of the engine changes so that the engine can provide the required thrust. In manned aircraft this function is already automated and thus executed by the auto-throttle. The flight management system does this by receiving desired input parameters and compares this to actual flight data. The input parameters are provided by the pilot or by extrapolating these automatically. For this design the process should be fully automated.

Sustainability

By developing a efficient inlet the propulsive efficiency will increase, hence increasing the overall efficiency of the engine. Additionally, when the minimisation in pressure losses are optimised, the SFC will further decrease. Since the inlet is far from the hot engine core, compared to other components, advance carbon reinforced epoxy materials can be used to produce to part. These considerations make the design more sustainable.

4.5.8 Environmental control

In order to protect the cargo being transported it is important that the environment in the cargo bay is carefully managed. This is split up into two main parts; thermal control and pressure control.

Both functions are full filled using a full electric environmental control system similar, but smaller, as the one on the Boeing 787. This system uses electrical pressurisation compressors for pressure control. The airflow from these compressors then first flows through air-conditioning packs where the temperature is managed and the air is dried [38]. The reason the air is dried is to prevent condensation, which could cause corrosion or electrical faults. The air is then led to both critical aircraft components, which need to be cooled, and the cargo bay. In the event this control system fails at least two positive pressure relief valves and one negative pressure relief valve are provided to protect the cargo bay from over or under pressurisation.

4.5.9 Fire protection system

To minimise the risk of damage or catastrophic failure due to fire five basic fire protection principles are used. Prevention, separation, detection, isolation and control.

Prevention: The first goal should be to prevent a fire from happening. This is accomplished by using noncombustible or self-extinguishing materials where possible. In addition all used sub-system will need to be certified for airworthiness, a process in which fire prevention is a major

part.

Separation: For a fire three elements are necessary; fuel, ignition source and oxygen. Separating these elements can prevent or control a fire. This is implemented by safely separating the most dangerous fuel, the jet fuel, from possible ignition sources as electronic subsystems and the cargo bay.

Detection: In the aircraft multiple smoke and fire sensors are placed that will detect fire. They are placed in the ceiling and walls of the cargo bay, as well as throughout the wings and centre body, near possibly dangerous (electrical) components.

Isolation: If a fire is detected the first move is to isolate it. When the fire occurs in the cargo bay this is done by immediately cutting of the air supply provided by the environment control system. Thereby effectively stopping the flow of oxygen to the cargo bay. If the fire occurs outside of the cargo bay this is done by closing all vents between the cargo bay and inside structure, preventing the fire from reaching the possibly flammable cargo.

Control: To control the fire 3M Novec 1230 Fire Protection Fluid is used to suppress an fire. This fluid is stored centrally as an fluid in the aircraft. When an fire occurs a network of pumps and pipes is used to get this to the extinguishers closest to the fire. Here it evaporates and suppresses the fire.

Sustainability

By using 3M Novec instead of the previously common Halon gas the environmental impact in case of an fire is severely limited. This fire protection gas reduces the greenhouse gases in fire suppressing with respect to Halon with 99%.¹⁵

4.5.10 Wing ice protection

In order to prevent ice from accumulating on the wing or control surfaces, a wing ice protections system is installed. Traditionally, systems like these often use hot bleed air from the engines, which is led through piccolo tubes through the wing and finally exhausted through holes in the surface.

For the ATLAS however, an electro-thermal ice protection system is being used. This system uses heating blankets, distributed over the wing and control surfaces, for ice protection. These blankets can be energised as soon as ice protection is required, requiring only electrical energy as provided by the aircraft's electrical system. This method is shown to be up to 50% more energy efficient as an traditional (pneumatic) system [38] since no excess energy is exhausted. Additionally, due to the fact that no exhaust holes in the surfaces are required, it decreases aircraft drag and noise production.

4.5.11 Electrical power system

The required power to drive all subsystems will be calculated in the power budget allocation in section 4.7. Based on the outcome of the power budget allocation, an APU can be selected. If some margin is added, a 40kW APU will be sufficient for supplying electrical power to all subsystems. As APU the Motor Sich AI-450-MS is selected.¹⁶ This APU is used as well on the Antonov An-148, and uses 118kg of fuel per hour. The characteristics of this APU:

- Providing electrical power to start the engine generators
- Electrical power supply with a power up to 40kW
- Generation of compressed air for aircraft conditioning system
- Generation of compressed air for aircraft anti-icing system

¹⁵http://www.3m.com/3M/en_US/novec/products/1230-fire-protection-fluid/sustainability/ [accessed on 19/06/15]

¹⁶<http://www.motorsich.com/eng/products/aircraft/auxiliary/ai-450-ms/> [accessed on 18/06/15]

4.6 Class II weight estimation

After the first class weight estimation, the design of the subsystems could start, as explained in the previous sections. For the second class weight estimation a more detailed design of these major subsystems is required. As a minimum the wing, engines, fuselage and tail, as well as the outcome of the first class weight estimation must be known. The second class weight estimation is performed using the Torenbeek method as described in [39]. To include some of the key characteristics of this aircraft some adaptations had to be made to this estimation. These are described in this section. The result of the second class weight estimation will be a new estimation of the empty weight. This estimation can then be used to update the previously empirical relationship between empty weight and maximum take-off weight.

General equation

The empty weight (W_E) of an aircraft consists of the structure weight (W_{struct}), powerplant weight (W_{pwr}), and fixed equipment weight (W_{feq}). This can be seen in Equation 4.30.

$$W_E = W_{struct} + W_{pwr} + W_{feq} \quad (4.30)$$

Variables calculation

In this section, all variables of Equation 4.30 will be either defined or calculated for this design, such that a new value for the empty weight will come out.

Structure weight

The structure weight can be divided into the wing weight W_w , empennage weight W_{emp} , fuselage weight W_f , nacelles weight W_n and landing gear weight W_g , as can be seen in Equation 4.31.

$$W_{struct} = W_w + W_{emp} + W_f + W_n + W_g \quad (4.31)$$

The weight of the wing (W_w) consist of the combined outerwing and midwing weights. It is calculated using a class II & 1/2 weight estimation as proposed and developed by Dr. A. Elham in [40]. This TU Delft semi-analytical weight estimation tool called EMWET (Elham Modified Weight Estimation Technique) uses a combination of both analytical structural sizing for the equivalent wing box panels and empirical methods as proposed by [32] for secondary and non-optimum structure weight contributions. Its accuracy for aircraft of different size and configuration is shown to be significantly better than the purely empirical class II wing weight estimation methods usually being used during a class II weight estimation. Additionally it offers excellent sensitivity to major design parameters including airfoil shape, planform shape, aerodynamic loads, engine load relief and material properties. [40] All of these parameters are fully implemented in the designed program and used during all iterations. The aerodynamic loads required for this were provided by Q3D, as described in Figure 5.2.6.

W_{emp} consist of the weight of the vertical and horizontal tail, which are calculated using the equations given in [39]. These equations however did for example not allow for incorporating weight saving due to the choice of advanced materials and weight optimisation methods as discussed in section 5.3. Therefore W_{emp} was scaled down with 50%, a slightly more conservative ratio than the weight savings reached in the wing weight.

W_f is calculated by adjusting the equation given in [39] for this design. The equation in [39] is based on reference aircraft, which have a pressurised fuselage. In this case, since it is a blended wing body, the fuselage (which will be referred to as the centre body) is shaped differently, and the cargo bay is pressurised instead. Therefore, W_f is defined as the sum of the actual cargo bay weight calculated in section 5.3 and the fuselage weight equation in [39] downscaled by a factor 0.87. The factor 0.87 comes from the fact that the centre body does not have a cockpit or windows and part of the calculated fuselage weight is already included in the cargo bay weight. W_n and W_g come directly from [39], since it is assumed that these are not different for this design compared to reference aircraft.

Powerplant weight

The powerplant weight can be divided into the weight of the engines W_e , the air induction system weight W_{ai} , the propellers weight W_{prop} , fuel system weight W_{fs} and propulsion system weight W_p , as can be seen in Equation 4.32.

$$W_{pwr} = W_e + W_{ai} + W_{prop} + W_{fs} + W_p \quad (4.32)$$

W_e comes directly from the actual weight of the engines selected. W_{ai} is set equal to 0, since for podded engines (which this design has) this weight is already included in the nacelle weight W_n (in the structure weight). Also W_{prop} is set equal to 0, since this is only applicable to propeller engined aircraft. Both the relation of W_{fs} and W_p are taken directly from [39], since it is assumed that these are not different for this design compared to reference aircraft.

Fixed equipment weight

The fixed equipment weight can be divided into 17 different variables, of which many are equal to 0 since this design is an unmanned cargo freighter. All non-zero components can be seen in Equation 4.33. This consists of the flight control system weight W_{fc} , the electrical system weight W_{els} , the instrumentation, avionics and electronics weight W_{iae} , the air-conditioning, pressurisation, anti- and de-icing system weight W_{api} , the auxiliary power unit weight W_{apu} , the baggage and cargo handling equipment weight W_{bc} and the paint weight W_{pt} .

$$W_{feq} = W_{fc} + W_{els} + W_{iae} + W_{api} + W_{apu} + W_{bc} + W_{pt} \quad (4.33)$$

All of these non-zero components are assumed to be the same for this design as for reference aircraft, so all necessary equations were directly taken from [39].

Results weight estimations

As mentioned before, the first class and second class weight estimations have been performed several times, since it is part of the iterative process. This section will show how the operational empty weight W_{OEW} and maximum take-off weight W_{TO} changed over the iterations, as well as the final result of both the first and second class weight estimation.

In Figure 4.23 the final result of the first class weight estimation can be seen, with in Table 4.9 the corresponding values. Note that on the y-axis the weight is given in Newtons. What immediately can be noticed is the relatively low operational empty weight and fuel weight, compared to the payload weight. This is due to a multitude of factors:

- **Unmanned aircraft:** Since the design is completely unmanned, no cockpit, on-board crew, emergency exits or windows are required. This decreases the operational empty weight.
- **Advanced materials:** The use of advanced materials leads to a significant weight saving in the structural weight.
- **Fuel efficient engines:** The use of fuel efficient engines leads to a decrease in fuel consumption and a reduction in total fuel weight.
- **Aerodynamic efficiency:** Due to the use of a blended wing body the drag is relatively low, leading to less thrust required and therefore a lower fuel weight.

Additionally the influence of all these weight savings is strengthened due to the amplifying relationship between fuel weight and operational empty weight. If the operational empty weight decreases the fuel weight also decreases and vice versa.

The second class weight estimation shows the division of the empty weight of the aircraft over the subsystems. In Figure 4.24 the final result of the second class weight estimation can be seen, with in Table 4.10 the corresponding values. Note that in Figure 4.24 the subsystems mentioned in the legend are plotted counter clockwise in the same order in the pie chart, starting from the top. What can be noticed is that the three largest components of the empty weight are the

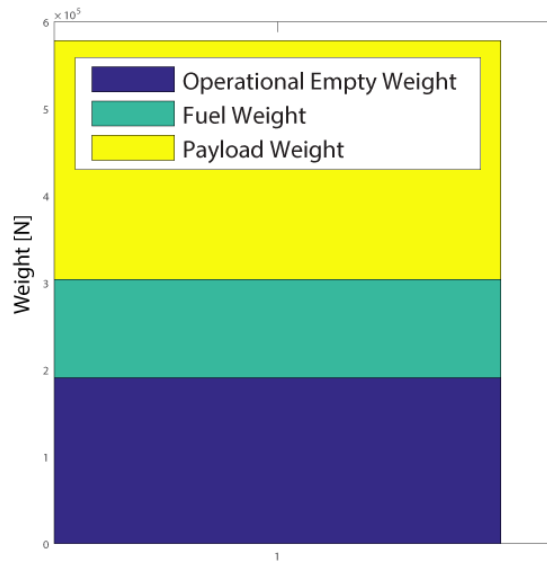


Figure 4.23: Final result of the first class weight estimation.

Table 4.9: Final result of the first class weight estimation

	W_{OEW}	W_F	W_{PL}	W_{TO}
Weight [N]	191,110	113,460	274,680	579,250

wing, the centre body and the engines. The percentage of the wing weight is less than reference aircraft [32]. This can be explained by the fact that the fuselage of this design generates part of the lift, so the wings can be downsized. Apart from this, the other subsystems seem to have a similar value as reference aircraft [32].

Table 4.10: Final result of the second class weight estimation.

	W_w	W_{emp}	W_f	W_n	W_g	W_e	W_{fs}	W_p
Weight [N]	40,930	9,240	38,870	6,380	13,980	37,410	6,670	600
	W_{fc}	W_{els}	W_{iae}	W_{api}	W_{apu}	W_{bc}	W_{pt}	
Weight [N]	7,310	10,250	1,440	3,940	2,320	7,730	1,740	

Centre of gravity estimation

The centre of gravity of the empty aircraft is estimated using weights of the components as calculated in the second class weight estimation and the positions of these components. The exact positions of the components are calculated and if not possible they are estimated using some hints of Roskam [39] and common sense. Since this aircraft is unmanned, there are some possibilities to move certain systems, what would sometimes not be possible for conventional aircraft. After the weight and position of each component is known, the centre of gravity of the empty aircraft can be calculated, and this turns out to be at 12.3m measured from the nose.

Moment of inertia estimation

The moment of inertia are calculating using the equations given in Roskam [39], and these moment of inertia will be used for the calculating the stability derivatives. The outcome will be six moment of inertia (I_{xx} , I_{yy} , I_{zz} , I_{xy} , I_{yz} and I_{zx}), of which I_{xy} and I_{yz} are equal to 0 due to symmetry. This means that no programming errors are made for this part.

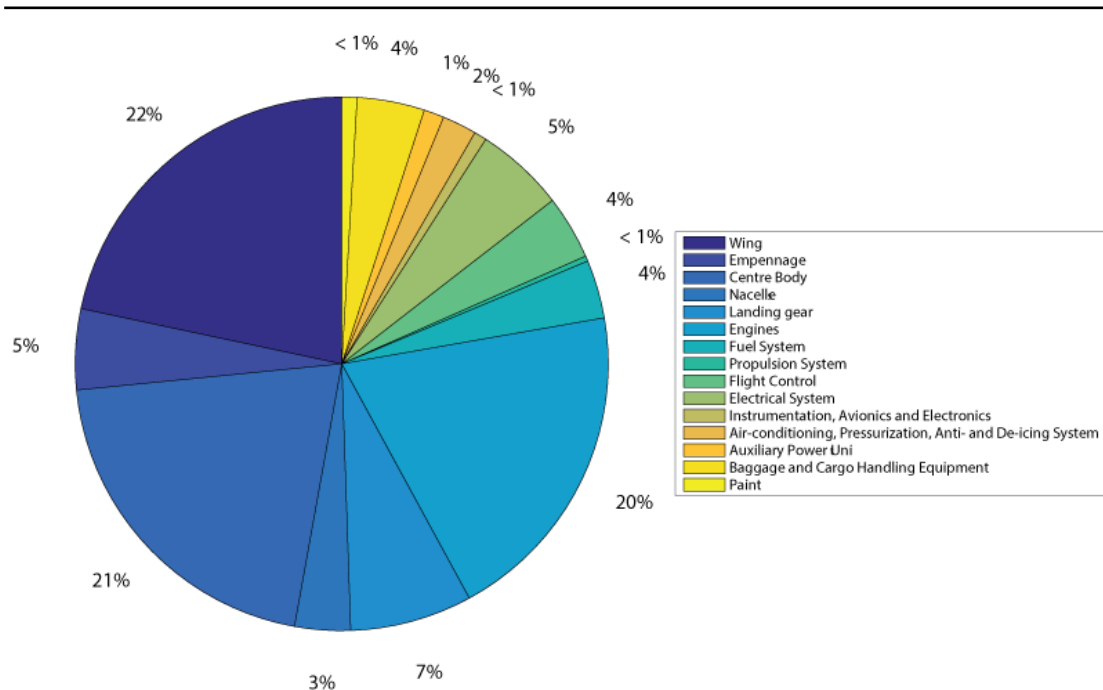


Figure 4.24: Final result of the second class weight estimation.

Verification

The first class weight estimation is verified using examples from the lecture slides of "Aerospace Design Systems Engineering Elements I" [20]. The difference is 0%, which is expected since all input variables are clearly stated and the equations are straightforward.

The second class weight estimation is verified using examples given in Roskam [39]. The values obtained from the program and from Roskam do not match exactly. This is due to some assumptions that had to be made, since not all parameters are given in the examples of Roskam. However, these values are close enough to say that the second class weight estimation is assumed to be verified.

The centre of gravity estimation is verified using some dummy inputs from which the total centre of gravity is known. These values match exactly, which implies that the tool works as intended. Also it is checked that the span wise position of the centre of gravity is 0 (since the aircraft is symmetric). On top of that, a plot is made of the centre of gravity positions of all individual components, including the position of the total centre of gravity as well, to see if it makes sense. All of the above implies that the centre of gravity estimation can be assumed to be verified.

The moment of inertia estimation is verified by checking if I_{xy} and I_{yz} are equal to 0 (because of symmetry). The moment of inertia estimation uses only simple equations, using the outputs of the second class weight estimation and the centre of gravity estimation. Since the second class weight estimation and the centre of gravity estimation have already been verified, the moment of inertia estimation is assumed to be verified as well.

Implication of being unmanned

The aircraft being unmanned has a significant impact on the second class weight estimation. The operational empty weight was greatly decreased due to the lack of crew, cockpit and required fuselage cutouts. Additionally the lack of the cockpit provides more freedom when placing subsystems.

Table 4.11: Weight budget allocation.

Subsystem	Weight [N]	Weight min [N]	Weight max [N]
Wing	40,930	32,744	49,116
Empennage	9,240	7,392	11,088
Centre body	38,870	31,096	46,644
Nacelle	6,380	5,104	7,656
Landing gear	13,980	11,184	16,776
Engines	37,410	29,928	44,892
Fuel system	6,670	5,336	8,004
Propulsion system	600	480	720
Flight control	7,310	5,848	8,772
Electrical system	10,250	8,200	12,300
Instrumentation, avionics, electronics	1,440	1,152	1,728
Air-conditioning, pressurisation, anti- and de-icing	3,940	3,152	4,728
Auxiliary power unit	2,320	1,856	2,784
Cargo handling equipment	7,730	6,184	9,276
Paint	1,740	1,392	2,088
Total	188,810	151,048	226,572

Sustainability

By providing the most accurate weight estimation, the risk of over-designing the aircraft decreases. This will ultimately help with getting the most fuel efficient aircraft, since no unnecessary weights have to be carried. Additionally since there was some freedom in the placement of the different subsystems they could be placed such that the centre of gravity was more favourable and the tail could be smaller. Thereby decreasing weight and material needed, and increasing fuel efficiency.

4.7 Budget allocation

This section will state and explain both the weight budget allocation and the power budget allocation. Because of the early stage the design is in currently, a 20% contingency factor is included in the budget allocation.

4.7.1 Weight budget allocation

For the weight budget allocation, the results of the second class weight estimation in section 4.6 will be used. In section 4.6, an estimation of the weight division of the different subgroups was already made. However, in those values the contingency was not yet incorporated. Using the 20% contingency factor as mentioned earlier to account for future growth or shrinkage, will give a minimum and a maximum expected value of the final weight of that particular subsystem. Using the values of Table 4.10 will result in the weight budget allocation as can be found in Table 4.11.

4.7.2 Power budget allocation

In this section the required power will be estimated based on [34] and the contingency factor of 20%. In [34] the power budget allocation of the McDD DC-10 is given as an example. The maximum take-off weight of the DC-10 is higher than the maximum take-off weight of this design. To be conservative, and take into account the fact that an unmanned aircraft probably needs more and better computers compared to a manned aircraft, the values will be based on the DC-10 in order to get a first estimation. Systems that are needed for the DC-10, but not for

Table 4.12: Power budget allocation.

Component	Power [W]	Power min [W]	Power max [W]
Exterior lighting	100	80	120
Cargo bay lighting	1,000	800	1,200
Avionics	7,250	5,800	8,700
Environmental control	1,600	1,280	1,920
Fuel	6,500	5,200	7,800
Flight control	14,000	11,200	16,800
Electrical power	6,000	4,800	7,200
Miscellaneous	250	200	300
Total	36,700	29,360	44,040

this design (for example toilets), will be neglected. The exterior lighting and cargo bay lighting power are decreased greatly compared to a DC-10. This is done because currently more energy efficient lighting is available (for example LED lights). On the other hand, the flight control is upscaled, since extra computing capabilities are required for an unmanned aircraft. Currently most aircraft have hydraulic actuators, since they are more reliable and have a higher power density.¹⁷ It is expected that by 2035 the reliability and power density of electrical systems are increased. So for this design the actuators like flaps, ailerons and rudder are electrical driven. This is also incorporated in the power of the flight control system. The power budget allocation of the ATLAS can be seen in Table 4.12. It should be noted that this power required is evaluated during cruise. The third and fourth column of Table 4.12 represent the minimum and maximum value when taking the contingency factor into account.

4.8 Aircraft system characteristics

This section provides a brief summary of the key system characteristics. Combined with the configuration layout this gives a brief but comprehensive overview of the designed aircraft. In addition some key supportive subsystems are discussed.

4.8.1 Key characteristics

The key characteristics of ATLAS describe the major design variables and can be used to compare the proposed design to other reference aircraft. These key characteristics can be found in Table 4.13.

4.8.2 Configuration layout

In order to provide a clear overview of the different system and there placement Figure 4.25 is constructed. It shows both the fuel and electrical layout, combined with important subsystems. It must be noted that for clarity only the major electrical connections are shown. The full electrical diagram can be found in subsection 6.5.2. It should also be noted that for clarity reasons some systems have only be drawn for one side of the aircraft, although they are present in both sides.

Additionally a side view with indicated centre of gravity range is created to show all possible positions of the centre of gravity with respect to the landing gear. This can be seen in Figure 4.15. Additionally, a front of ATLAS can be seen in Figure 4.26.

¹⁷<http://www.mobilehydraulictips.com/end-hydraulics-aerospace-fast/> [accessed on 18/16/15]

Table 4.13: ATLAS key characteristics.

Parameter	Value
b	49.9 [m]
S	221 [m ²]
A	11.3 [-]
L/D	19.5 [-]
Cruise height	12,500 [m]
Operational cost ¹⁸	$0.134 \cdot 10^{-3}$ [USD/kg/km]
Production Cost	33 M [USD]
OEW	191 [kN]
$MTOW$	579 [kN]
Thrust	95,429 [N]
SFC	$1.24 \cdot 10^{-5}$ [Kg/Ns]
Fuel burn /Payload ¹⁹	0.41 [kg/kg]
Fuel burn per 100 tonne-kilometre ²⁰	7.47 [L/10 ⁻⁵ kg/km]

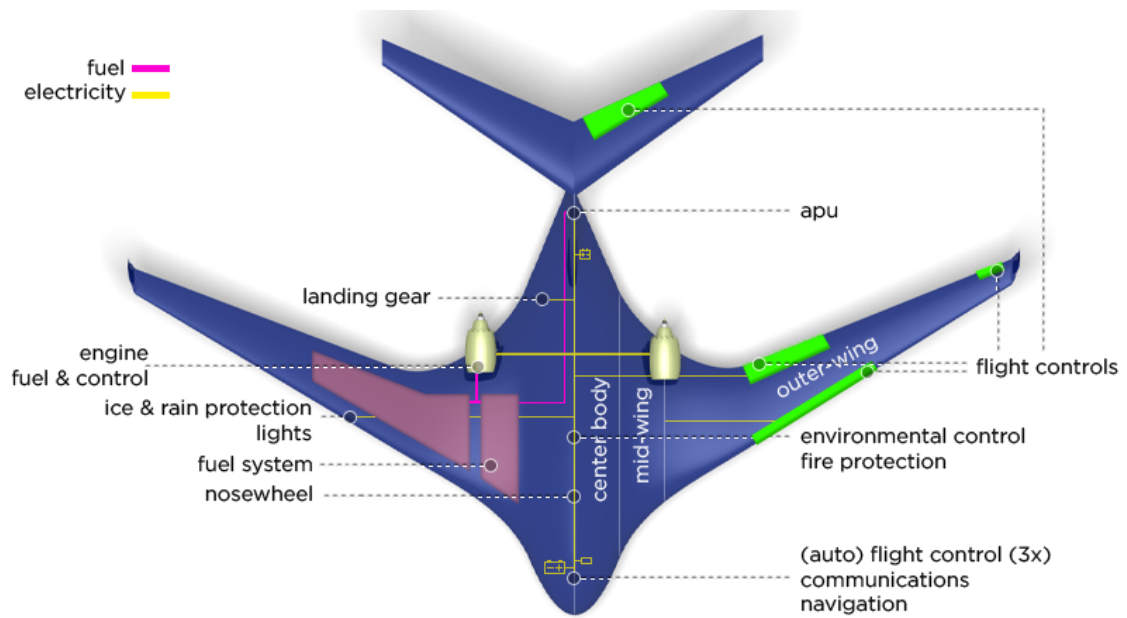


Figure 4.25: Configuration layout of ATLAS.

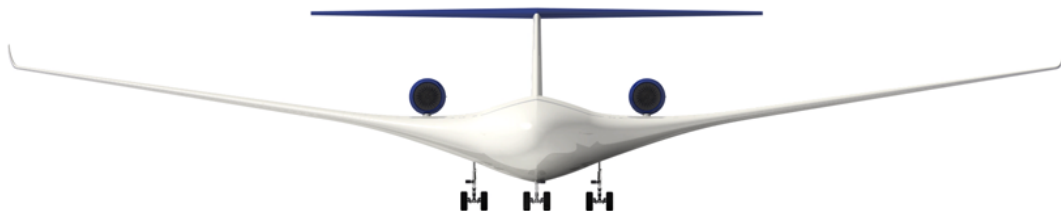


Figure 4.26: Front view of ATLAS.

5 Design evaluation

This chapter will continue on the design decisions made in chapter 4 by evaluating the design. The chapter will start by analysing the aircraft performance. Next, the aerodynamic characteristics will be explained, after which the winglets are designed. Following this, the structural analysis is performed and the stability and control characteristics are evaluated. The next step is to perform the financial analysis. To conclude, the sensitivity analysis, verification & validation procedures, technical risk assessment, and sustainability development strategy will be explained.

5.1 Performance analysis

This section will show the performance analysis of ATLAS. First the payload range diagram will be shown. After that, both the climb and descent performance will be analysed. Next, the stall and turning performance will be calculated. This is followed by the evaluation of the take-off and landing performance. Lastly, the SEL noise contour and the emissions will be analysed.

5.1.1 Payload range diagram

The payload-range diagram shows the relationship between the payload that the aircraft carries and the range that it can fly. The diagram for ATLAS is shown in Figure 5.1. The horizontal line in the diagram shows the range that the aircraft can fly with maximum payload. The first diagonal part of the diagram shows the payload that needs to be replaced by fuel weight in order to fly further. The final diagonal part of the diagram indicates that the maximum amount of fuel that the aircraft can carry has been reached. If the aircraft has to fly further the payload weight needs to be reduced even further. The dotted lines indicate the range for a typical payload of 28,000 kg.

Sustainability

It was already stated that the ATLAS is more fuel efficient than an Boeing 747-400F. As a simple comparison, the ferry range of the 747-400F is approx. 8500 nmi. The ferry range of the ATLAS is approx. 9500 nmi, while it uses 46% less fuel.

5.1.2 Climb performance

After take-off the aircraft needs to climb to cruise altitude. Since the engines are more efficient at cruise altitude, the climb route is optimised to get as high as possible as fast as possible. The rate of climb (ROC) is the vertical velocity of the aircraft. Figures 5.2 and 5.3 show the rate of climb of the aircraft at different altitudes vs the true Mach number. The rate of climb is directly proportional to the excess power available. The equation for the ROC is given in [35, p. 375], the first term represents the excess power and the second term represents the power that is needed in order to accelerate. When the aircraft flies at a constant velocity the second term is zero.

$$ROC = \frac{(T - D)V}{W} \left[1 + \frac{V}{g} \frac{dV}{dH} \right] \quad (5.1)$$

The ROC decreases non-linearly with altitude because the lower atmospheric density reduces engine thrust (thus excess power) [41]. The black dotted lines indicate the maximum rate of climb for different altitudes and therefore the optimal Mach numbers to fly at in order to climb fastest.

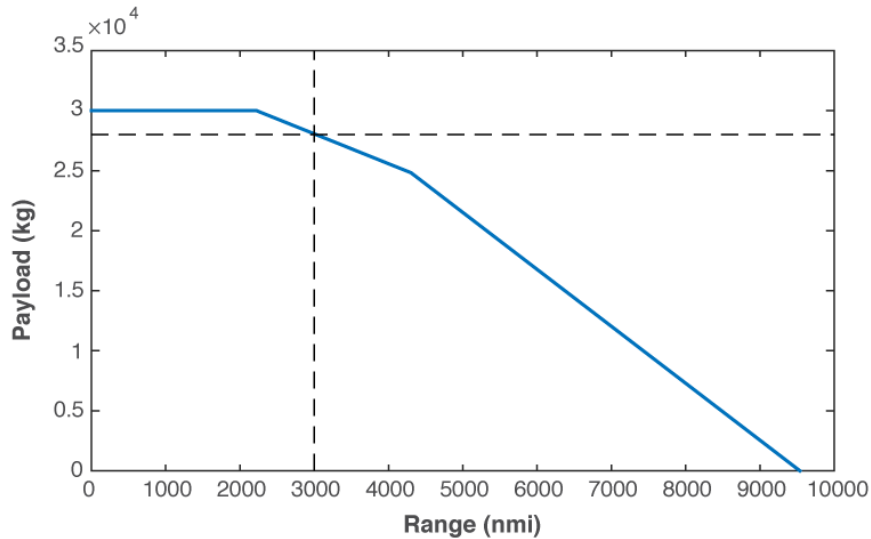


Figure 5.1: Payload range diagram. Indicated with the dotted lines is the range (3000 nmi) for the typical payload weight (28000 kg).

For the optimal climb (with respect to climb time) path the mean climb angle was calculated to be 5.33 degrees. The ground distance covered during the climb is 133.9 km and the time to climb is 1491 seconds (approx. 25 minutes).

5.1.3 Descent performance

At the end of the cruise phase of the flight the aircraft needs to decent to the airport altitude. The next generation air transportation system (NextGen) plan mandates the development of advanced air traffic management technologies and procedures to accommodate safely, efficiently and reliably a significant increase in traffic demand in the already congested terminal environment. A concept of operations for NextGen terminal airspace, referred to as super-density operations, envisions the use of advanced ground and flight deck automation and optimised vertical profiles. One method for increasing the vertical profile efficiency is a continuous descent approach (CDA). CDAs are arrival procedures in which the aircraft descends continuously from cruise to landing with engines at or near idle. CDAs contrast against todays typical dive and drive procedures in which aircraft fly powered constant-altitude segments, referred to as level segments, at intermediate altitudes after their initial descent from cruise altitude. Flying these level segments, which may be chosen on the basis of local traffic, schedule constraints and weather, generally increases fuel burn, greenhouse gas emissions and noise pollution. For this reason, the CDA trajectory has also been referred to as a sustainable green trajectory [42].

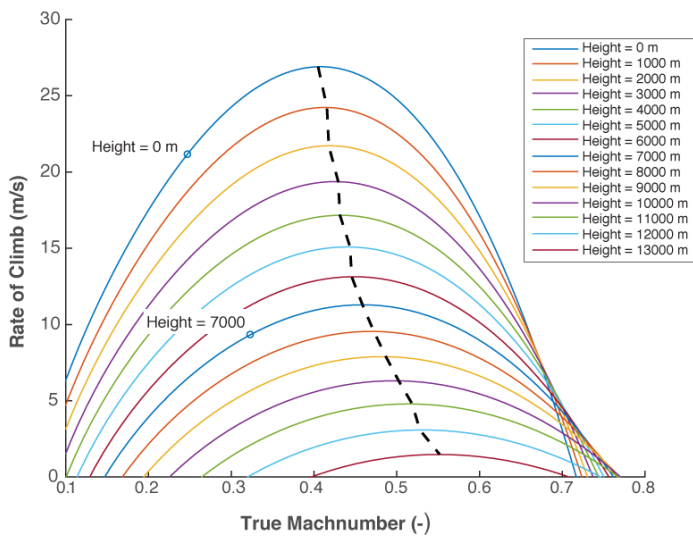


Figure 5.2: Rate of climb at different altitudes versus true Mach number for MTOW.

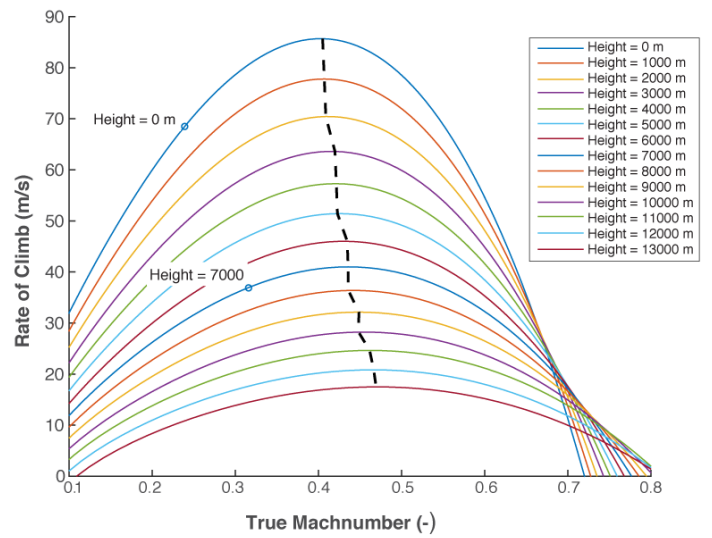


Figure 5.3: Rate of climb at different altitudes versus true Mach number for OEW.

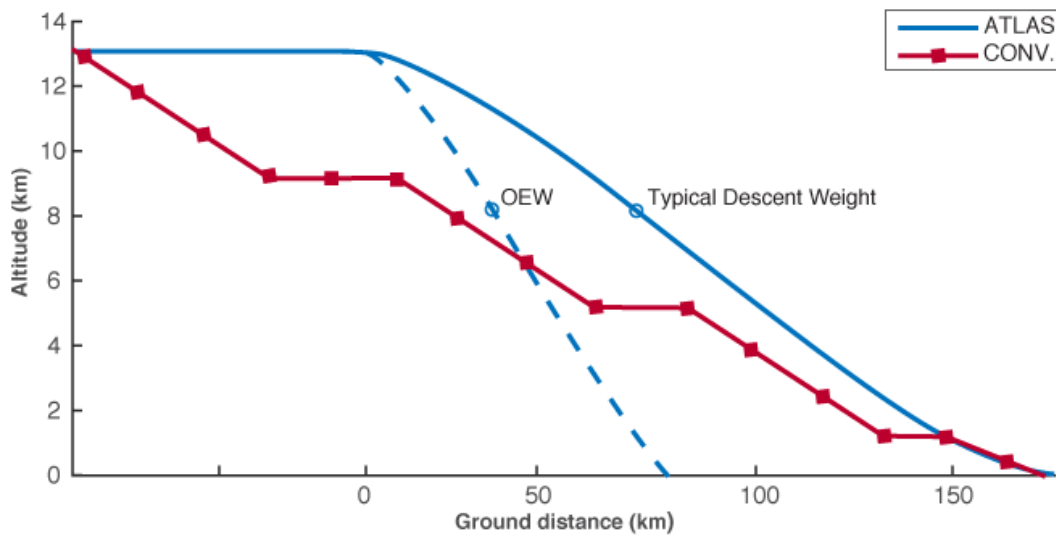


Figure 5.4: Continuous descent approach of the ATLAS versus a conventional approach.

Since the expectation is that CDAs will be widely used in 2035, such a descent trajectory was chosen for the ATLAS. Figure 5.4 shows the continuous descent trajectory of the ATLAS (typical descent weight and OEW) and a "dive and drive" trajectory of a conventional aircraft. Besides the benefits mentioned above, one can clearly see that the ATLAS starts its descent nearly 100 km closer to the airport. This implies that the ATLAS flies longer at cruise altitude where the engines operate more efficiently. The downside of CDAs is that due to the different approach speeds of different aircraft the separation between them will have to be bigger. This means that the capacity of airports will decrease.

To start the descent the thrust is gradually decreased to idle thrust. The drag is increased by a factor 2. This is done by deploying the spoilers. At 3000 meters altitude the aircraft needs to gradually stop descending, so the thrust is increased to $\frac{1}{6}$ max thrust and the spoilers are withdrawn again. These descent settings do not apply to final approach, since there the goal is

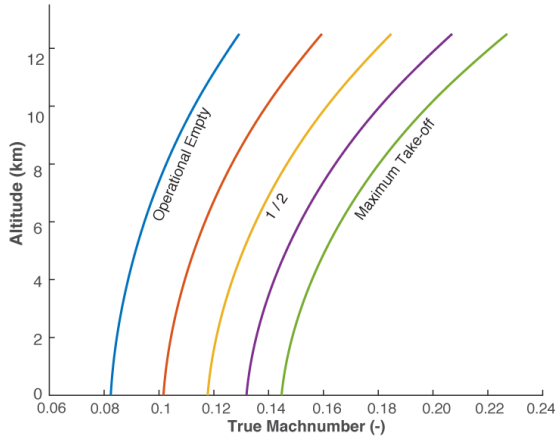


Figure 5.5: Stall speeds for different weights without high lift devices.

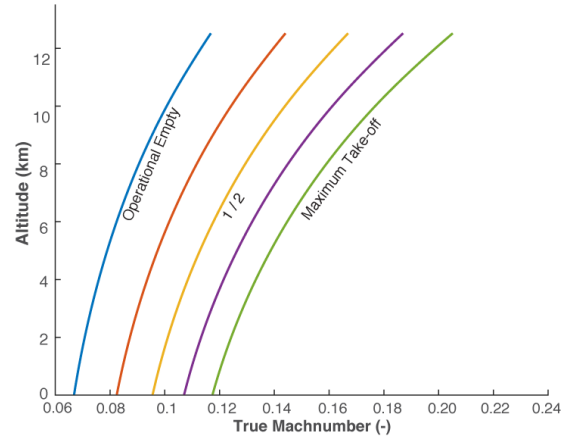


Figure 5.6: Stall speeds for different weights with high lift devices.

to fly as close to $1.2V_{min}$ as possible without going slower.

The equation for the rate of descent is similar to the equation for the rate of climb:

$$ROD = \frac{(D - T)V}{W} \left[1 + \frac{V}{g} \frac{dV}{dH} \right] \quad (5.2)$$

For the ATLAS' continuous descent trajectory the ground distance during descent is 163.2 km, the descent time is 1243 seconds (approx. 21 minutes). The mean descent angle is -4.38 degrees and the max. descent angle in the trajectory is -6 degrees.

5.1.4 Stall performance

One of the most crucial things to know is when the aircraft stalls. To this end Figure 5.5 shows the stall speeds at different altitudes and weights. The stall speed was calculated by rewriting the lift formula. The equation is given in [35, p. 581]. The stall speed is especially important at landing, since at landing the aircraft should fly as slow as possible. As the bank angle θ increases the load factor n increases as well. This increases the stall speed. For a bank angle of 30° the stall speed increases by 7.2%.

Figure 5.6 shows the stall speeds when the High Lift Devices are deployed. In fact, the main reason that flaps are extended during landing is to give the aircraft a lower stall speed so the approach to landing can be flown more slowly.

5.1.5 Manoeuvring performance

Based on the same rewritten lift formula as used for subsection 5.1.4 a relationship can be found between the maximum achievable load factor and a given equivalent airspeed. This relationship, for a flaps-up configuration, is shown in Figure 5.7. The maximum load factor, the design limit load factor, can be calculated using the following equation (imperial units) [39].

$$n_{lim} \geq 2.1 + \frac{24,000}{W + 10,000} \text{ with } n_{lim} \geq 2.5 \quad (5.3)$$

In this case the calculate n_{lim} is lower than 2.5 so the minimum value of $n_{lim} = 2.5$ must be taken.

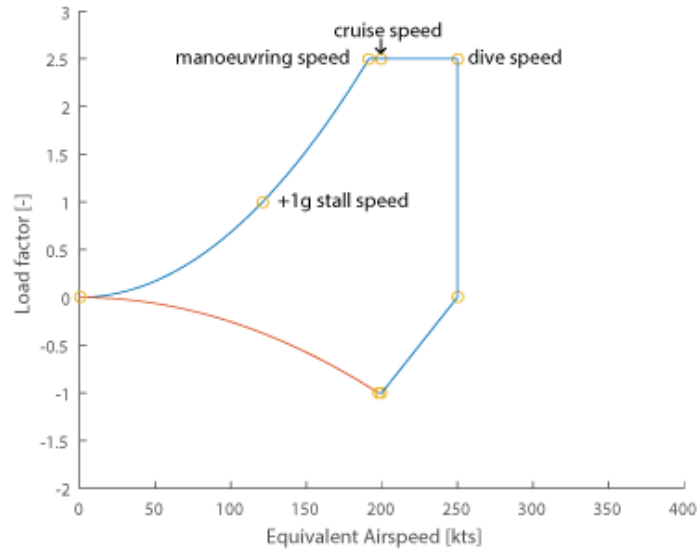


Figure 5.7: Maximum achievable load factor for a given equivalent airspeed.

5.1.6 Turning performance

The next step is to evaluate the turning performance. It should be noted that it turns out that the zero-lift drag is relatively low, and the engines are powerful. Therefore, the graphs in this section will show both the case for a 4g turn, as well as a 2.5g turn. The value 2.5 is chosen because this is the maximum load factor the airplane will be designed for (see subsection 5.1.5).

The first step is to calculate the drag for a range of airspeeds for a given load factor. The airspeed is calculated using Equation 5.4. Here n is the load factor, for which a range of values is taken. Also for C_L a range of values is chosen, ranging from almost 0 to the maximum lift coefficient. After that the drag is calculated using Equation 5.5.

$$V_{true} = \sqrt{\frac{n \cdot W_{TO}^2}{S \cdot \rho \cdot C_L}} \quad (5.4)$$

$$D = \left(\frac{C_{D0}}{C_L} + \frac{C_L}{\pi \cdot A \cdot e} \right) \cdot n \cdot W_{TO} \quad (5.5)$$

Plotting the airspeed versus the drag results in Figure 5.8. As mentioned before, that the zero-lift drag is relatively low and the engines are powerful results in a graph where it seems like the drag is always decreasing when airspeed increases. This is not true, as can be seen in Figure 5.9. Here it can be seen that the drag will increase rapidly, but only at a relatively high airspeed. To get realistic values, the remaining plots of this chapter will show the case for both the 4g and the 2.5g turn.

The next step is to calculate the maximum achievable load factor for a given airspeed. These are the most left points in Figure 5.8, and the intersections of the curves with the maximum thrust line. The result can be seen in Figure 5.10.

After the maximum achievable load factors are known, the minimum turn radius, minimum turn time, and bank angle for a "rate one" and "rate two" turn can be evaluated. The minimum turn radius is calculated using Equation 5.6, and the turn time is calculated using Equation 5.7. In Figure 5.11 and Figure 5.12 it can be seen that for a 2.5g turn the minimum turn radius is 462m and the minimum turn time is 28.5s.

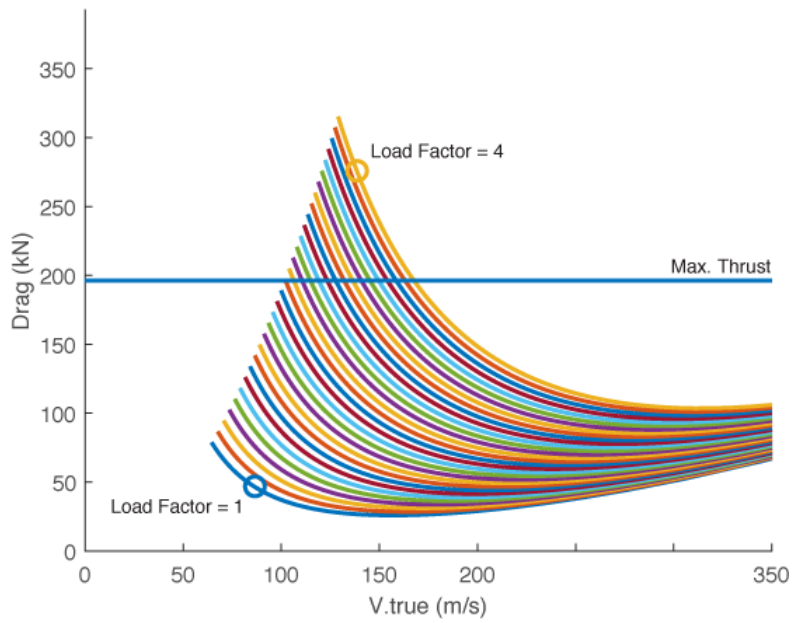


Figure 5.8: Drag as a function of airspeed and load factor.

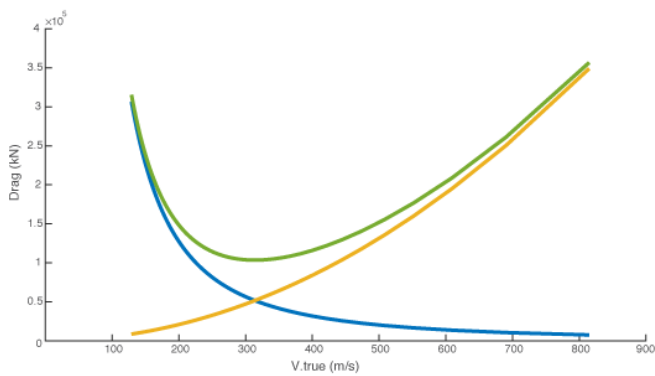


Figure 5.9: Drag components versus airspeed.

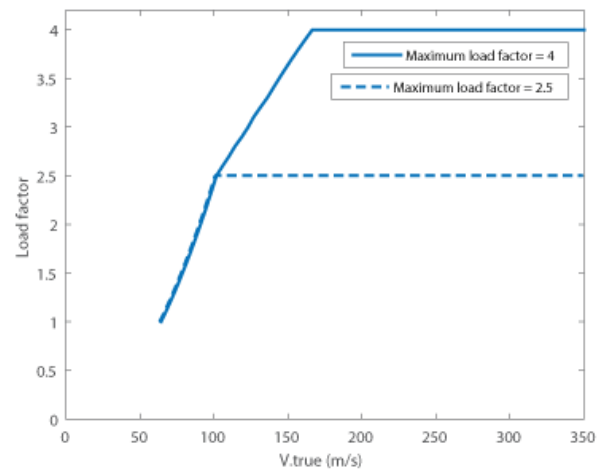


Figure 5.10: Achievable load factor as a function of airspeed.

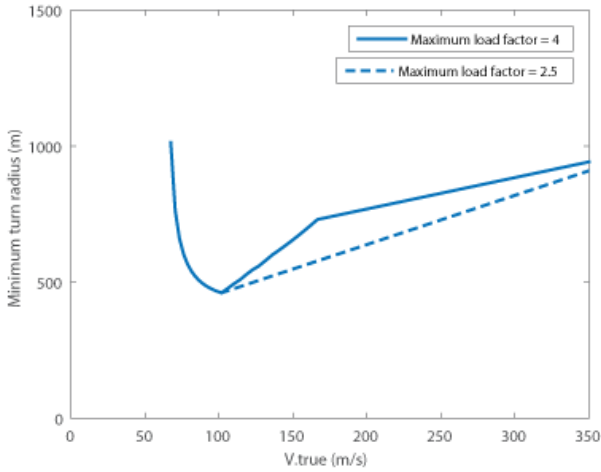


Figure 5.11: Minimum turn radius as a function of airspeed.

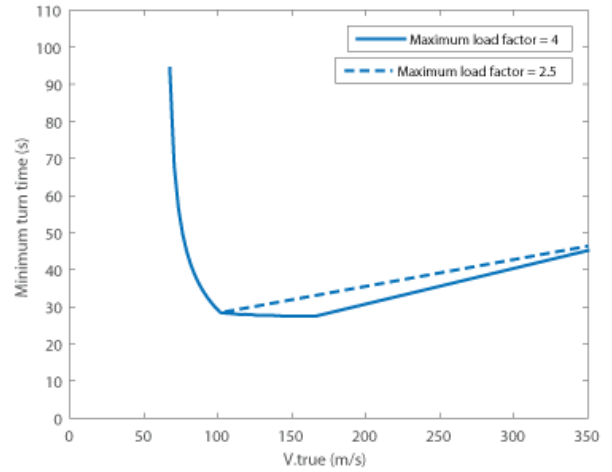


Figure 5.12: Minimum turn time as a function of airspeed.

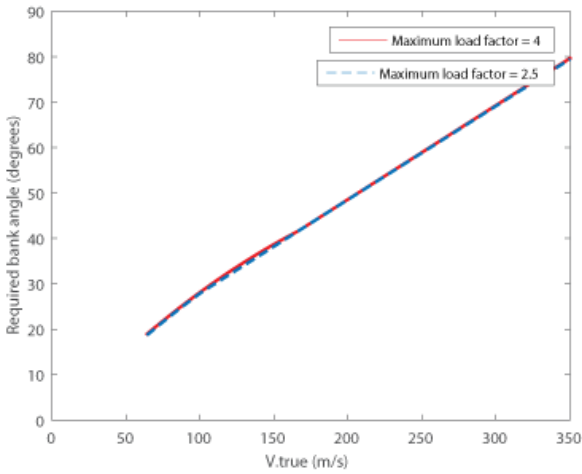


Figure 5.13: Required bank angle for a rate one turn as function of airspeed.

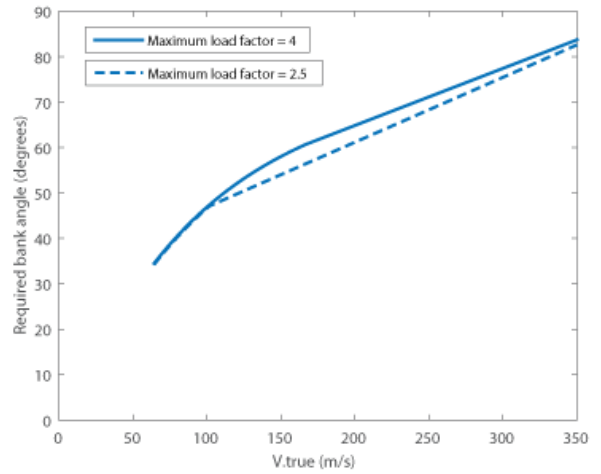


Figure 5.14: Required bank angle for a rate two turn as function of airspeed.

$$R_{turn} = \frac{V_{true}^2}{g \cdot \sqrt{n^2 - 1}} \quad (5.6)$$

$$T_{turn} = \frac{2 \cdot \pi \cdot R_{turn}}{V_{true}} \quad (5.7)$$

The bank angle ϕ for a "rate one" and "rate two" turn is calculated using Equation 5.8. A "rate one" turn means making a 180° turn in 60 seconds, and a "rate two" turn means making a 360° turn in 60 seconds. Therefore the value of Ω is $\frac{\pi}{60}$ for a "rate one" turn, and $\frac{2\pi}{60}$ for a "rate two" turn. The results can be seen in Figure 5.13 and Figure 5.14.

$$\phi = \arccos\left(\frac{1}{\sqrt{\left(\frac{V_{true} \cdot \Omega}{g}\right)^2 + 1}}\right) \quad (5.8)$$

5.1.7 Take-off and landing performance

From the landing gear position which will be calculated in subsection 4.5.6, the aerodynamic characteristics calculated in section 5.2, the centre of gravity position at maximum take-off weight calculated in section 5.4, and tail characteristics calculated in subsection 4.5.4, the necessary elevator deflection and area can be defined or calculated in order to be able to rotate at take-off. Rotating can occur when the moment induced by the weight is counteracted by the lift generated by the wing and down force generated by the horizontal tail. The moment induced by the weight is calculated using Equation 5.9. At maximum take-off weight, this results in a moment of 817kNm. The moment counteracted by the wing and the tail can be calculated using Equation 5.10. Using a value of 1.1 for $C_{L,maxtail}$, and combining Equation 5.9 and Equation 5.10, the equations can be solved for $S_{elevator}$.¹ It turns out that a elevator surface area of $15m^2$ is required. Using the ratio between the elevator area and the total horizontal tail area (0.224), this turns out to be a reasonable value as can be seen in [28].

$$M_{weight} = W_{TO} \cdot (x_{maingear} - CG_{max}) \quad (5.9)$$

$$M_{wing,tail} = C_{L,\alpha,0} \cdot \frac{1}{2} \rho V_{TO}^2 \cdot S \cdot (x_{maingear} - \bar{c}_{wing}) + C_{L,maxtail} \cdot \frac{1}{2} \rho V_{TO}^2 \cdot S_{elevator} \cdot (x_{maingear} - \bar{c}_{tail}) \quad (5.10)$$

The aircraft is designed to be able to take-off and land at a runway of 1500m, as can be seen in section 4.4. This runway length is low compared to reference medium range aircraft [43]. This short runway length gives great benefits to ATLAS in terms of usage, since it is able to land and take-off at more airports than its competitors.

5.1.8 SEL noise contour

The following section will provide a preliminary investigation on the noise pollution generated by the ATLAS. One of the top level requirements is that the 55 decibel Sound Exposure Level (SEL) noise contour should be 50% smaller than the one generated by an Airbus A320. The SEL is defined as the time-integrated A-weighted (i.e. frequency corrected) sound level that is normalised to a time period of one second [44]. This section describes how the noise has been calculated for the baseline and the blended wing body design, after which the results are presented.

Noise algorithm

To predict the noise exposure as accurately as possible, a *Matlab* program is built around the INMTM (Integrated Noise Model / Management of Trajectory and Missions) tool developed by *Cleansky*. This tool, which uses the same algorithms as the Federal Aviation Administration's (FAA) standard Integrated Noise Model (INM), is able to calculate the SEL on a pre-defined grid below a specified flight trajectory [45]. The input required by the INMTM tool consists of a trajectory file and a grid file. The trajectory file primarily specifies the flight path of a certain movement by defining six vectors, as shown in Table 5.1. It also allows the user to specify the engine type and location. The grid file describes the outer limits of the grid, as well as the size of the cells in x-direction and y-direction, as shown in Table 5.2.

¹<http://airfoiltools.com/airfoil/details?airfoil=n0012-il> [accessed on 19/06/15]

Table 5.1: Input parameters for INMTM trajectory file.

Symbol	Parameter	Unit
x	x-coordinate	[m]
y	y-coordinate	[m]
h	altitude	[m]
V	true airspeed	[m/s]
T	net corrected thrust per engine	[N]
m	flight mode	[-]

Table 5.2: Input parameters for INMTM grid file.

Symbol	Parameter	Unit
x_min	minimum x value	[m]
x_max	maximum x value	[m]
x_sz	cell size in x-direction	[m]
y_min	minimum y value	[m]
y_max	maximum y value	[m]
y_sz	cell size in y-direction	[m]

To define the trajectory file, use is made of actual radar observations at Amsterdam Airport Schiphol (AAS). The data, originating from October 22, 2010, includes the aircraft's position with respect to the control tower, the landing or departure time, the current time, and the aircraft type code. From the data set both an approach and departure trajectory of an Airbus A320 movement are extracted. To maximise the speed of the program all data points with an altitude exceeding 8,500 meters are not included in the noise analysis, for both the A320 and the ATLAS. If, during the analysis of the results, it turns out that noise is still significant above these altitudes, the algorithm should be adapted. How every parameter used for the input trajectory files is defined, is shown in Table 5.3. With all vectors known the INMTM tool could be run to generate the SEL across the grid for both aircraft.

Table 5.3: The origin of each parameter needed to define the INMTM input trajectory file for both the A320 and the ATLAS.

	A320		ATLAS	
	Departure	Approach	Departure	Approach
x	AAS Data set	AAS Data set	AAS Data set	AAS Data set
y	AAS Data set	AAS Data set	AAS Data set	AAS Data set
h	AAS Data set	AAS Data set	Climb performance (subsection 5.1.2)	Descent performance (subsection 5.1.3)
V	$\Delta s/\Delta t$	$\Delta s/\Delta t$	Climb performance (subsection 5.1.2)	Descent performance (subsection 5.1.3)
T	$0.75 \cdot T_{max}(h)$	$0.25 \cdot T_{max}(h)$	$T_{max}(h)$	Descent performance (subsection 5.1.3)
m	n/a	n/a	n/a	n/a

Due to the fact that the INMTM tool is only able to predict noise exposure of existing aircraft, two corrections are implemented in the noise module: one to account for BWBs and one to account for a reduction in size. A noise comparison by the Nasa Langley Research Center between multiple Boeing BWB concepts and comparable state of the art aircraft, shows that the most conservative reduction between a Boeing 777 and equal sized BWB is 4 dB for departure and 10.5 dB for approach [46]. An explanation that the sound reduction for approach is larger than for departure is that airframe noise has a more significant contribution with respect to engine noise

during approach than during departure [47]. Converting the decibel values to absolute noise levels, the noise reduction of a BWB is 60.2% and 91.1% for take off and approach, respectively. However, since the Boeing BWB concept neither has a tail nor a fuselage, a 30% correction was applied to the reductions.

A change in aircraft size is represented in the noise module by both a change in required thrust, which is accounted for in the definition of the trajectory file, and by a change in aircraft weight. The aircraft weight is a rough approximation of the airframe size and hence the airframe generated noise [47]. Therefore, a sizing factor has to be implemented to approximate the change in airframe noise, which is assumed to be only significant during approach. Using [47] the airframe noise (in dB) during approach can be estimated by Equation 5.11, where W is the aircraft weight in lbs. The Matlab program uses this formula to compute the airframe noise generated by an Airbus A320 and the concept designs. The absolute noise difference is then used to scale the noise levels, either up or down.

$$DB_{airframe} = 40 + 10\log(W) \quad (5.11)$$

Results

The noise profiles generated by the module described in the previous section consist of values for the SEL for each cell in the predefined grid. Using *Matlab* the 55 dB noise contours could be plotted over the size of the grid for the A320 and the ATLAS. A map of Schiphol area has been added to each figure to get a better feeling for the size of the noise contours. The comparisons are shown in Figure 5.15 and Figure 5.16. A table with comparisons of the area of the 55 dB noise contours is presented in Table 5.4. From this it follows that the ATLAS meets the 50% noise reduction requirement. The most significant reasons for the noise reduction are the aerodynamically efficient airframe and the short ground distances required to climb with respect to the A320.

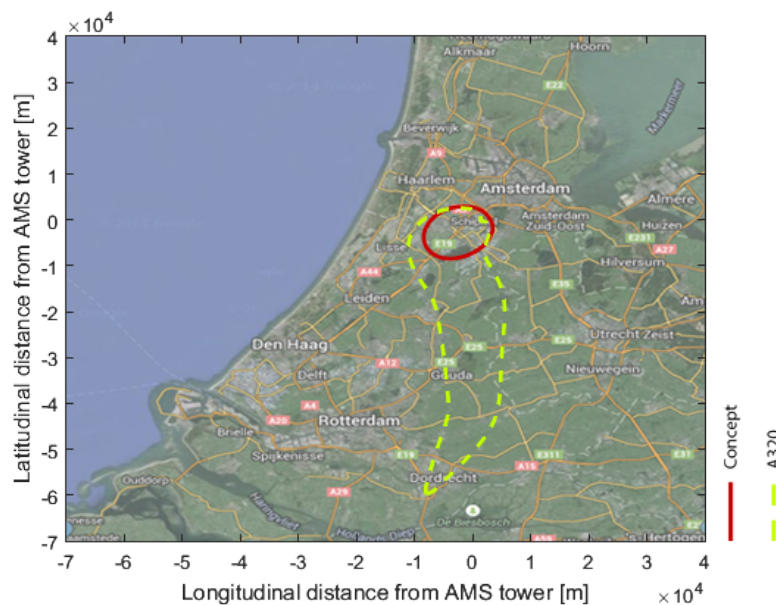


Figure 5.15: Noise comparison between baseline and the ATLAS - Departure.

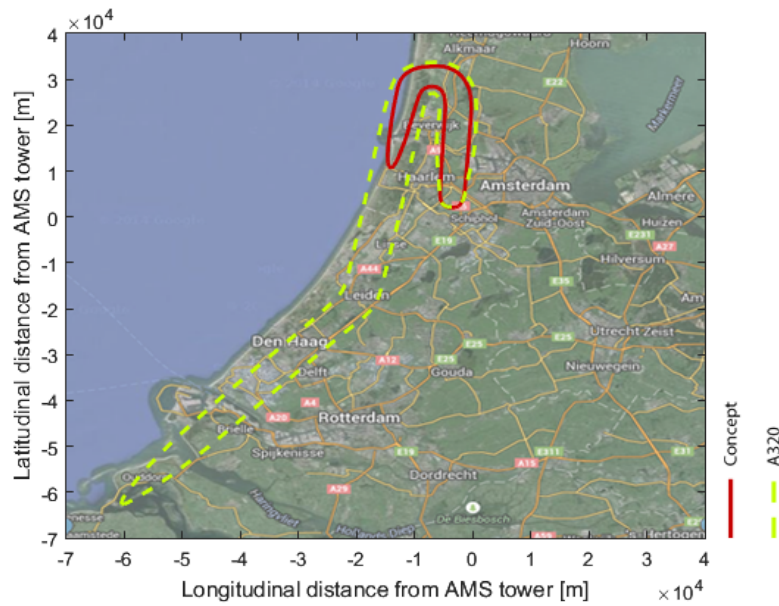


Figure 5.16: Noise comparison between baseline and the ATLAS - Approach.

Table 5.4: SEL comparison.

Aircraft	Mode	SEL area [km^2]	% difference w.r.t. A320
A320	Departure	596	0
	Approach	829	0
ATLAS	Departure	102	-82.3
	Approach	210.5	-74.6

Verification and validation

The noise program consists mainly of two parts: the generation of the INMTM trajectory file, which is verified in the following trajectory file subsection, and actually running the INMTM model, which verification is described in the INMTM tool subsection.

Trajectory file

The x, y, and altitude coordinates were taken from the data set directly. The data set has been provided by Air Traffic Control, hence coordinates are assumed to be correct. On top, for the extracted trajectories the coordinates have been manually checked for outliers, which were not encountered. To verify the velocity vectors of the A320, references have been obtained to compare the results². These were found to be in good accordance. All other required input values are taken from other sections of the program, which have all been verified in their respective sections.

INMTM tool

The INMTM tool has already been verified and validated by the program's developers according to [45]. The verification and validation process consisted of three parts:

- Accuracy of the tool with respect to the FAA's INM tool.
- Robustness of the tool.
- Ability of the program to be integrated in other noise optimisation frameworks.

For an more detailed description of the program's verification and validation process, the reader is referred to [45].

²<http://www.satavirtual.org/fleet/A320PERFORMANCE.PDF> [accessed on 18/06/15]

5.1.9 Fuel consumption

One of the driving requirements of the ATLAS design was the low fuel consumption. Using the drag calculated in section 5.2 and specific fuel consumption found in subsection 4.5.7 the fuel consumption can be calculated. For ATLAS this is found to be is $7.47 \frac{L}{10^{-5}kg \cdot km}$.

This is 54% of the fuel consumption of the 747-400F per 100 tonne payload, per kilometre. Which was calculated in chapter 2. While this is a significant improvement the requirement was 25% of the fuel consumption of the 747-400F. This requirement is therefore not met. However, in the calculations it is assumed that the 747-400F is completely filled with cargo. Since ATLAS is a relatively small aircraft, it will for ATLAS be more common to fly with maximum payload compared to a 747-400F. This is of course good for the fuel consumption of ATLAS compared to the 747-400F.

An preliminary analysis on multiple aircraft characteristics is therefore performed to see what results would be required to make this requirement. This resulted in the following options:

- **Improved L/D:** An lift over drag ratio of 40 would be required to meet the fuel requirement.
- **Reduced SFC:** A decrease in specific fuel consumption of 60% with respect to the current LEAP 1A engine would be required to meet the fuel requirement.
- **Combination of improved L/D and reduced SFC:** The most realistic option would be an combined improvement of aerodynamic efficiency and decreased specific fuel consumption. Multiple combinations would of course be possible, but at an L/D of 25 the required reduction in SFC would be around 46%.

5.1.10 Emissions

To become the cargo aircraft of the future, the ATLAS needs to be sustainable. One way of measuring sustainability is the produced emissions. In this section the CO₂ emissions of the ATLAS will be compared to those of the Boeing 747-400F. Below the CO₂ production of the ATLAS and 747-400F is calculated and compared.

ATLAS

Range: 3000 nmi
Payload: 28000 kg
Fuel: 10930 kg

Boeing 747-400F

Range: 4445 nmi
Payload: 112630 kg
Fuel: 119123 kg

$$CO_2 = \frac{10930 * 3.157}{28000 * 3000} = 4.11 \cdot 10^{-4} \frac{kg}{kg \cdot nmi}$$

$$CO_2 = \frac{119123 * 3.157}{112630 * 4445} = 7.51 \cdot 10^{-4} \frac{kg}{kg \cdot nmi}$$

Where '3.157' is the conversion factor from Fuel to CO₂. For every kg of Jet-A fuel that is burned, 3.157 kg of CO₂ is produced. The ATLAS produces only 54% of the 747-400F' CO₂. That is an reduction of 46%, which means that the ATLAS is more sustainable than the current standard.

5.2 Aerodynamic characteristics

The aerodynamic analysis of the aircraft give insight into the performance, the stability and the structural loads of the aircraft. This section will explain the methods for estimating the zero lift drag coefficient, the zero lift pitching moment coefficient and other aerodynamic properties and their use.

5.2.1 Atmospheric conditions

In this section the atmospheric conditions the aircraft will encounter are calculated. These atmospheric properties are important to analyse the aerodynamics of the aircraft. Temperature,

Table 5.5: Values for physical constants.

Symbol	Description	Value
μ_0	Air reference viscosity	$1.716 \cdot 10^{-5}$
T_0	Reference temperature	273.15 K
S	Sutherland's law constant	110.4 K

density and pressure can be calculated as described in [48, p. 75]. The values of physical constants at sea level and temperature rates in different regions of the atmosphere have been standardized. International Organization for Standardization (ISO) has published the International Standard Atmosphere (ISA) as an international standard, ISO 2533:1975 [22]. To calculate the Reynold's number for an airflow, Equation 5.13 is used. The dynamic viscosity (μ) is calculated with Sutherland's law (Equation 5.12) and reference constants specific for air [49].

$$\mu = \mu_0 \cdot \left(\frac{T}{T_0} \right)^{3/2} \cdot \frac{T_0 + S}{T + S} \quad (5.12)$$

$$Re = \frac{\rho V L}{\mu} \quad (5.13)$$

5.2.2 Estimating C_{D_0}

To provide an aerodynamic analysis of the performance, the zero lift drag coefficient (C_{D_0}) has to be estimated. C_{D_0} is estimated for every aircraft subsystems separately and then summed to get the total. These specific values are calculated at cruise conditions.

C_{D_0} of Wing segments (body, outer wing, empennage, nacelles)

This section describes how to estimate C_{D_0} for wing segments. This estimation is applied to the body segment, the outer wing segment and the horizontal and vertical tail (empennage) segments. The nacelles are also approximated as circular wing segments, since they have a large diameter. However, only the outer surfaces of the nacelles are considered as wetted surface area.

$$C_{D_0, \text{wing segment no wave}} = R_{wf} \cdot R_{LS} \cdot C_f \cdot [1 + L' \cdot (t/c) + 100 \cdot (t/c)^4] \cdot \frac{S_{wet}}{S} \quad (5.14)$$

To calculate C_{D_0} for the wing segments Equation 5.14 is used. The wing fuselage interference factor (R_{wf}) is 1.0 since the design is a blended wing body. Lifting surface correction factor (R_{LS}), friction coefficient (C_f) and the thickness location parameter ($L' = 1.2$) are factors. Maximum thickness over chord (t/c) depends on airfoil of the segment. The wetted area for wing segments is calculated with Equation 5.15 [50]. Equations and factors are retrieved from [51].

$$S_{wet} = [2 + 0.5 \cdot (t/c)] \cdot S_{segment} \quad (5.15)$$

To calculate the wave drag, the Mach drag divergence (M_{DD}) number is calculated. k_α is the airfoil technology factor (0.95 for supercritical sections, 0.87 for normal sections). By using Lock's empirical equation for drag rise, the critical Mach number (M_{crit}) can be calculated together with the wave drag coefficient ($C_{D_{wave}}$), using Equations 5.16 through 5.18. [52]

$$M_{DD} = \frac{\kappa_\alpha}{\cos \Lambda} - \frac{t/c}{\cos^2 \Lambda} - \frac{C_l}{10 \cdot \cos^3 \Lambda} \quad (5.16)$$

$$M_{crit} = M_{DD} - \left(\frac{0.1}{80} \right)^{(1/3)} \quad (5.17)$$

$$C_{D_{wave}} = 20 \cdot (M - M_{crit})^4 \cdot \frac{S_{segment}}{S} \quad (5.18)$$

Table 5.6: C_{D_0} values for different components.

Coefficient	Value
$C_{D_0, body}$	0.00541
$C_{D_0, outer wing}$	0.00491
$C_{D_0, empennage}$	0.00185
$C_{D_0, nacelles}$	0.00136
$C_{D_0, fuselage}$	0.000529
C_{D_0}	0.0141

The total zero lift drag coefficient $C_{D_0, wing segment}$ for a wing segment can be computed with Equation 5.19. It incorporates sweep and compressibility effects.

$$C_{D_0, wing segment} = C_{D_0, wing segment no wave} + C_{D_{wave}} \quad (5.19)$$

C_{D_0} of the fuselage

To calculate C_{D_0} for the fuselage Equation 5.20 is used.

$$C_{D_0, fuselage} = R_{wf} \cdot C_f \cdot \frac{S_{wet}}{S} \quad (5.20)$$

Generally an equation for C_{D_0} incorporates a thickness over length parameter to account for pressure drag. However, this design has a fuselage which is located behind the wing and is not thicker than the wing. Thus, the pressure drag has already been accounted for by the C_{D_0} calculation of the body. The remaining drag is only friction drag and interference drag. This is calculated with Equation 5.20. The interference factor ($R_{wf} = 1.015$) and C_f are determined with [51]. The wetted area for the fuselage is calculated with Equation 5.21 with diameter d and length l of the fuselage in contact with airflow.

$$S_{wet} = \pi d \cdot l \quad (5.21)$$

C_{D_0} of the Aircraft

With the methods described above the individual C_{D_0} components are calculated. The total drag is calculated with Equation 5.22. The values are displayed in Table 5.6. The aircraft C_{D_0} is 0.0141. For conventional aircraft this value typically lies around 0.020. In consequence this aircraft can achieve higher L/D ratios than conventional aircraft.

$$C_{D_0, aircraft} = C_{D_0, body} + C_{D_0, outer wing} + C_{D_0, empennage} + C_{D_0, nacelles} + C_{D_0, fuselage} \quad (5.22)$$

5.2.3 Estimating C_{m_0} and $x_{a.c.}$

To provide an aerodynamic basis for the stability analysis, the zero lift pitching moment coefficient (C_{m_0}) and the aerodynamic centre of the aircraft have to be calculated.

$$C_{m_0, wing} = \frac{A \cos^2 \Lambda}{A + 2 \cos \Lambda} \cdot \frac{c_{m_0, root} + c_{m_0, tip}}{2} + \frac{\Delta C_{m_0}}{\epsilon_t} \epsilon_t \quad (5.23)$$

$$C_{m_0, fuselage} = \frac{(k_2 - k_1)}{36.5 \cdot S \cdot \bar{c}} \cdot w^2 \cdot i_{cl_{rear}} \cdot L_{rear} \quad (5.24)$$

$$C_{m_0, wing fuselage} = (C_{m_0, wing} + C_{m_0, fuselage}) \cdot \frac{C_{m_0, M}}{C_{m_0, M=0}} \quad (5.25)$$

The $C_{m_0, wing}$ is calculated using Equation 5.23. In this equation c_{m_0} is the airfoil zero lift pitching moment coefficient, acquired with XFLR5 analysis. The $\Delta C_{m_0}/\epsilon_t$ relation is a factor. ϵ_t is the wing twist. The $C_{m_0, fuselage}$ contribution of the fuselage is calculated with Equation 5.24. In this

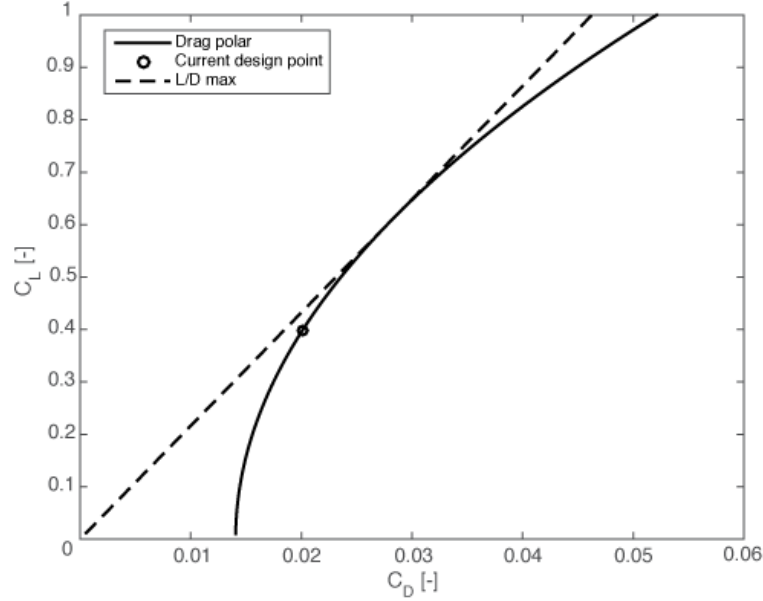


Figure 5.17: Drag polar during cruise.

equation $k_2 - k_1$ is a factor. w is the span of the fuselage, L_{rear} is the rear length of the fuselage. The inclination angle (i_{cl}) is only non zero for the rear of the fuselage. The $C_{m_0, wing fuselage}$ is calculated with Equation 5.25. The $C_{m_0, M}/C_{m_0, M=0}$ term is a compressibility factor. The aerodynamic centre of the aircraft is assumed to be at the quarter chord length of the mean aerodynamic chord of the trapezoidal wing. Equations and factors are retrieved from [51].

5.2.4 Analysis of aerodynamic performance

This section performs an analysis on the performance of the aircraft during cruise, the longest mission segment.

$$C_{L_{design}} = 1.1 \cdot \frac{1}{2} \left(\frac{W}{S_{cruise\ begin}} + \frac{W}{S_{cruise\ end}} \right) \frac{2}{\rho V_{cruise}^2} \quad (5.26)$$

$$C_D = C_{D_0} + \frac{C_L^2}{\pi A e} \quad (5.27)$$

The design lift coefficient ($C_{L_{design}}$) (Equation 5.26 [53]) is the required C_L for the average wing loading during cruise. The equation takes a negative trim lift of 10% into account. To compute the Oswald factor, the induced drag from XFLR5 in combination with Equation 5.27. The Oswald factor e is lower than the initial estimation of 0.85, with winglets only $e = 0.74$ could be achieved. In Figure 5.17 it is visible that the maximum Lift over Drag (L/D_{max}) is at a slightly higher C_L than the current design point. To fly at L/D_{max} either the cruise altitude should be higher or the cruise airspeed should be lower, since this would enable the aircraft to fly at a higher C_L . It should be noted that trim drag is not accounted for, thus the aerodynamic performance may be less than projected. To improve aerodynamic performance the body segment could be optimised for a more elliptical lift distribution.

5.2.5 Aerodynamic parameters

In this section other aerodynamic parameters are calculated using the DATCOM method. These equations require single inputs for parameters such as sweep and aspect ratio. For these equations the trapezoidal wing approximation is used. The slope of the lift curve (C_{L_α}) is corrected for 3D effects using Equation 5.28. Here $\beta = \sqrt{1 - M^2}$ and η is the airfoil efficiency factor, typically

Table 5.7: Aerodynamic parameters.

Coefficient	Value [Unit]
$C_{L_{cruise}}$	0.398 [-]
$C_{D_{cruise}}$	0.0201 [-]
e	0.740 [-]
$C_{L_{\alpha}}$	5.76 [-]
$C_{L_{max,sea-level}}$	1.74 [-]
$C_{L_{max,take-off}}$	1.60 [-]
$C_{L_{max,landing}}$	1.80 [-]
$\alpha_{trim,cruise}$	0.305 [°]
$\alpha_{stall,sea-level}$	20.4 [°]
$\alpha_{stall,take-off}$	18.5 [°]
$\alpha_{stall,landing}$	17.6 [°]

0.95. Ideally, the aircraft only generates lift with the wings to minimise trim drag. So the incidence angle of the wings is set to the α_{trim} , the required angle of attack during cruise. α_{trim} is calculated with Equation 5.29 using the zero lift angle of attack (α_0), which was retrieved from airfoil analysis. The maximum lift coefficient is calculated with Equation 5.30. The stall angle is then calculated with Equation 5.31. The stall angles with deployed high lift devices are lower, but within range of the specified landing conditions ($\alpha = 9.5$). Results are shown in Table 5.7. [54]

$$C_{L_{\alpha}} = \frac{2\pi A}{2 + \sqrt{4 + \left(\frac{A \cdot \beta}{\eta}\right)^2 \cdot \frac{1 + \tan^2 \Lambda_{0.5c}}{\beta^2}}} \quad (5.28)$$

$$\alpha_{trim} = \frac{C_{L_{design}}}{C_{L_{\alpha}}} + \alpha_0 \quad (5.29)$$

$$C_{L_{max}} = 0.9 \cdot \cos \Lambda \cdot C_{l_{max}} \quad (5.30)$$

$$\alpha_{stall} = \frac{C_{L_{max}}}{C_{L_{\alpha}}} + \alpha_0 + \Delta\alpha_{C_{L_{max}}} \quad (5.31)$$

5.2.6 Lift distribution

In this section the lift distribution is determined for the main wing. The lift distribution is required to determine the structural loads of the wing.

XFLR5

The full 3D lift distribution has been analysed in XFLR5. XFLR5 provides preliminary estimation of the 3D lift as experienced by the aircraft based on the Vortex Lattice Methods. It should be noted that XFLR5 assumes incompressible, irrotational and inviscid flow. It is also less accurate for higher Reynolds numbers. More accurate analysis can be provided by completing the Navier-Stokes equations, requiring significant computer resources.

It can be seen that the body is less effective at generating lift in Figure 5.18a. The main reason is the high sweep of these sections, which was necessary to minimise wave drag for these thick wing segments. The lift distribution used to size structural components is shown in Figure 5.18. The distribution is not nearly elliptical, this explains why the Oswald factor is less than for conventional aircraft.

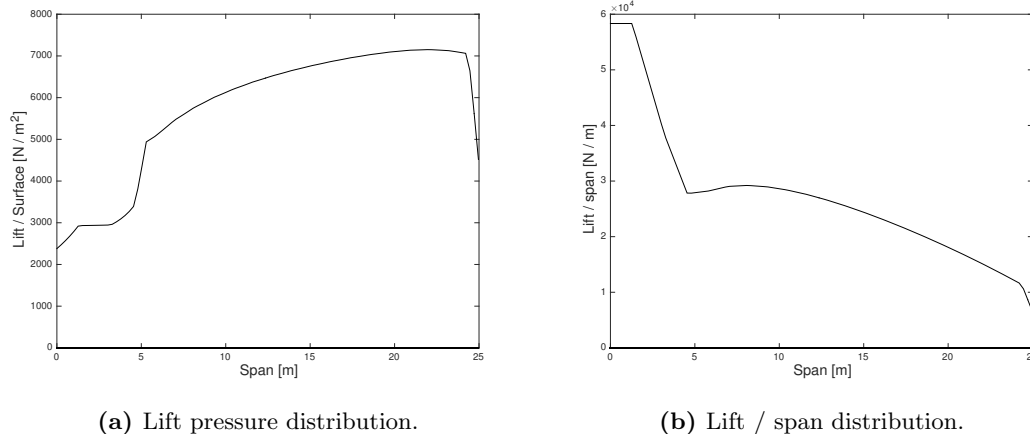


Figure 5.18: Lift distribution.

Q3D

Additionally an alternative aerodynamic estimation tool was implemented to provide the fast lift distribution estimations required for the wing weight estimation. This quasi three-dimensional aerodynamic solver developed at the TU Delft [40] uses a combination of the strip method combined with simple sweep theory. The strip method being used combines strip theory, in which the aircraft is divided into discrete segments and aerodynamic forces are calculated on these segments, with vortex lattice methods. A more detailed explanation of this combination can be found in [55] and [56]. This method allows the solver to analyse the tapered swept wings while still providing the fast results required for design optimisation. It was verified with a full CFD analysis of the Fokker 100 wing. [40]

5.2.7 Winglet design

One of the objective during the aerodynamic design was to increase the aerodynamic performance of the aircraft. Winglets are small surface areas located at the wingtip. They are extensions of the wingtip designed to reduce the tip vortices. The intend is always to reduce the aircraft's drag by partial recovery of the tip vortex energy. The winglets are a simple extension of the outer wing of 1.5 meters. Other than the improved lift distribution the winglets also have a positive effect on the stability of the aircraft. [57][58]

Stability coefficients

To perform a stability analysis of the aircraft, a 3D model for the wing and tail is made in XFLR5. To perform the stability analysis, the geometry of the wings and empennage was modelled as accurately as possible. The computed coefficients are shown in Table 5.8.

Verification of XFLR5

In this section the different analysis methods of XFLR5 are verified. It is divided into the 2D analysis, the lift distribution and the stability analysis.

2D analysis

To verify the 2D analysis of airfoils, a comparison is made between experimental data and XFLR5 computations. The NACA 63-412 airfoil was used for the analysis. The experimental data was retrieved from [59]. In Figure 5.19 the $C_L - \alpha$ curves are shown. The linear part of the curves is similar, but the $C_{L_{max}}$ is underestimated. The α_{stall} is overestimated, however, this value is

Table 5.8: Stability coefficients.

Coefficient	Value	Coefficient	Value
CXu	-0.00619	CYb	-0.43434
CLu	0.00001	Clb	-0.13138
Cmu	0.00000	Cnb	0.04276
CXa	0.12453	CYp	-0.18424
CLa	4.44303	Clp	-0.33090
Cma	-0.63910	Cnp	-0.01066
CXq	-0.00484	CYr	0.18225
CLq	4.62283	Clr	0.07140
Cmq	-5.16161	Cnr	-0.02358

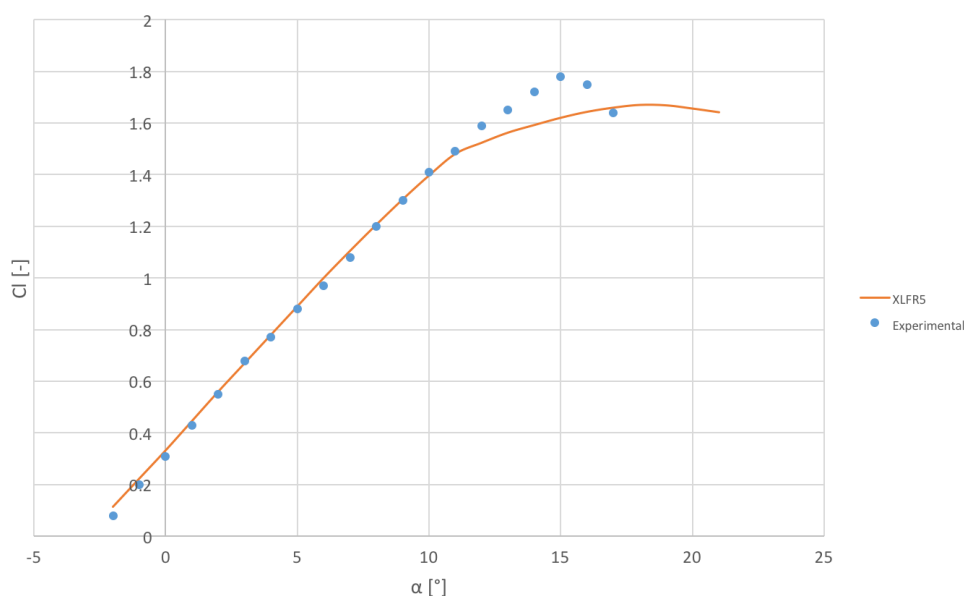


Figure 5.19: Comparison of NACA 63-412 airfoil with $Re = 9.0 \cdot 10^6$.

calculated with the DATCOM method. The results of XFLR5 used in the 2D analysis are either similar or conservative.

Lift distribution

XFLR5 is also used in 3D performance analysis. The calculations are primarily based on the lift distribution over the wing. Components as induced drag are a function of the lift distribution. XFLR5 is compared to the already verified program Q3D. The results of XFLR5 resemble the results of Q3D closely, as shown in Figure 5.20. Q3D did not compute the centre body lift.

Stability analysis

The verification of the stability analysis of XFLR5 was done in a document by the developers of the program.³ It compares XFLR5 to AVL⁴ and an experiment. In this document it was shown that results of XFLR5 resemble those of AVL and the experiment.

³http://www.xflr5.com/docs/XFLR5_and_Stability_analysis.pdf [accessed on 19/06/15]

⁴<http://web.mit.edu/drela/Public/web/avl/> [accessed on 19/06/15]

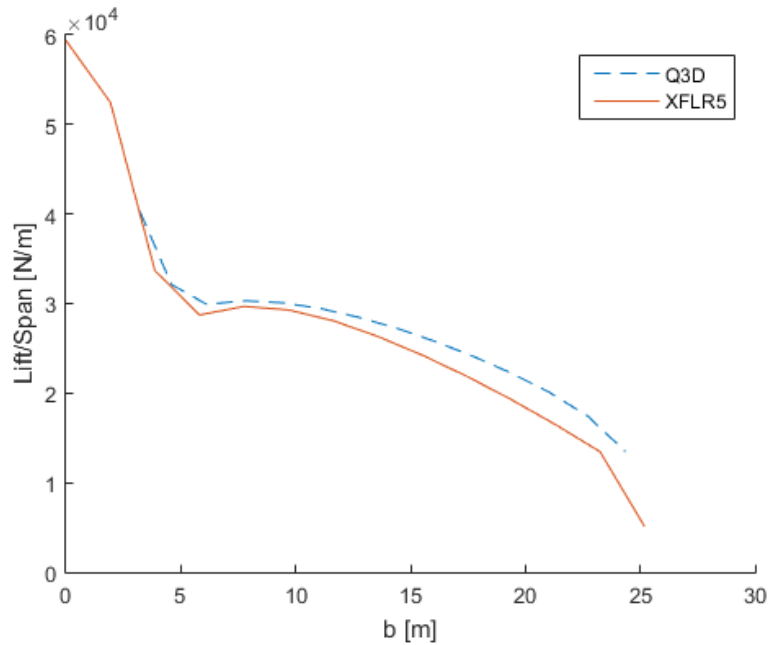


Figure 5.20: Lift distribution XFLR5 vs Q3D.

Implication of being unmanned

The implications on aerodynamics of an unmanned aircraft are minimal. Shapes do not have to accommodate humans. But the general principles are not effected by the aircraft being unmanned.

Impact on safety

A factor which greatly influences the public acceptance is safety. In this section the impact on safety because of aerodynamics will be presented.

There can be a malfunction of control surfaces. They can stop responding to commands or there is a structural failure. Either of them, would have a high intensity impact on safety. Failure of these modes will make the aircraft uncontrollable and unstable. To avoid such a catastrophic event, a mitigation strategy can be implemented. Which can be as follows:

- Strict regulations on maintenance checks.
- Software implementation which does the self testing system for safety to check for the need of repair & maintenance and predict potential operational failure and fatigue in wings structure.

Sustainability

The current design is a blended wing aircraft and hence the overall lift to drag efficiency increases which allows the aircraft to use less fuel in order to perform a certain task. This fuel efficiency as a result of aerodynamic design, makes the aircraft more sustainable and environmental friendly.

5.3 Structural analysis

Next to assuring the required flight performance and aerodynamic efficiency the design should also be capable of handling the loads it encounters during the phases of flight. This chapter will show the loads the structure has to cope with. Also the range of these loads and at which part of the structure these loads reach a maximum will be shown. After the loads acting on the

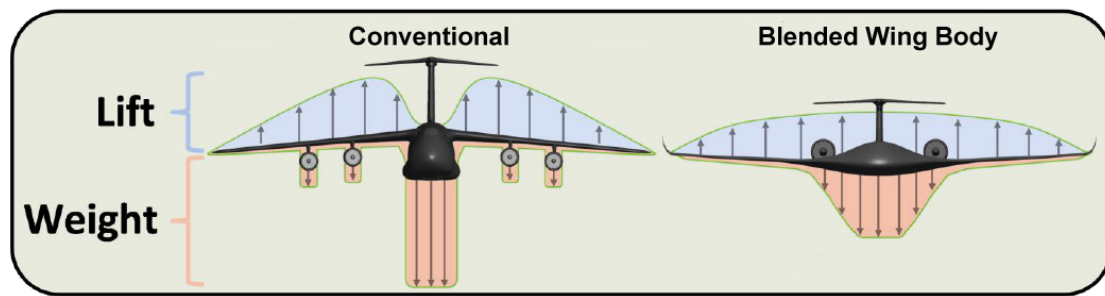


Figure 5.21: Comparison of lift and weight loads between conventional aircraft (left) and blended wing body (right) [6, p. 19].

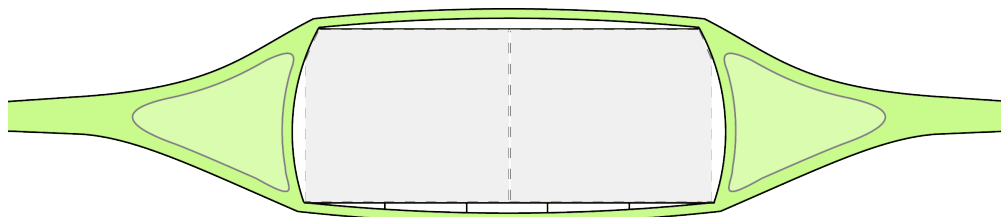


Figure 5.22: Front view of cross-section of wings and centre body showing integrated bulkhead and spar configuration.

structure have been analysed, the material selection will be elaborated on. As a last part of this section, the implications of being unmanned for the structural analysis will be stated and the impact of the structural analysis on sustainability and safety will be provided.

Structural solution

As explained in subsection 4.5.3 the multibubble cargo bay will only carry the pressure loads acting on it, a surrounding structure is needed to cope with the compression, tension, torsion and buckling loads acting on the wing and fuselage. This structure should also function as an enforcement between the cargo bay and the outer skin.

As depicted in Figure 5.21 the lift and weight distribution on a blended wing body is more distributed span wise along the wing and centre body compared to a conventional aircraft. [6] Also the large wing root bending moment at the side of the fuselage for a conventional aircraft is distributed more over the total centre body for a blended wing body. This implies that the ultimate stress acting on the transition from the wing to the centre body is less than for a conventional design. Inspired by the Lockheed Martin F-16 bulkhead design [60], the structural solution of integrated bulkheads and spars is analysed to cope with the loads. In Figure 5.22 the front view of the cross section of the wings and centre body this structural solution is depicted. Although the ultimate stress acting on the transition from the wing to the centre body is less than for a conventional design, this transition point between the centre body and wing is still expected to encounter the highest loads with respect to the mid wing and outer wing. The next section will explain the methodology used to find out how many bulkhead and spars have to be used in order to cope with the loads acting on the aircraft. In Figure 5.23 and Figure 5.24 the reference frame for the front and top view respectively, including the loads acting on the structure are depicted.

Structural analysis method

The loads and stresses that are carried by the surrounding structure are analysed by a numerical discrete element analysis. The wing is divided into n elements in its span direction, and for each of the elements the bending moments, shear forces, and torques are calculated. Depending on

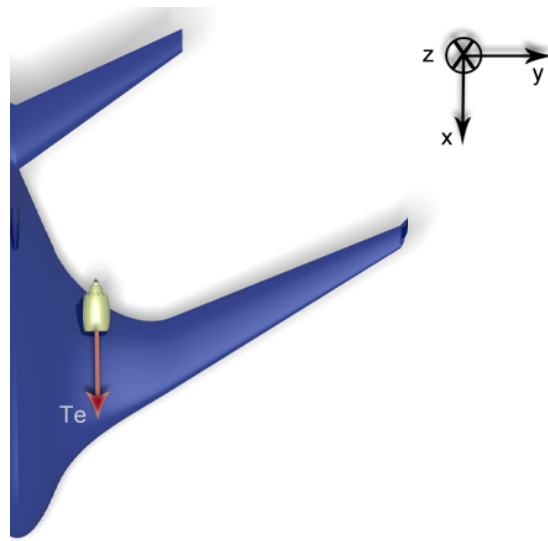


Figure 5.23: Reference frame for the top view of the aircraft including the loads acting on the structure.

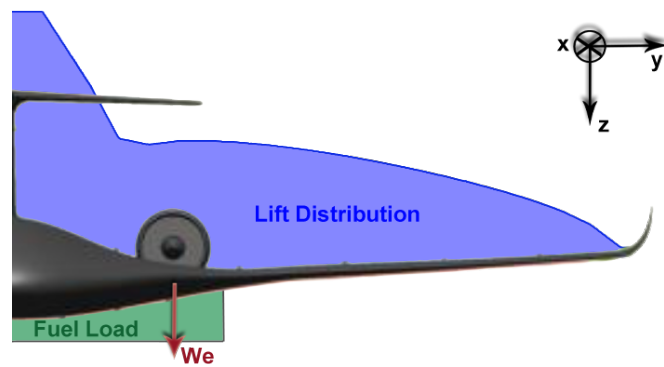


Figure 5.24: Reference frame for the front view of the aircraft including the loads acting on the structure.

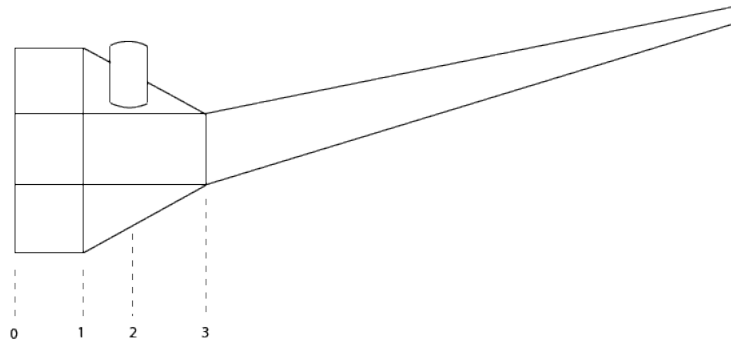


Figure 5.25: Top view of the wing box indicating the different sections analysed.

Table 5.9: Four wing sections used to model the wing.

Wing section	Cross section	Loads
0-1	Figure 5.26	Lift, Fuel weight Thrust, Engine weight
1-2	Figure 5.27	Lift, Fuel weight Thrust, Engine weight
2-3	Figure 5.27	Lift, Fuel weight
3-4	Figure 5.28	Lift

the moment of inertia, these loads can be translated in bending, shear, and ultimately Von Mises stresses.[61]

To accurately describe the loads and moments of inertia on specific wing span locations, the wing is divided into four sections, which can be seen in Figure 5.25. When going from one cross section to another, there is a change in how either the loads or moment of inertia are calculated. Which changes apply for each specific section is depicted in Table 5.9. It is assumed that the most front spar and most rear spar of the wing box are located at $0.25c$ and $0.75c$ respectively. Also, the fuel tank is located solely in the wing, i.e. it does not continue in the centre body. Furthermore, because of symmetry the structure is analysed as a cantilever beam for half its span only.

Assumptions

In order to be able to get to an appropriate estimation of the loads acting on the design, a few assumptions have to be made. Each assumption is briefly explained below. Also the assumptions are divided into primary and secondary assumption, as can be seen in Table 5.10 and Table 5.11. This division is made since the impact of the primary assumptions on the validity of the structural approach will be significantly larger than the impact of the secondary assumptions. The impact of the assumptions on the results will be reflected in Figure 5.3.

Structural Loads

In order to be conservative in the computation of the stresses the worst case scenario in flight is analysed. This implies that the lift distribution from the aerodynamics department, as provided in subsection 5.2.6, is corrected with the maximum loading factor. Also, the cargo bay is assumed



Figure 5.26: Wing box cross-section view for centre body.

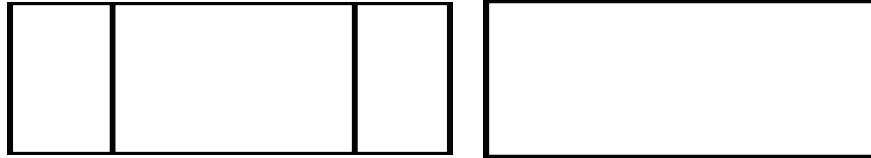


Figure 5.27: Wing box cross-section view for mid wing. **Figure 5.28:** Wing box cross-section view for outer wing.

Table 5.10: Primary assumptions for the structural analysis approach.

Primary assumptions	
1	The lift distribution, fuel load distribution, engine weight and the engine thrust are assumed as the only external forces acting on the wing.
2	Drag and the structural weight are neglected.
3	The lift is assumed to act at the quarter chord line of the wing.
4	It is assumed the wing box is symmetrically and rectangular shaped.
5	It is assumed that no deflections and no deformations take place in the wing box.
6	The centroid of the cross section of each analysed segment is assumed to be in the centre.
7	It is assumed that the spar configuration in the mid wing section can be approached as a single cell cross section instead of a multi-cell cross section.

to be empty, since the weight of cargo would decrease the bending moments caused by the lift of the wing, and therefore the Von Mises stresses as well. In the following subsections the resulting loads and stresses are plotted.

Bending moments

As explained in section 5.3 the bending moments are measured without the payload weight, since the weight of cargo would decrease the bending moments. In Figure 5.29 and Figure 5.30 the bending stress in x and z direction respectively are shown along the span of the wing and centre body.

The bending moment in x direction is influenced by the lift distribution, the fuel distribution and the engine weight. As can be seen in Figure 5.29, the lift distribution has the most impact on the bending moment, generating a quadratic behaviour. The bending moment in z direction is only influenced by the engine thrust, since it is assumed that the drag can be neglected. In Figure 5.30 this can be seen in the linear increase in bending moment from the point on the wing where the engine is located.

With these bending moments and the moments of inertia that have been determined along the cross section of the outer wing, mid wing and centre body, the bending stresses can be calculated via Equation 5.32.

$$\sigma_y = \frac{M_z}{I_{zz}}x + \frac{M_x}{I_{xx}}z \quad (5.32)$$

Table 5.11: Secondary assumptions for the structural analysis approach.

Secondary assumptions	
1	The fuel load is assumed to be constant along the fuel tank span.
2	Sweep is neglected for the torque calculations.
3	The thickness of the webs is assumed to be equal for all spars.

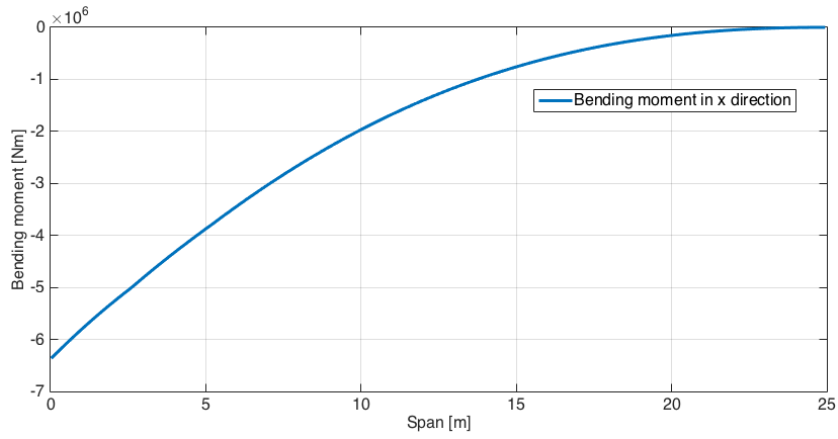


Figure 5.29: Bending moment in x direction.

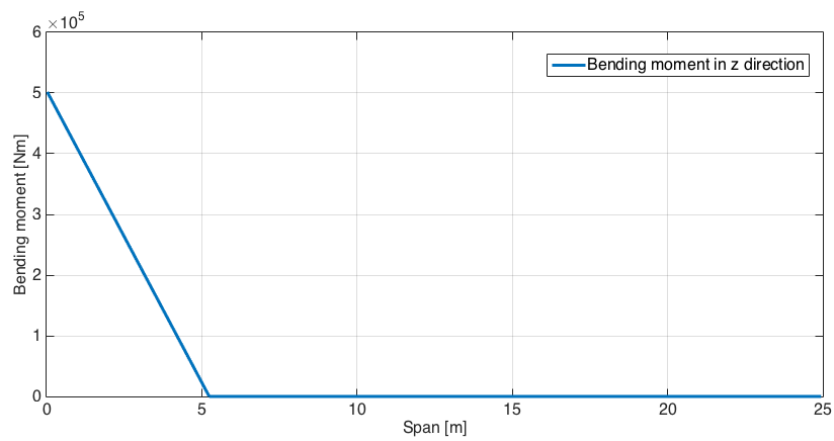


Figure 5.30: Bending moment in z direction.

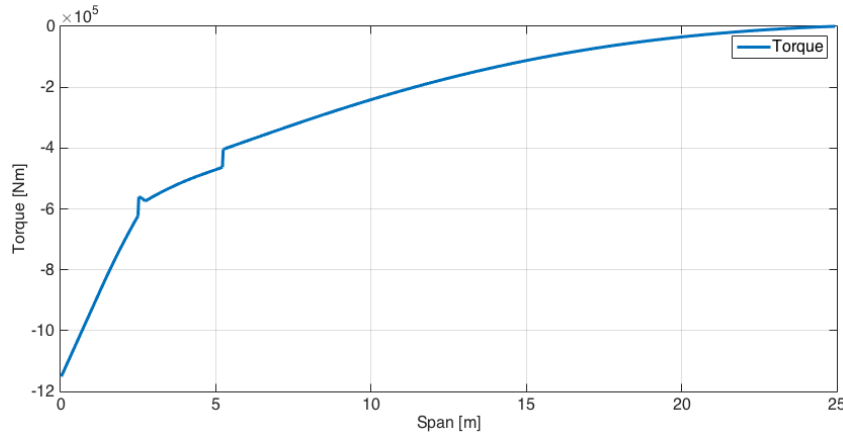


Figure 5.31: Torque distribution along the wing span.

Torque

The torque distribution is shown in Figure 5.31. This moment is mainly caused by the contribution of the distributed lift force. The lift acts at the aerodynamic centre of the wing chord, which for this analysis is assumed to be at the quarter chord line of the wing. Therefore, the lift force does not act through the shear centre of the wing box and thus induces a torque. The kink in the plot at a span of 4 meters is caused by the contribution of the engine. The influence of the engine is small: since top mounted engines are used, the thrust induced torque is counteracted by the engine weight induced torque. The kink in the plot at 2.5 meters is caused by the local decrease in lift the occurs due to wing fuselage interaction. Note that for the centre body section the torque increases linearly instead of quadratically. This is caused by the fact that wing box chord is constant in the centre body.

Shear forces

In the stress analysis of a wing often the induced bending moments have a predominant influence on the total stresses. However, most loads that cause bending stress also induce shear stresses. These also contribute to the Von Mises stresses and should thus be analysed as well. In Figure 5.32 and Figure 5.33 the horizontal and vertical shear loads are plotted respectively. The only contribution to the shear force in x-direction is the engine thrust force, therefore, for each span location larger than the engine location the shear force is zero. In the z-direction there is mainly a contribution of the lift force. At the location of the engine there is an decrease in the shear force due to the engine weight. The largest shear force in x-direction is equal to the engine thrust, $9.5 \cdot 10^4$ N, whereas the largest shear force in the z-direction is $-6.4 \cdot 10^5$ N. From the shear forces and torque the shear flows follow from Equation 5.33. The shear stresses can be computed using Equation 5.34.

$$q = -\frac{S_x}{I_{zz}} \int_0^s t x ds - \frac{S_z}{I_{xx}} \int_0^s t z ds + \frac{T}{2A} \quad (5.33)$$

$$\tau = \frac{q}{t} \quad (5.34)$$

Von Mises

Based on the bending and shear stresses, the Von Mises stresses can be calculated using Equation 5.35. The Von Mises stress plots for the four extreme locations of the wing box are shown in Figure 5.34. The bending moment is the major contributor to the Von Mises stresses. The sudden decrease in stress between the centre body and the mid wing is caused by the required buckling resistance of the centre body. In order to cope with the buckling loads in the centre

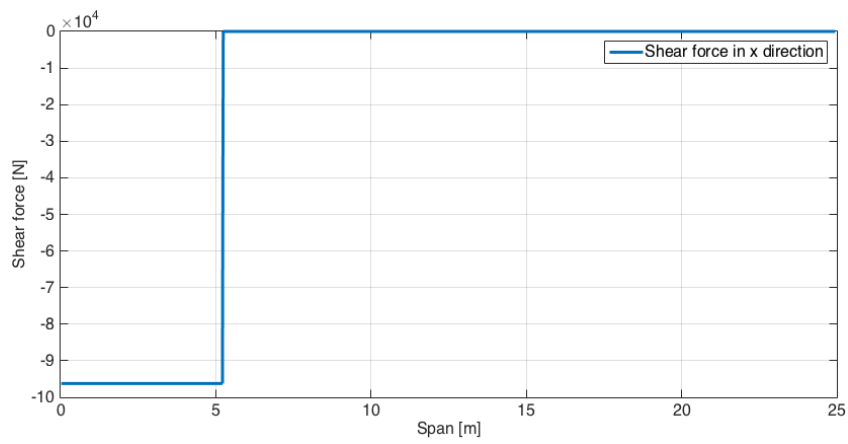


Figure 5.32: Horizontal shear force distribution.

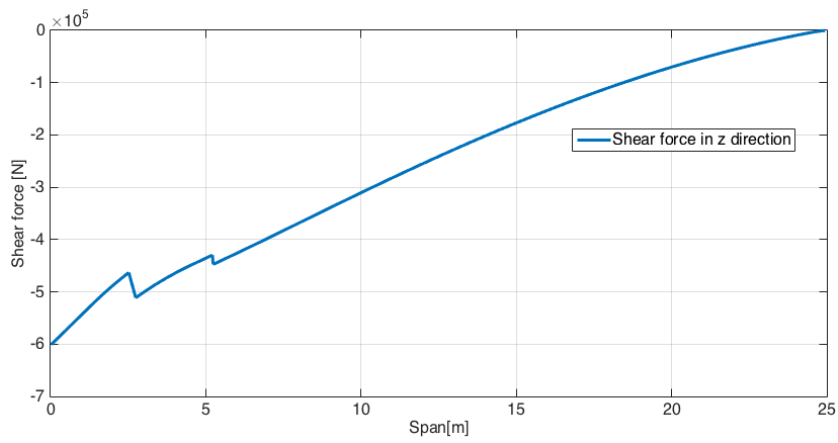


Figure 5.33: Vertical shear force distribution.

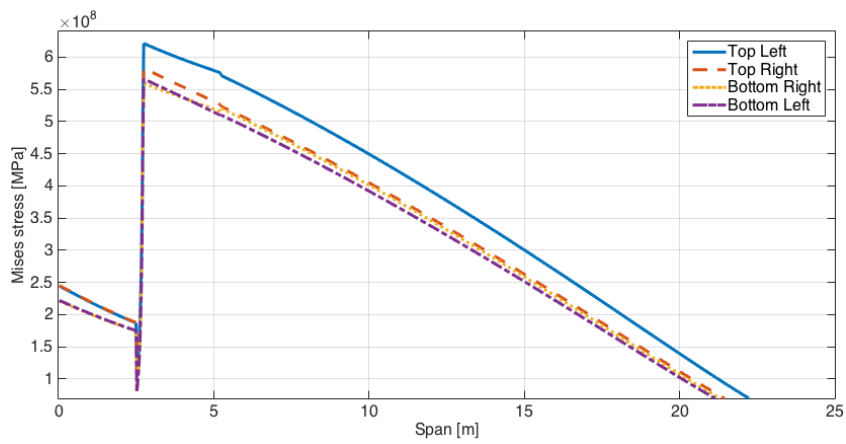


Figure 5.34: Von Mises stress.

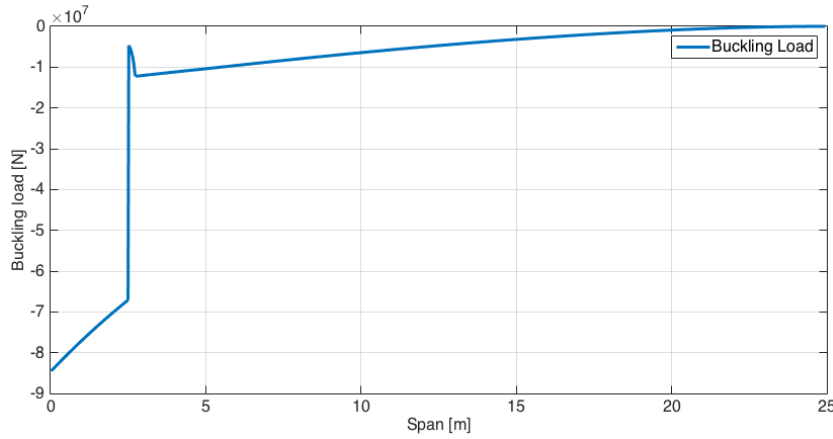


Figure 5.35: Buckling loads.

body, the required moment of inertia around the x-axis had to be higher than for the mid- and outer wing. This also increased the moment of inertia around the z-axis for the centre body, which increased the overall bending and shear strength of this cross section and thus decreases the local stresses.

All Von Mises stresses calculated have been multiplied with a 0.2 safety factor. The maximum stress of 625 MPa occurs at the transition from the centre body to the mid wing in the top left corner of the wing box.

$$Y = \sqrt{\frac{1}{2}\sigma^2 + 3\tau^2} \quad (5.35)$$

Buckling loads

The buckling load is of particular interest for this design due to the fact that there is no continuous wing box that goes through the fuselage. Therefore, the magnitude of the compressive load that is induced by the bending moment in the spars that form the bulkhead around the fuselage should be calculated. The results of these calculations (corrected with a 0.2 safety factor) are shown in Figure 5.35. Then, using Equation 5.36 [62], the minimum required moment of inertia around the x-axis can be calculated.

$$I_{buckreq} = \frac{P_{buck}L_{beam}^2}{4\pi^2 E} \quad (5.36)$$

Verification

The structural analysis module is verified using system tests. For each of the plots it is assured that the following conditions were satisfied:

1. Changes in the plot behaviour occur at logical locations along the span, i.e. at the engine location, fuel tank location, or at the transition from one wing section to another;
2. The plot curves are compliant with analytical equations, i.e. the bending moment shows quadratic behaviour or the torque shows linear behaviour at the centre body section;
3. The order of magnitude of the results are checked empirically, using [61].

The discretisation error is quantified in order to determine an acceptable number of elements in the analysis. Since it is difficult to compute the lift distribution analytically, it is decided to not compare the numerical result with the analytical result. Instead, the maximum discretisation error found for a range of n-values is defined, as seen in Table 5.12, where the discretisation

Table 5.12: Discretisation errors for various n-values.

n	$\Delta S_z(y = 10)$ [N]	% difference
10	$7.5 \cdot 10^4$	10.56
100	$7.4 \cdot 10^3$	1.13
500	$1.5 \cdot 10^3$	0.23
1000	$7.3 \cdot 10^2$	0.11
10000	70	0.02
100000	10	0.01

Table 5.13: Material properties.

Composite Type	Ultimate stress compression [MPa]	Ultimate stress tension [MPa]	Shear strength [MPa]	Young's Modulus [GPa]	Density [$\frac{kg}{m^3}$]
T-65035 3K 976 plain weave fabric	652	648	103.4	65.5	1570
T-65035 3K 976 8-harness satin weave fabric	608	707	88	66.8	1575
AS4 6k/PR 500 RTM 5-harness satin weave fabric	738	770	82.8	64.4	1565
Aluminium Alloy	Yield Stress [MPa]	Shear Strength [MPa]	Young's Modulus [GPa]	Density [$\frac{kg}{m^3}$]	
2024-T86	440		310	72.4	2780
7075-T6	503		331	71.7	2810
7178-T6	538		360	71.7	2830

errors have been defined comparing the vertical shear force using Equation 5.37. From this, the n-value, based on accuracy and computation time, was taken to be $n = 1000$.

$$Error = 1 - \left(\frac{\Delta S_z - S_z}{S_z} \right) \quad (5.37)$$

Material selection

After the loads acting on the centre body, mid wing and outer wing are analysed, a proper material had to be selected. This material should comply with the following criteria. It should be able to cope with the maximum compression and tension stresses, the maximum Von Mises stress, the maximum buckling load and should be as light as possible. Therefore the material will be analysed on the yield stress for compression and tension, the Young's Modulus E , the shear strength and the density. In the following paragraphs different types of aluminium alloys and composites will be compared.

Aluminium versus composites

For the material selection different types of aluminium alloy and composite material are analysed to find a suitable material for the design. These different material types are shown in Table 5.13 [63]⁵. As can be seen in Table 5.13 for composite materials the ultimate stress is provided as properties for compression and tension strength. This is because the fibres of the composite get brittle during yielding and the material fails. For the aluminium alloys the same yield strength is provided for compression and tension strength.

⁵<http://asm.matweb.com/search/SpecificMaterial.asp?bassnum=MA2024T6> [accessed on 18/06/15]

Table 5.14: Selected composite characteristics explained.

Code	Meaning
AS4	Commercial name for carbon fibre
6k (6000)	Amount of filaments per strand
500 RTM	500 parts per resin transfer mold
5-harness satin weave fabric	Weave pattern, the fill yarn floats over four warp yarns and under one. Multi-directional fibres

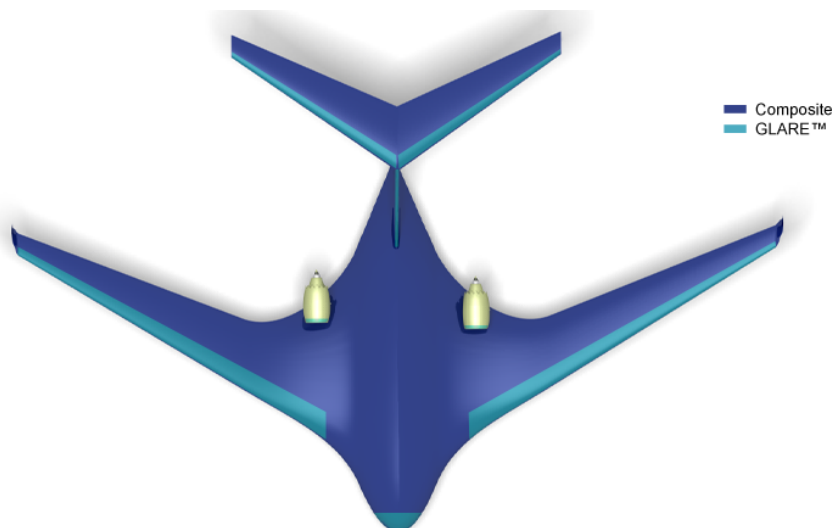


Figure 5.36: Materials used for the ATLAS structure.

During the process of selecting the most suitable material the criteria of being lightweight plays the most important role. Therefore it is found that the aluminium alloys are not suitable for the design, since their density is almost twice as large as the composite materials.

As shown in Figure 5.34 and Figure 5.35 the maximum Von Mises stress the material should be able to withstand is 625MPa and the maximum buckling load 85MN . Since the AS4 6k/PR 500 RTM 5-harness satin weave fabric composite is able to withstand this stress and load, and because it has a relative low density it was chosen as the most suitable material for the design. The characteristics for this composite are more thoroughly explained in Table 5.14. ^{6 7}

Material for impact sensitive parts of the design

As explained in Table 5.3 a composite material was chosen for the skin and structural parts of the design. However, for impact sensitive parts of the design, this composite is not favourable. For example when a bird strike would occur against the wing, a material is needed that can withstand this kind of impact. Since GLARE performs well with these kind of loads, this material has been selected for the leading edges of the wings and tail. [64] In Figure 5.36 a sketch of the material build up for the ATLAS is provided.

Matching material failure stress and Von Mises stress

From the structures module the main results are the maximum Von Mises stresses along the wing and the required moment of inertia to cope with the buckling load. As the program is not designed to find an optimal solution, it has to be checked manually whether the maximum Von

⁶<http://www.acpsales.com/Woven-Fabric-Style-Guide.html> [accessed on 18/06/15]

⁷<https://www.solidconcepts.com/technologies/composites/> [accessed on 18/06/15]

Table 5.15: The dimensions of the wing box cross-sections required to cope with the Von Mises stresses and buckling loads.

Wing box dimensions [m]					
Centre body		Mid wing		Outer wing	
Spar width	0.2	$t_{frontspar1}$	0.01	$t_{frontspar}$	0.01
Spar height	0.0904	$t_{frontspar2}$	0.01	$t_{rearspar}$	0.01
t_{flange}	0.025	$t_{rearspar1}$	0.01	$t_{topskin}$	0.005
t_{web}	0.025	$t_{rearspar2}$	0.01	$t_{bottomskin}$	0.005
$t_{topskin}$	0.007	$t_{topskin}$	0.005		
$t_{bottomskin}$	0.007	$t_{bottomskin}$	0.005		

Mises stresses do not exceed the material failure stresses as described in the material selection. If the Von Mises stresses are too high at any section, or if the required moment of inertia exceeds the actual moment of inertia, more material should be added at the critical wing section. After doing this, the program should be run repeatedly and the structure should be checked whether it can cope with the loads. The final thicknesses required in the different wing sections are shown in Table 5.15.

Conclusion

Using the above methods a preliminary estimation of the structural loads within the wing fuselage combination can be obtained. The structural analysis model translates the significant forces to stresses and is able to check for material failure, so that an initial feel for the structural dimensions can be found. However, the accuracy of the model can be improved. Most of the assumptions that are taken into account can be incorporated in the program with additional resources. For detailed recommendations, please refer to chapter 10.

Implication of being unmanned

The innovative design requirement of being unmanned also has an influence on the structural configuration. Most importantly, no windows and emergency exits are required, thereby needing fewer cutouts, which ultimately decreases the weight of the structure. In fact, the only discontinuities in the structural design are the cut-outs required for the loading and unloading.

Impact on sustainability

The sustainable design approach that is apparent throughout the design of the ATLAS is also incorporated in the structural design. With the use of composite materials for large sections of the load bearing structure, the weight of the aircraft is relatively lower compared to state of the art aircraft. Through the snowball effect the entire weight and size of the aircraft reduces, which decreases the amount of material that is needed. Also, due to the weight efficient aircraft the operational costs of the aircraft reduce, such as a decrement in the fuel requirement, which is beneficial in terms of fossil fuel depletion.

The downside of using composite materials is the end of life behaviour: most composites are not recyclable and the production of composite fibres is not a sustainable process. However, with the continuing research in biodegradable composites [65], the environmental footprint of using composite materials will be reduced by 2035.

Impact on safety

The fatigue performance of the pressure vessel is improved with the use of composite materials, which have increased fatigue performance with respect to metals [66]. This reduces the possibility of material failure in the fuselage during the operational life of the aircraft. Another advantage

of the use of composites is that defects can easily be solved by locally re-laminating the structure.

A downside of using composites is that composite materials cannot be elongated to the extent that metals can. Therefore, if the maximum stresses are exceeded and material failure occurs the strength of the structure is gone entirely, which has large impacts to being a fail-safe system. This has been solved by implementing safety factors over the found stresses. Using GLARE at impact sensitive locations, the generally bad impact behaviour of composites is tackled [64].

5.4 Stability and control characteristics

After the structural analysis has been performed, the stability and control characteristics of the ATLAS are described in this section. Firstly, the aircraft's balance is investigated. Secondly, the static longitudinal stability is researched. Thirdly, the dynamic stability of the aircraft is determined.

Aircraft balance

The aircraft balance is based on the most forward and most aft position possible of the centre of gravity (CG) of the aircraft. These CG positions are influenced by the CG position of the operational empty weight, the CG position of the fuel and the CG position of the containers when placed in the aircraft. The CG position of the operational empty weight is determined during the second class weight estimation. The result of the aircraft balance is given in Figure 5.37. Based on these CG positions the position of the landing gear can be determined. As can be seen, the front loading and rear loading are the most forward and most aft CG positions. After adding the fuel, the MTOW CG stays in between these positions.

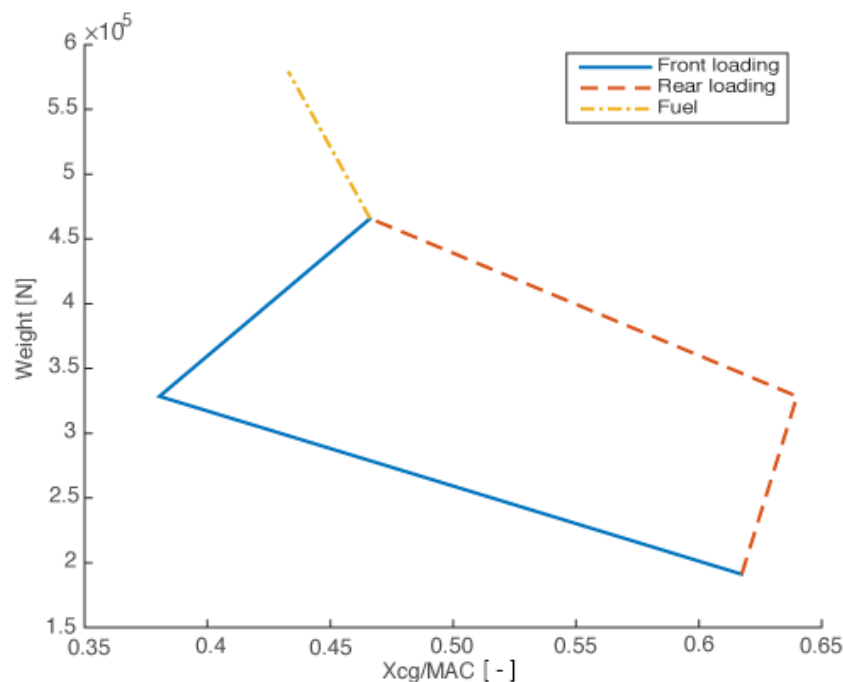


Figure 5.37: Loading diagram of the ATLAS.

5.4.1 Static longitudinal stability

The static longitudinal stability is based on the controllability and the stability curve in a so called X-plot. This plot is created with the theory from [67]. The CG ranges during flight have to be between the controllability and the stability curve. On the y-axis the ratio of horizontal tail surface area over the surface area of the wing is given. This ratio can be used to change the CG range the aircraft can fly on. In Figure 5.38 the X-plot is given for the ATLAS. As can be seen, the most forward CG position for the aircraft is between the stability and the controllability curve, which makes it both stable and controllable. This is also the case for the normal loading CG, when flying with only 2 containers in the front of the aircraft. Even when flying with two containers in the back of the aircraft, which normally is not favourable for stability, the aircraft is still stable. As can be seen in the plot, a safety margin of 5% is taken which makes sure the CG stays within the stability range.

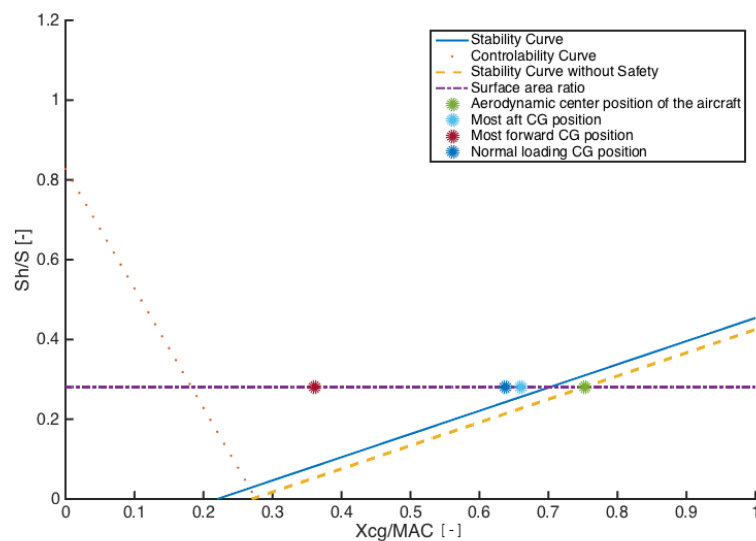


Figure 5.38: X-plot of the ATLAS showing the stability and controllability range.

5.4.2 Dynamic stability

The aircraft is subjected to five eigenmotions. The response of the aircraft to these eigenmotions are analyzed in this section. The different eigenmotions are described below.

- **Short period:** The short period mode is usually a heavily damped oscillation with a period of only a few seconds. The motion is a rapid pitching of the aircraft about the CG. The period is so short that the speed does not have time to change, so the oscillation is essentially an angle of attack variation.
- **Phugoid:** The longer period mode, called the phugoid mode is the one in which there is a large-amplitude variation of air-speed, pitch angle, and altitude, but almost no angle-of-attack variation. The phugoid oscillation is really a slow interchange of kinetic energy (velocity) and potential energy (height) about some equilibrium energy level as the aircraft attempts to re-establish the equilibrium level-flight condition from which it had been disturbed. The motion is so slow that the effects of inertia forces and damping forces are low.
- **Aperiodic roll:** Aperiodic roll mode is simply the damping of rolling motion. There is no direct aerodynamic moment created tending to directly restore the wings original position, which means that there is no returning spring force or moment proportional to roll angle. However, there is a damping moment, which is proportional to the roll rate, created by the slewing-about of the wings. This prevents large roll rates from building up when roll-

Table 5.16: Eigenvalues of the eigenmotions of the ATLAS for different flight conditions.

Eigenmotions	Begin Cruise	Mid Cruise	End Cruise
Short Period	-5.535 -0.1421	-5.536 -0.142	-5.536 -0.1437
Phugoid	-3.27e-06 + 9.63e-04i -3.27e-06 - 9.63e-04i	-3.88e-06 + 9.97e-04i -3.88e-06 - 9.97e-04i	-4.63e-06 + 1.036e-03i -4.63e-06 - 1.036e-03i
Aperiodic Roll	-1.080	-1.081	-1.082
Dutch Roll	-0.0223 + 0.462i -0.0223 - 0.462i	-0.0224 + 0.463i -0.0224 - 0.463i	-0.0225 + 0.464i -0.0225 - 0.464i
Spiral	-3.063e-05	-3.296e-05	-3.568e-05

control inputs are made or it damps the roll rate to zero when there are no roll-control inputs.

- **Dutch roll:** The Dutch roll may be described as a yaw and roll to the right, followed by a recovery towards the equilibrium condition, then an overshooting of this condition and a yaw and roll to the left, then back past the equilibrium attitude, and so on. The period is usually on the order of 3-15 seconds, but it can vary from a few seconds for light aircraft to a minute or more for airliners. Damping is increased by large directional stability and small dihedral and decreased by small directional stability and large dihedral.
- **Spiral:** The spiral mode is a mode that starts when the aircraft has an initial roll angle. If the aircraft has spiral stability, the aircraft's attitude will return to level flight conditions. However, if the aircraft is unstable in spiral mode, the roll angle will keep increasing if the aircraft is flying stick-fixed and the pilot or computer does not intervene.

The stability of the eigenmotions can be analysed by checking the eigenvalues of the first matrix in the equations of motion. The symmetric and asymmetric equations of motion are given in [68], together with their derivation. If the real parts of all the eigenvalues are negative, the motion is considered to be stable. In Table 5.16 the eigenvalues of the specific eigenmotions can be found. They are taken on begin cruise, mid cruise and end cruise flight conditions. As can be seen in the table, all the real parts are negative, which implies stability for all the eigenmotions of the ATLAS.

The response of the ATLAS to specific inputs that can initiate these eigenmotions are plotted in Figure 5.39, 5.40, 5.41, 5.42 and 5.43, being the short period, phugoid, aperiodic roll, dutch roll and spiral respectively. As can be seen, the response of the aircraft is always damping and returning to a constant value. Even the response of the spiral motion is stable, since the aircraft returns to a roll angle of 0 degrees from the initial position.

Implication of being unmanned

Spiral instability is a dangerous situation for unmanned aircraft, because when the computer fails while the aircraft is rolling, it does not recover by itself. This could be dangerous for people on the ground, since the aircraft is not able to control its emergency landing or crash position. It is thus favourable to have spiral stability for the unmanned aircraft, giving the backup systems time to kick in. Early versions of the ATLAS were not stable in spiral, but by implementing an increasing dihedral over the span of the wing made it stable. This makes the ATLAS a safer aircraft.

5.5 Financial analysis

In this chapter a financial analysis on the ATLAS is given. This is mainly done following the cost estimation methods that are given in Roskam part VIII [69]. Firstly the development, production, maintenance and operating cost are investigated. Following this, the Return on Investment (RoI) is calculated together with the Break Even Point (BEP) and finally the cost breakdown structure

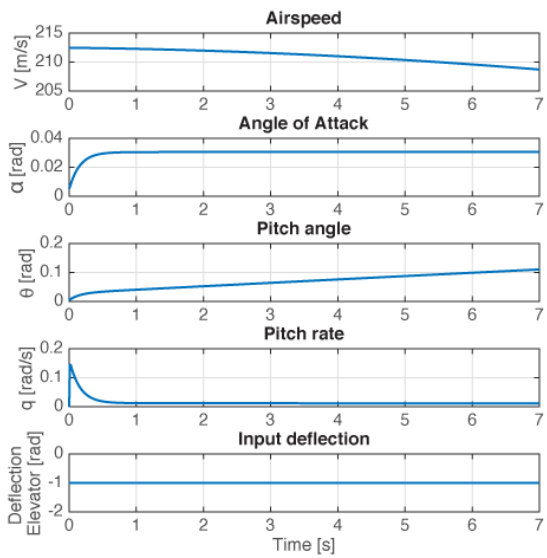


Figure 5.39: Short period: ATLAS' response to an input of -1 degree deflection on the elevator.

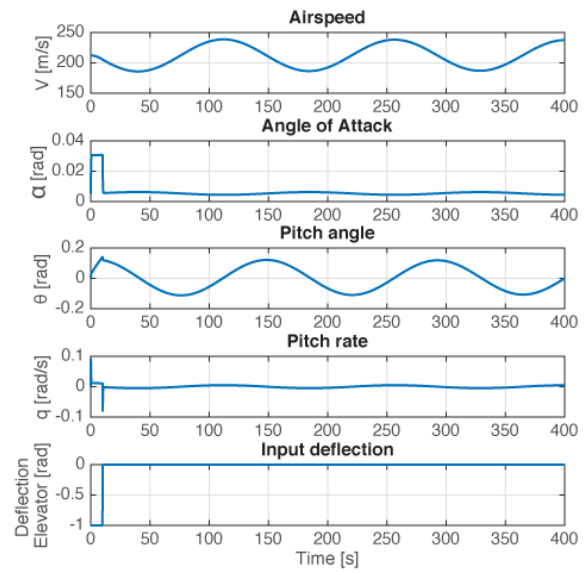


Figure 5.40: Phugoid: ATLAS' response to a step input of -1 degree deflection on the elevator.

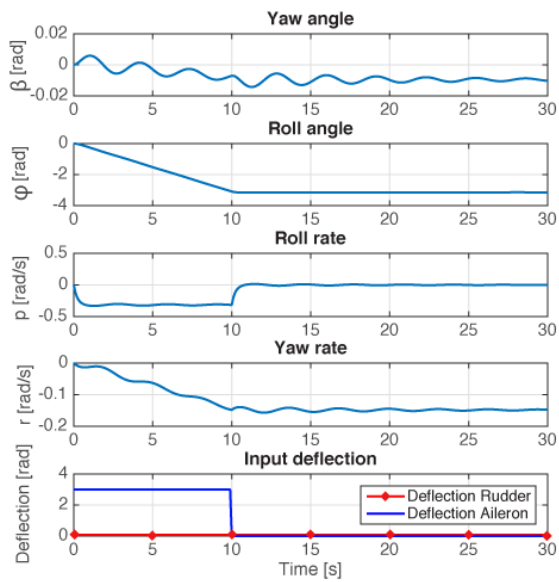


Figure 5.41: Aperiodic roll: ATLAS' response to a step input of 3 degrees on the ailerons.

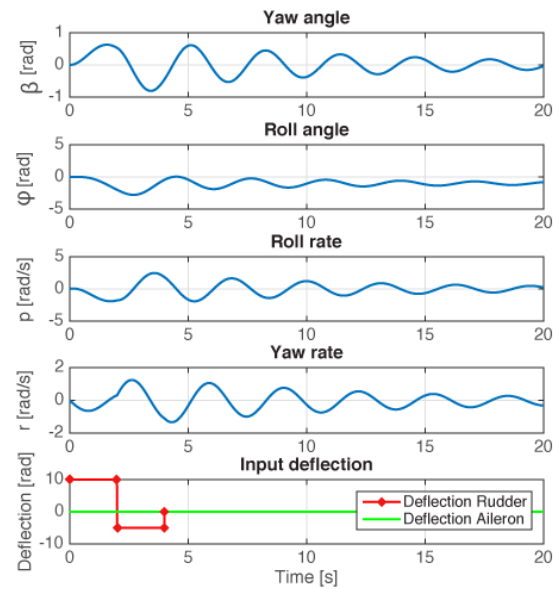


Figure 5.42: Dutch roll: ATLAS' response to step inputs of 10 and -5 degrees on the rudder.

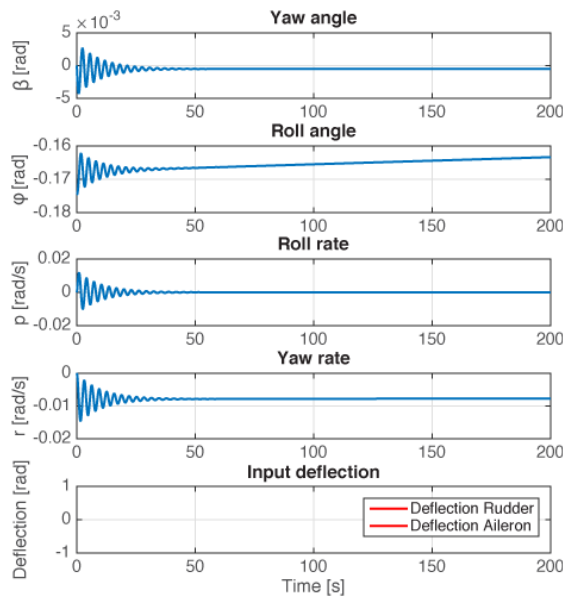


Figure 5.43: Spiral: ATLAS' response to an initial roll angle of -10 degrees.

is given for the post-preliminary design phase. As described in the section 2.5, it is assumed that 500 ATLAS aircraft will be produced. The ATLAS is also designed to have a life time of at least 40 years, which is also taken into consideration for the cost calculation.

5.5.1 Development cost

The development cost are the cost made while developing the aircraft. This depends on the following parameters.

- Airframe engineering and design cost
- Development support and testing cost
- Flight test aircraft cost
- Flight test operational cost
- Test and simulation facilities cost
- Research and development profit
- Cost to finance the Research, Development, Test and Evaluation (RDTE) phases

The total development cost for the project are 958 Million (M) USD. These are divided over the parameters as shown in Figure 5.44. Dividing the total development cost by the total aircraft produced gives the share of development cost per aircraft: 1.916 M USD.

5.5.2 Production cost

Since the mid-term review a second class weight estimation is performed. This means that the production cost can be calculated quantitatively. The unit price per aircraft depends on the following parameters.

- Manufacturing costs: Airframe engineering and design cost, aircraft program production cost, production flight test operations cost and the cost to finance the manufacturing phase.
- Profit margin: Enterprises will want to make a profit on the aircraft manufacturing activities. This profit margin is suggested to be 10% of the manufacturing costs.

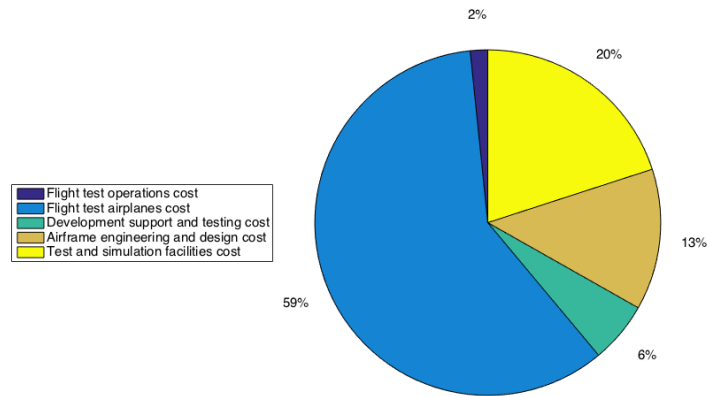


Figure 5.44: Research, development, test and evaluation cost for the ATLAS.

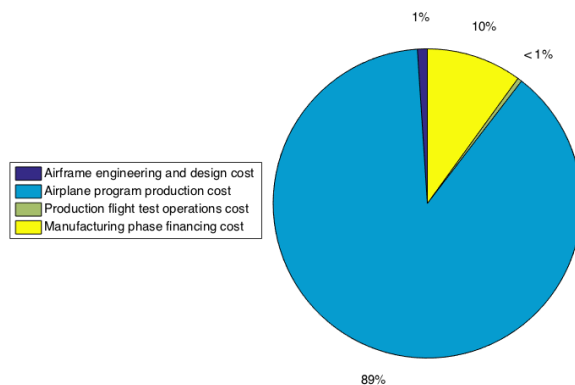


Figure 5.45: Production cost division for the ATLAS.

- Research and development costs: All the costs to develop the aircraft before it can be sold. These are calculated in subsection 5.5.1.

In Figure 5.45 the costs are depicted in a pie chart. The total production cost for the entire program are 16.3 Billion (B) USD. Dividing the total production cost cost by the amount of aircraft produced gives the share of production cost per aircraft at 32.5 M USD.

5.5.3 Maintenance cost

The maintenance cost are part of the direct operating cost (DOC) and its unit is United States Dollars (USD)/Nautical miles (nmi). The maintenance cost estimation is based on the following parameters according to Roskam.

- The labour cost of airframe and system maintenance.
- The labuour cost of engine maintenance.
- The cost of maintenance materials for the airframe and systems.
- The cost of maintenance materials for the engines.
- The applied maintenance burden.

In Figure 5.47 the maintenance cost comparison for the ATLAS is given. This is combined with the other direct operating cost to get a clear overview of the different cost contributions. The maintenance cost for an ATLAS are 1.83 USD/nmi.

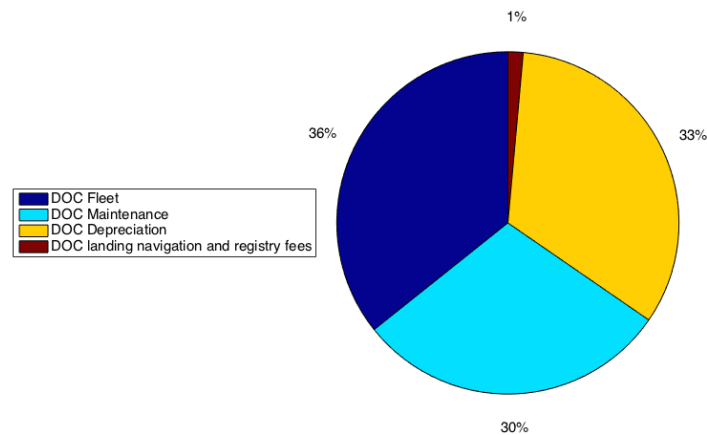


Figure 5.46: Direct operating cost of the ATLAS split in its main contributors.

5.5.4 Operating cost

Operating costs are split in two main categories, the direct operating costs and the indirect operating costs (IOC). The direct operating costs are more important for our design, since a top level requirement is stated on the DOC. The DOC are calculated in USD/nmi but can easily be converted to DOC/tkm (tonne kilometer), which gives more insight when comparing different freighter aircraft. The DOC estimation is based on the following parameters.

- Direct operating costs of flying: Crew cost, fuel and oil cost and cost of airframe insurance.
- Direct operating cost of maintenance: The maintenance cost depends on the parameters as described in subsection 5.5.3.
- Direct operating cost of depreciation: Dependant on the depreciation cost for different aircraft subsystems.
- Direct operating cost of landing fees, navigation fees and registry taxes: Dependant on landing fee cost, navigation fee cost and registry taxes.
- Direct operating cost of financing: The direct operating cost of financing the aircraft depends on how an operator is financing his fleet of aircraft.

In Figure 5.46 the DOC is split in his main parameters. In Figure 5.47 the DOC is split in all it's sub-parameters, which shows the contribution of everything to the DOC. What can be seen is that because of the high fuel efficiency of the ATLAS, the fuel share of the DOC is relatively low compared to conventional aircraft. The total DOC in USD/tonne kilometre (tkm) for the ATLAS are \$0.131. The requirement on DOC stated that the DOC should be less than 25% of the DOC per tonne of payload of a Boeing 747-400F being 0.1668 USD/Available Tonne Mile (ATM) in 1995. This is converted to USD/tkm and corrected for inflation, to 0.5455 USD/tkm. 25% of this value gives us 0.1363 USD/tkm, which means that the ATLAS DOC requirement is met.

5.5.5 Aircraft unit price and cost

Since all the main cost components are known, the aircraft unit cost and price can be calculated. The aircraft unit cost consist of the total manufacturing cost and the total research and development cost divided by the total amount of aircraft produced. This gives an aircraft unit cost of approximately 34.5 M USD, or 30.2 M EUR. This means that the requirement of aircraft unit cost being lower than 50.0 M EUR is met. This inherently gives the aircraft unit price, since the profit margin of 10% is used. The suggested aircraft unit price is 33.2 M EUR.

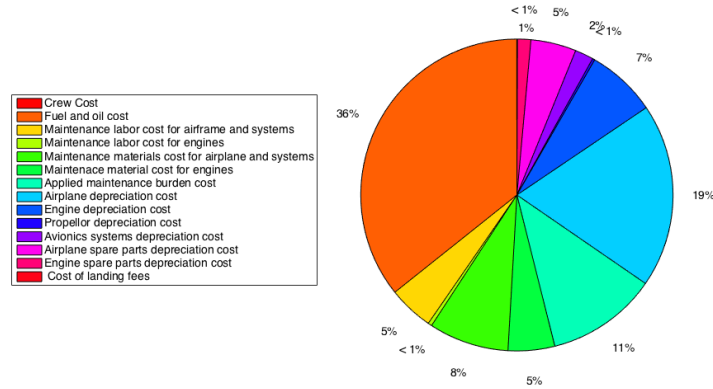


Figure 5.47: Direct operating cost of the ATLAS split in all sub contributors.

5.5.6 Return on investment

Return on Investment (RoI) is the benefit to the investor resulting from an investment of some resource. A high RoI means the investment gains compare favourably to investment cost. As a performance measure, RoI is used to evaluate the efficiency of an investment or to compare the efficiency of a number of different investments. In purely economic terms, it is one way of considering profits in relation to capital invested. The RoI for the ATLAS is calculated using Equation 5.38 from Roskam, where V_{bl} is the aircraft's block speed (373 knots), AEP ($\$3.79 \cdot 10^7$) is the aircraft unit price, tx_{inv} is the investment tax credit rate (0.10 in the US), tx_{rev} is the revenue tax rate (0.20 in the US), $U_{ann_{bl}}$ is the annual block hours flown by an aircraft (computed to be 3547 hours) and REV_{nmi} is the revenue generated per nautical mile flown, which are given in Table 5.17 for different air cargo operators, together with the corresponding RoI. The other parameters are defined before. The air cargo operators are FedEx⁸, UPS⁹ and Asia Pacific¹⁰ respectively.

$$RoI = \frac{(REV_{nmi} - DOC - IOC) \cdot V_{bl}}{AEP \cdot (1 - tx_{inv})} \cdot (1 - tx_{rev}) \cdot U_{ann_{bl}} \quad (5.38)$$

5.5.7 Break even point

The Break Even Point (BEP) is the point at which cost or expenses and revenue are equal: there is no net loss or gain, and one has 'broken even'. A profit or a loss has not been made, although opportunity costs have been invested, and capital has received the risk-adjusted, expected return. It is shown graphically as the point where the total revenue and total cost curves meet. In the linear case the break-even point is equal to the fixed costs divided by the contribution margin per unit. For the ATLAS it is calculated using Equation 5.39. All the parameters are defined before. The BEP can be found in Table 5.17 for different air cargo operators.

$$BEP = \frac{AEP}{(REV_{nmi} - DOC - IOC) \cdot U_{ann_{bl}} \cdot V_{bl}} \quad (5.39)$$

5.5.8 Cost break-down structure

The Cost Break-down Structure (CBS) contains the cost elements of the post-preliminary design project activities. It has the shape of an AND tree and serves to identify the elements that

⁸http://www.transtats.bts.gov/carriers.asp?pn=1&Sel=C&Carrier=FX&Carrier_Name=Federal%20Express%20Corporation [accessed on 18/06/15]

⁹http://www.transtats.bts.gov/carriers.asp?pn=1&Sel=C&Carrier=5X&Carrier_Name=United%20Parcel%20Service [accessed on 18/06/15]

¹⁰http://www.transtats.bts.gov/carriers.asp?pn=1&Sel=C&Carrier=PFQ&Carrier_Name=Asia%20Pacific [accessed on 18/06/15]

Table 5.17: Return on investment and the break even point given for different air cargo operators.

	FedEx	UPS	Asia Pacific
REV_{nmi} [USD/nmi]	2.4056	0.7574	1.5462
RoI [-]	1.806	0.374	1.06
BEP [yrs]	0.492	2.380	0.839

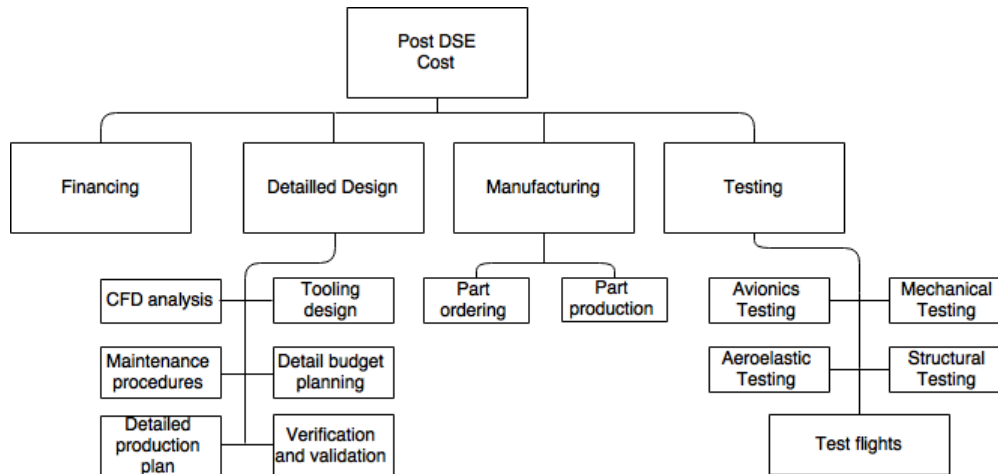


Figure 5.48: Cost break-down structure for the post-preliminary design project activities

contribute to the overall development and production cost of the product or system, for which a preliminary design has been produced. The CBS of the ATLAS can be found in Figure 5.48.

5.6 Sensitivity analysis

A sensitivity analysis investigates the sensitivity of a design (solution) for a change in major system parameters. In this report, it is primarily used to test the robustness of design options for such a change or to establish the degree of feasibility of the final design.

During any design process, major system parameters can change. This is seen during this preliminary design process and is also expected to be seen in the further development of this aircraft design. Therefore it is important to test the robustness of the design to changes in these major system parameters. This is done by performing a sensitivity analysis. For this sensitivity analysis the following major system parameters are changed.

- **Lift over drag (L/D):** A more accurate value for this will be available after a full computational fluid dynamics analysis (CFD) is performed.
- **Specific fuel consumption (SFC):** The actual specific fuel consumption of the engines will be known after testing the actual engine.
- **Operational empty weight (OEW):** The empty weight calculated is an estimation and is likely to change during the further design process. The final value will be known when the first aircraft is built and weighed.
- **Cruise speed & height:** The cruise speed & height differ from the system parameters above since they are chosen instead of estimated. However, during the design process it can occur that for optimisation they need to be changed. Since this has a large impact on the design, also the effect of these parameters on the design was evaluated.

The effect of changing these system parameters is assessed on the key performance indicators, identified to be the maximum take-off weight, production cost, direct operational cost and fuel

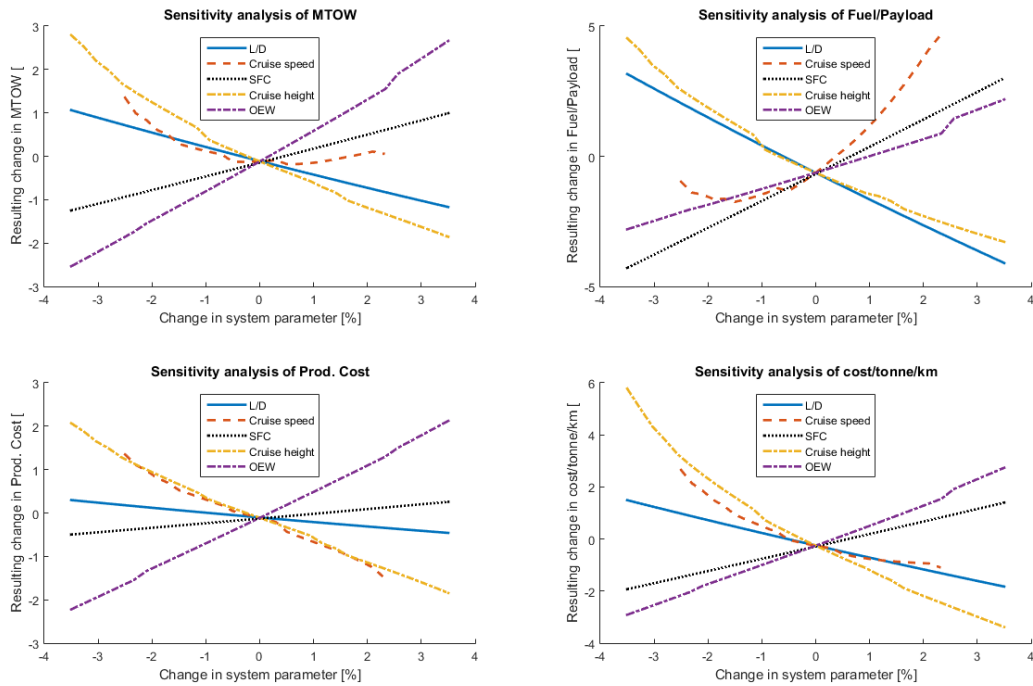


Figure 5.49: Response of key performance indicators to a change in major system parameters.

consumption. Both the fuel consumption and the operating cost are given as a percentage of payload weight. This is done to enable comparison between other aircraft. For all these characteristics, an increase will worsen the aircraft performance and a decrease will improve its performance. The results can be seen in Figure 5.49.

- Lift over drag:** As expected, an increase in lift over drag has a positive effect on all performance indicators. However, if a decrease is to be found, this would negatively influence all performance indicators. It can be seen that the most affected performance indicator is the fuel over payload. Since a low fuel consumption is one of the driving requirements for this design, further improvement of the lift over drag would be beneficial.
- Specific fuel consumption:** One of the other key factors in the fuel consumption is the specific fuel consumption. From the results presented in Figure 5.49 it can immediately be seen that an increase in engine efficiency, and thereby decrease in specific fuel consumption, leads to a reduction in operating cost and fuel consumption. Additionally, since less fuel is required, the fuel weight decreases, consequently decreasing the maximum take off weight. This decrease in maximum take-off weight also decreases the production cost.
- Empty weight:** The empty weight is an aircraft characteristic that should be carefully managed. In the aircraft development process it is often seen that the aircraft weight has a tendency to increase during the design process [67], an effect that is strengthened by the snowball effect. This effect can be seen in the sensitivity analysis; the increase in OEW leads to an increase in full consumption, eventually further increasing the MTOW. As an effect of the increase of MTOW and fuel consumption, also the production and direct operating costs increase.
- Cruise speed & height:** These are the system parameters that can be adjusted by the design team. It is however clear that their effect is more complex. A decrease in cruise speed for example leads to an increase in L/D, which then lowers the fuel consumption. The direct operating cost however increase due to the fact that they are calculated per kilometre and not per hour. A lot of operating cost components are per hour, so when it takes longer to fly the same distance it becomes more expensive. These are only a few of the effects coming into play when the cruise speed is changed. The same complication goes for the cruise height. The general trend for this however that

an increase in cruise height leads to an improved performance. This however is limited by some factors currently not in the scope of this analysis. For example the negative effect of flying higher, where the air density is lower, on the stability of the eigenmotions.

Finally it can be seen that some of the relationships are almost linear. These relationships can therefore quite easily be used to calculate the change in aircraft performance due to a change in one of the system parameters. It must be noted however that this is only shown to be valid for the current small scale of changes, i.e. between 0 and 3.5%.

5.7 Verification & validation procedures

During the design of the ATLAS, preliminary estimation tools are used to assess the complex reality of interest. These tools are therefore based on assumptions, simplifications and approximations in order to obtain the par of reality of interest. The mathematical and simulation models used by each engineering department are verified and validated during this final design phase. The sections containing these procedures can be found at the end of each corresponding chapter.

The tasks of this design are divided into multiple individual interconnected modules, which is depicted in Figure 4.1 in chapter 8. Each module has a clearly identifiable purpose, input and output values. This also enables every module to be verified individually.

Validation of ATLAS could be done using the aircraft simulation software of SIMONA, the flight simulator of the Aerospace Engineering faculty of Delft University of Technology. In this way it can be checked if the actual responses of the eigenmotions match with the calculated ones, by inserting inputs. For this a detailed model of the outer dimensions, control derivatives and other detailed characteristics have to be available and uploaded in SIMONA. Another way of validating the program is by comparing the results to an already validated CFD program. However, since this does not lay in the scope of this project, only partial validation will be done by comparing the concepts with reference aircraft or other studies where possible.

5.8 Technical risk assessment

Technical risk assessment is the activity of identifying and ranking of technical risks that may occur in the development of the system or product, with the consequence that technical performance, schedule or cost requirements are not met. To this purpose elements, characteristics, technologies or conditions are identified that may form a risk, the probability that they occur is estimated and the consequence for the success of the mission of the system, if the risk occurs, is assessed. The risks are plotted in a Risk Map, which shows on one axis the probability of occurrence and on the other the consequence. For the highest-ranking risks (high probability and consequence combination) measures in terms of alternative design or additional development activities are identified to decrease the risk (risk mitigation). In Table 5.18 the current intensity of design risks is shown. In Table 5.19 the intensity of design risks after implementing mitigation recommendations is shown.

Aerodynamics

The aerodynamic risks stem from the inaccuracy of VLM, because it analyses airflow inviscidly. Several aspects have been analysed with empirical equations and others have only been analysed with VLM. A more accurate analysis can be performed using CFD analysis, decreasing the probability that parameters change. Instability is catastrophic but less likely than an increase in drag, which is moderate.

- A1** Cruise drag is higher.
- A2** Aircraft is statically unstable.
- A3** Aircraft is dynamically unstable.

Propulsion

The engine parameters are scaled with a program that neglects fuel consumption changes. The scaling can also result in heavier engines. Engines are also expected to be improved by 2035. If this improvement falls short of expectations, the fuel consumption increases. These parameters will become more fixed while the design approaches the production date. The inlets for the engines are designed with empirical equations, a lower probability of pressure loss at the inlets can be achieved by designing with CFD analysis.

- P1** Specific fuel consumption too high.
- P2** Engines heavier than projected.
- P3** Pressure loss at inlet.

Structures

The fuselage deformation was not accounted for in the analysis due to the complex shapes. Ribs and stringers have not been designed. The fuselage may become heavier to withstand deformation. A factor has been implemented to account for these risks. To decrease the probability of these risks, the structure should be analysed with FEMs. This improves the accuracy of the design and therefore decreases the probability of these risks.

- S1** Increase in structural weight of the fuselage to withstand deformation.
- S2** Increase in structural weight because of ribs and stringers.

Operations

Airports can be slow to adept for this aircraft, since the technology of the design is new and the containers are not the current standard for air transport. Considering the timeframe until production, there is a long period to overcome this resistance. Also the aircraft can still be loaded with current ULDs, albeit less efficiently.

- O1** Airports do not adept.
- O2** Compatibility of cargo containers.

Tail

The downwash estimations for the tail were rudimentary. The incidence angle of the tail can be incorrect. A CFD analysis should be performed to determine the downwash more accurately.

- T1** Tail incidence angle is off.

Cost

The direct operating cost is dependent on the fuel price which is in direct correlation with the oil price. An increase in direct operational cost is possible but not severe.

The tooling cost can be higher than expected because the design uses new technologies. A factor has already been implemented for this, reducing the probability of this risk.

The research and development aircraft are used to test the aircraft. Due to design errors aircraft or aircraft parts might be lost in this process. This can increase the cost significantly.

The financing of the project can also be a problem. The design requires investors and the design uses a lot of new technology. To convince investors high aerodynamic performance and low fuel consumption are selling points. This decreases the probability of this risk.

The certification process might require more tests than regular aircraft since it is unmanned. This drives up the cost for the certification process. A factor has been taken into account to reduce the probability of this risk.

Cost risks end up being the most difficult risks to mitigate due to the long time frame and uncertainties. These risks have to be carefully tracked during the design process.

- C1** Direct operating cost increases.
- C2** Tooling cost higher than expected, new technology.
- C3** Research & development aircraft loss.

Table 5.18: Risk map.

	Impossible	Very unlikely	Unlikely	Likely	Very likely
Catastrophic		A2 A3			
Severe		O1, O2	P3 C3 C4		
Moderate			C2 C5	A1 P1 P2 S1 S2 T1 C1	
Marginal					
Negligible					

Table 5.19: Mitigated risk map.

	Impossible	Very unlikely	Unlikely	Likely	Very likely
Catastrophic	A2, A3				
Severe	P3	O1, O2	C3 C4		
Moderate	S1 S2 T1	A1	P1 P2 C2 C5	C1	
Marginal					
Negligible					

C4 Finance risk.

C5 Higher certification cost.

5.9 Sustainability development strategy

Sustainable development is one of the most important aspects nowadays in the aeronautical industry. To continuously reduce the human impact on the environment, it is important to implement a sustainability strategy that will be used throughout the whole life cycle of an aircraft. The sustainability strategy of this aircraft is applicable on the four different aspects of the aircraft's life cycle. These aspects are the design phase, the operational phase, the end-of-life phase and the organisation of the team that is designing the aircraft [70].

For this final design phase the objective is to translate this strategy into sustainability driven design choices. At the end of the previous chapters it was explained what decisions for the design were made to make the design more sustainable, and what the implication of this is. Therefore in this chapter the overall sustainability strategy is explained, including the sustainability strategy of the group.

Requirements

During concept trade-off in the conceptual design phase, the sustainable requirements were taken into account with a relatively high weight factor. These requirements were about the noise contour, fuel consumption and CO_2 production. During the first trade-off, the sustainability requirements were translated in to three criteria which were given large weights with respect to the whole process. The low fuel requirement received 12.1%, Low Emissions 9.3% and Low Noise 7.2% which together made up 28.6% of the all the criteria. The non sustainable concepts were eliminated in this way.

During the final trade off sustainability was given a weight of 25.1% of all the criteria. This ensured that the final proposed concept is designed for low fuel consumption, low emissions and low noise.

Environmental footprint

One of the objectives in the sustainable strategy is to design an aircraft carefully considering the impact on the climate and the planet's resources. During this design the environmental footprint is considered in the three sustainable requirements for low noise, low fuel consumption and low CO_2 emissions.

Group organisation

The group believes that a sustainable design starts with a sustainable mindset by the group itself. Therefore small things as printing as little as necessary, reusing cups, and closing laptops during discussions were agreed on from the first week on. Sustainability is a standard topic of the morning meeting, to make sure everybody pays attention to this. In the end the group thinks that the group organisation is the basis of delivering a sustainable design.

Conclusion

Concluding it can be said that sustainability is taken into account throughout the design. During the concept trade-off, for all three sustainability requirements the this concept is performing better than reference aircraft. Much effort has been put into bringing the fuel usage down. Although the fuel requirement is not met, it can be proudly said that ATLAS is 43% more fuel efficient compared to a Boeing 747-400F. Also the noise contour requirement is met, as can be seen in subsection 5.1.8. ATLAS produces 46% less emissions compared to a Boeing 747-400F. All in all it can be said that the sustainability performance of the ATLAS is significantly improved with respect to the current standard.

6 Operations

This chapter will explain the operational part of ATLAS. This chapter will start by evaluating the unmanned control. After that, the operations and logistic concept will be explained. Next, the manufacturing, assembly and integration plan will be stated. After that, the reliability, availability and maintainability (RAM) characteristics will be explained. To conclude, the data and electrical block diagrams will be described.

6.1 Unmanned control

Unmanned flying is a new development in aviation. The aircraft is either controlled by a pilot on the ground or it is programmed to be completely autonomous. The ATLAS is designed to be operated using an unmanned systems, which has implications on the overall- and subsystem-design. These implications are discussed in the chapters where the subsystems are described. This section contains the description of the unmanned control system of the aircraft. First a section is devoted to the regulations and their implication on the unmanned system. Second, the unmanned system's design is given and explained, discussing the communication flows and the sensors and subsystems used. Finally, the unmanned system's safety is assessed, using a descriptive safety protocol.

6.1.1 Regulations

Since the unmanned flying is a relatively new development in aviation, there are no regulations specified on an aircraft with such a system. Almost all unmanned aircraft flying right now are military designs and their rules are less strict than the rules for civil aviation. The European Aviation and Safety Agency (EASA) has written a policy for airworthiness certification of unmanned aircraft systems (UAS). This policy is discussed in this section and taken into account when designing the unmanned system, since this will make it easier to get the ATLAS certified. [71]

The policy statement contains the following two main objectives.

- **Airworthiness objective:** With no persons on-board the aircraft, the airworthiness objective is primarily targeted at the protection of people and property on the ground. A civil UAS must not increase the risk to people or property on the ground compared with manned aircraft of equivalent categories.
- **Environmental protection objective:** Where applicable, a UAS must comply with the essential requirements for environmental protection as stipulated in basic regulations. The top level requirements for ATLAS are already complying with these environmental regulations.

For the routine certification of civil UAS, existing type-certification procedures are retained. However, in the future a type-certificate specifically for UAS will be created. Guidance from EASA to get a UAS certified is given below.

Ground/control station

The control station and any other equipment remote from the aircraft can be considered as a 'part and appliance' on the grounds that it is functionally attached to the aircraft and has the same characteristics as parts and appliances installed in an aircraft. Accordingly, UAS control stations and other remote equipment performing functions that can prejudice take-off, continued flight, landing or environmental protection shall be considered as part of the aircraft and included in the type-certification.

Demonstration of capability

Normal aircraft are certified by demonstrating their capabilities in a so called design organisation approval. However, alternative procedures may be accepted based on appropriate justification that the UAS is reaching its requirements. This is accepted because the process of demonstrating the capability of an aircraft has not yet been rewritten for UAS.

Airworthiness codes

UAS certification will be based on a determination of equivalence with the existing Certification Specifications (CS). For the ATLAS this means it has to comply with CS-25. EASA states that it can be expected that dedicated UAS codes or sub-parts will be developed when additional UAS certification experience is gained. This type-certification basis will consist of certification specifications selected and tailored from the applicable manned aircraft airworthiness codes. Next to this, special conditions and interpretative material related to UAS specifics is added, where existing requirements do not contain adequate or appropriate safety standards.

Emergency recovery capability

While there is no mandatory airworthiness requirement to fit or configure systems to provide an emergency recovery capability, it is advised to fit such a system in order to mitigate the effects of certain failure conditions. Such a capability will normally consist of either:

- A flight termination system (e.g. an aircraft recovery parachute) which aims to immediately end the flight and to reduce the kinetic energy at impact. This however does not necessarily ensure the impact point location.
- Emergency recovery procedures with functions that could be implemented through UAS flight crew command or through an automatic pre-programmed course of action. This is intended to navigate the unmanned aircraft to pre-selected emergency sites and then to make a safe landing or to have a controlled crash.

In providing an emergency recovery capability, it should be accepted by airlines that the unmanned aircraft may suffer loss or damage as a consequence of its use, but no additional hazard must be created to persons or property on the ground. If the emergency recovery capabilities rely on the pre-selection of emergency sites, the following guidelines on emergency sites are provided by EASA:

- Emergency sites shall be unpopulated areas.
- Factors such as gliding capability and emergency electrical power capacity should be considered in determining the location of emergency sites.
- When assessing the total probability of UAS catastrophic events, failure to reach those emergency sites should be taken into consideration.
- Any assumptions made at type-certification as to the location of emergency sites should be identified as a limitation in the flight manual.

Command and control link

Consideration of the following airworthiness factors will be included in the UAS type-certification basis according to EASA:

- The UAS flight crew (if necessary) should be provided with a continuous indication of the command and control link signal strength together with the maximum link range.
- Any single failure in the command and control system (uplink or downlink) should not affect normal control of the unmanned aircraft.
- Uplinks and downlinks are sensitive to electromagnetic interference. The command and control link should be adequately protected from this hazard.
- Contingencies for failures or interruptions of the command and control link must be defined and evaluated as part of the airworthiness certification. Some examples are lapse times, intermittent failures, alternate modes of command and control and total loss of the command and control link.

Level of autonomy

The level of UAS autonomy is likely to have impact on the following certification issues. These should be taken into account when designing the unmanned system.

- Human machine interface (trading autonomy level versus the possibility of UAS flight crew intervention)
- Compliance with Air Traffic Control (ATC) instructions
- Command and control link integrity
- Handling of UAS failures and compliance with safety objectives
- Specific autonomy techniques which have to prove safe behaviour
- Collision avoidance
- Type of airspace
- Avoidance of noise sensitive areas and objectives

System safety assessment

The system safety assessment should consider the system characteristics of a UAS design viewed as a whole and not confined to the unmanned aircraft. Compliance with the safety objectives can be shown by taking into account any mitigating provisions such as an emergency recovery capability, if provided. However, the use of the emergency recovery capability should not be used as a 'catch-all' for every failure case or every non-compliance.

6.1.2 Unmanned system design

The goal of the unmanned control system is to control the aircraft in a safe manner. First, basic requirements are stated on the unmanned control system. Second, the communication flows of the system are depicted in some diagrams. Third, the communication between ATC, the control room and the aircraft is described. Finally, the appropriate sensors and subsystems of the unmanned system are investigated.

Requirements

Following the regulations, requirements can be created that should be satisfied by the unmanned control system. These requirements are stated below.

UCCF-Tech-UAS-01 The aircraft shall be designed to perform the flight unmanned.

UCCF-Tech-UAS-02 The aircraft shall be able to communicate with Air Traffic Control.

UCCF-Tech-UAS-03 Air Traffic Control shall be able to communicate with the aircraft.

UCCF-Tech-UAS-04 The aircraft shall be able to navigate using a navigation system.

UCCF-Tech-UAS-05 The unmanned control system shall be fail-safe.

UCCF-Tech-UAS-06 The unmanned control system shall navigate the unmanned aircraft to pre-selected emergency sites to make a safe landing or a controlled crash, when an unrecoverable failure occurs.

UCCF-Tech-UAS-07 The unmanned control system shall be able to control the aircraft in all its operations.

Communication flow diagrams

The basic communication flow is depicted in Figure 6.1 and Figure 6.2 for respectively flight preparation and flight operations.

Flight preparation communication

The preparation for flight communication flow diagram starts with a flight plan, consisting of way-points, inputted by the airliner. This data is decrypted and send to the data handler. The data handler performs a subsystem check of all the aircraft's subsystems and the subsystems report their status to the data handler. This status is send to the data encryption module, together with the proposed way-points. The way-points are send to ATC and the aircraft's status

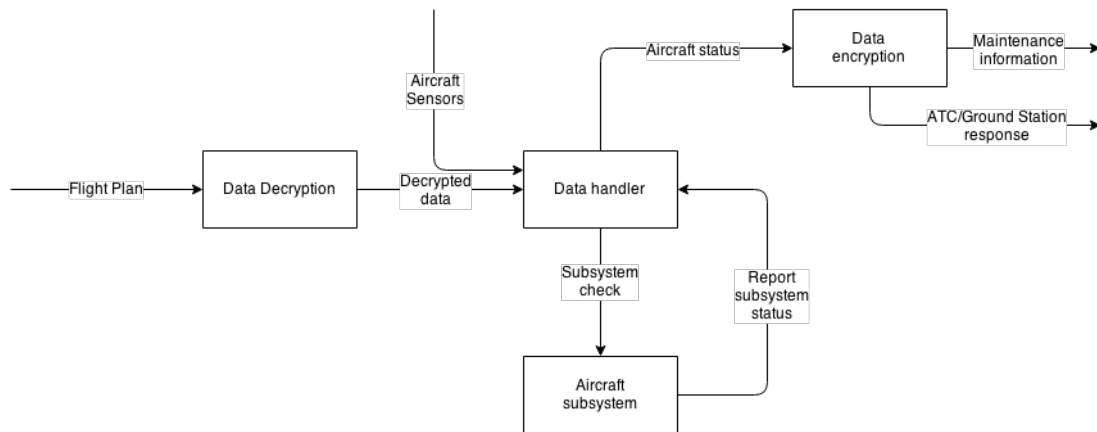


Figure 6.1: Communication flow diagram of the aircraft while preparing for flight.

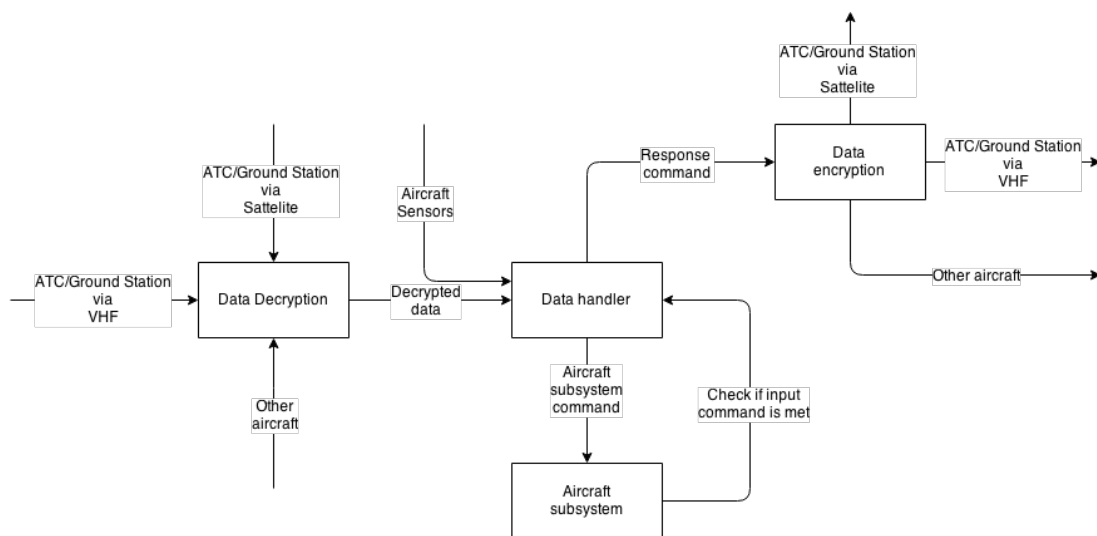


Figure 6.2: Communication flow diagram of the aircraft during flight operations.

is send to the airliner maintenance crew and the ground station. If necessary, they can perform maintenance operations before flight.

Flight operation communication

The flight operations flow starts with an input command from either Air Traffic Control (ATC) (via satellite communication, Very High Frequency (VHF) communication or the transponder), from other aircraft in the neighbourhood or the airliner’s ground station. This data is encrypted to make sure that the aircraft cannot be hacked. Than, the data is decrypted and send to the data handler. The data handler uses input from the aircraft’s sensors and sends a command to the aircraft subsystems that perform the required actions to fulfil the incoming command. The aircraft subsystems send their status back and together with the aircraft sensors it is checked if the input command is met. If necessary, a response is sent to the data encryption module which will send a response to either ATC, other aircraft or the airliner’s ground station.

ATC, control room and aircraft communication

The communication between ATC, the control room, the aircraft and vice versa is currently done using Very High Frequency (VHF) communication, satellite communication or the aircraft’s transponder. A general overview of this communication is given in Figure 6.3. The same communication methods can be used when flying unmanned, provided that the flight computer is adapted in such a way that it can process these commands to the aircraft’s subsystems. Very

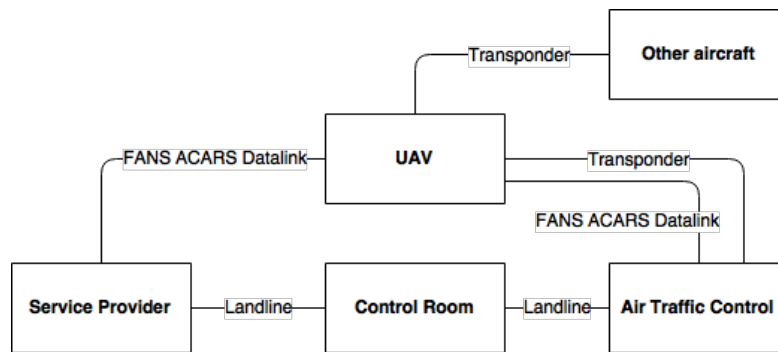


Figure 6.3: Communication flow diagram between ATC, the control room, the service provider, the UAV and other aircraft.

High Frequency is used when the aircraft is flying over land or in range of the on land radio towers. The satellite communication system is used when flying over the ocean and/or being out of range of the land towers. An airliner can use this communication system from different Communication Service Providers (CSPs). This is mainly done via the Future Air Navigation System (FANS-1/A) datalink communication environment, in combination with the Aircraft Communications Addressing and Reporting System (ACARS). An illustration of the high level FANS ACARS datalink service provider networks is shown in Figure 6.4, with an explanation given below. [8]

ATC is connected to the network of the CSP to whom they have contracted the FANS-1/A service. A CSP FANS-1/A service enables a FANS-1/A air traffic controller access to the datalink networks supporting FANS-1/A through providing the required connectivity to a FANS-1/A air traffic controller and providing an inter-networking function with other CSPs. The inter-networking function enables ATC to address all of their uplinks to a single CSP address such that ATC does not need to keep track of what specific CSP network an aircraft is currently using. The connected CSP then determines whether or not to attempt delivery over its own datalink network or to send via the inter-networking link to another CSP network for delivery. ATC inter-networking allows airlines to have their choice of CSP and participate in ATC datalink services regardless of what CSP a given air traffic controller is connected to. Airlines have different preferences for what CSP they use and sometimes they may also have different CSP preferences based on datalink media and region.

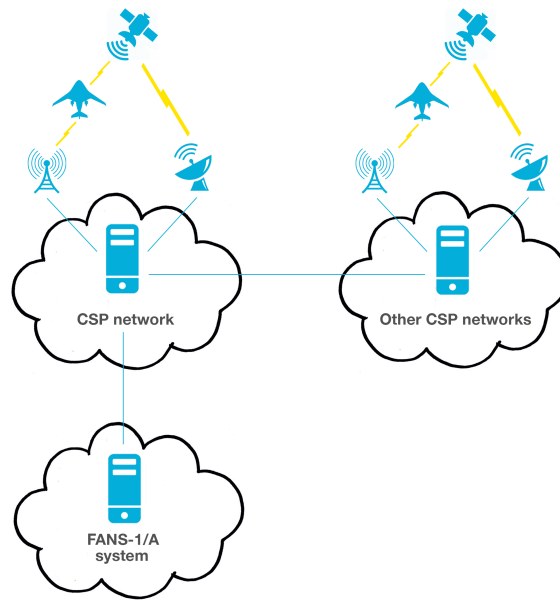


Figure 6.4: FANS ACARS datalink service provider networks.

The uplink and downlink can either be performed via VHF (transponder) or satellite communication. This is dependant on the position of the aircraft. SATCOM is one of the biggest CSPs and their satellite coverage for the communication (using Inmarsat) is given in Figure 6.5. The datarates that can be reached via Inmarsat are 10.5 kbps (kilobits per second). If lower datarates can be used, Inmarsat also provides 600 bps and 1200 bps data channels.

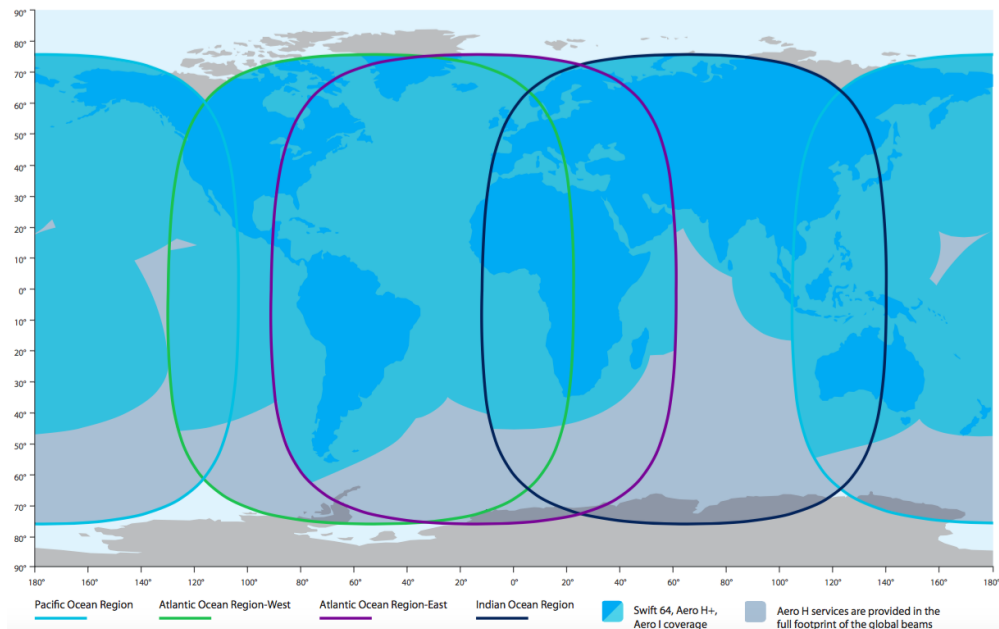


Figure 6.5: SATCOM satellite coverage using the Inmarsat satellites [8].

Using the satellite communication system is more expensive and only used when necessary, for example when flying over the ocean. If possible, it is preferred to use the VHF network. The worldwide VHF ACARS coverage is given in Figure 6.6. The old VHF ACARS protocol is able

to have a datarate of 2400 bits per second (bps), while the newer VHF mode 2 is able to reach datarates of 31.5 kbps. The satellite and VHF coverage combined makes it possible for the ATLAS to fly almost everywhere.

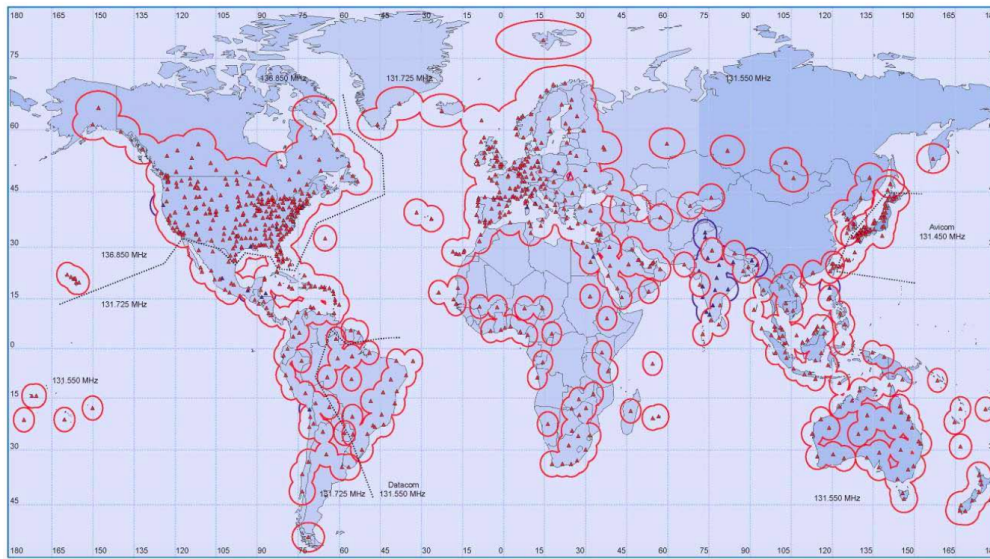


Figure 6.6: Worldwide VHF ACARS coverage [8].

Sensors and subsystems

The unmanned cruise flight is performed by flying over pre-programmed way-points. To make sure all other phases of the unmanned flight can be performed safely as well, the following sensors and subsystems are implemented in the aircraft. Their relation is discussed in subsection 6.5.1 in Figure 6.16.

- **Lidar:** A forward looking Doppler lidar is used to detect the wake vortices generated by aircraft, since they can be a potential hazard for other aircraft flying too close to these vortices. Pilots can often estimate the distance they have to fly behind other aircraft based on experience, but for unmanned aircraft a dedicated system is required.
- **Cameras:** Four cameras are placed on the aircraft to have a visual view around the aircraft. These cameras can be used during taxi, take-off and landing to position the aircraft correctly with respect to the taxiway and runway, next to the Instrument Landing System. Two cameras are enough to create the desired 3D image, but extra cameras are taken on board for redundancy.
- **Thermal imaging:** When flying at night, the cameras cannot be used as efficient as during daytime. To make sure the aircraft can also operate at night, four thermal imaging cameras are placed on the aircraft so a desired 3D image can be created. Again, two extra cameras are taken to be redundant.
- **Traffic collision avoidance system (TCAS):** A traffic collision avoidance system or traffic alert and collision avoidance system is an aircraft collision avoidance system designed to reduce the incidence of mid-air collisions between aircraft. It monitors the airspace around an aircraft for other aircraft equipped with a corresponding active transponder, independent of air traffic control, and warns the ATLAS of the presence of other transponder-equipped aircraft which may present a threat of mid-air collision. It is a type of airborne collision avoidance system mandated by the International Civil Aviation Organisation to be fitted to all aircraft with a maximum take-off mass (MTOM) of over 5,700 kg.
- **FLARM:** FLARM is a small-size, low-power device which broadcasts its own position and speed vector (as obtained with an integrated GPS) over a license-free ISM band radio transmission. At the same time it listens to other devices based on the same standard.

Intelligent motion prediction algorithms predict short-term conflicts and warn the aircraft's system accordingly. FLARM incorporates a high-precision 16-channel GPS receiver and an integrated low-power radio transceiver. Static obstacles are included in FLARM's database.

- **Ground proximity warning system (GPWS):** Uses a radar altimeter to detect proximity to the ground or unusual descent rates. GPWS is common on civil airliners and larger general aviation aircraft.
- **Terrain awareness and warning system (TAWS):** Uses a digital terrain map, together with position information from a navigation system such as GPS, to predict whether the aircraft's current flight path could put it in conflict with obstacles such as mountains or high towers, that would not be detected by GPWS (which uses the ground elevation directly beneath the aircraft). This digital terrain map could also be used to find a suitable emergency landing position.
- **'Smart' computer:** The 'smart' computer system consists of two computers. One main computer and one backup computer that can perform the same tasks as the main one. The computer can make decisions on its own, based on the input data given to it and its predetermined flight plan. If the computer is not sure on what decision to make, it can communicate with the airliner on the ground, so human intelligence can decide on further action.
- **Communication subsystem:** Commands via the communication subsystem can be given via a command and control link (C2-link), which uses either the FANS ACARS protocol or the aircraft's transponders. It also uses a GPS system to determine its position, so the aircraft can check if it is still flying according to its flight plan.

6.1.3 Unmanned system safety

To ensure that the unmanned system is safe, a descriptive system has been designed to mitigate certain safety risks. It uses the following system modes:

- **Emergency recovery mode (ERM):** Control room is warned. On-board computer tries to find solution by looking for an alternate component/system that can take over the function of the failing component/system.
- **Forced landing mode (FLM):** Control room is warned. Nearest airport is autonomously located and contact is made with ATC to make an emergency landing.
- **Emergency landing mode (ELM):** Control room and ATC warned. This flight termination can always be initiated from ground control room, even if some systems are failing. Nearest airport is located by system and decision is made if A/C can make it there with current conditions, if not an emergency landing is initiated by selecting an emergency landing site. This site is selected based on wind, surroundings, size, shape, surface, slope and civilisation. The system checks which systems are not working. For example, if the landing gear is not working, a belly landing is initiated. For loss of thrust a weighted decision is made if gliding to a nearby airport is possible. If flaps are not working a new landing distance is determined. For each component failing the emergency landing is simulated by the on-board computer to have a controlled crash. After landing power is turned off and emergency signal is given. A prediction is made where the aircraft will land, which is communicated with the control room.
- **Ground handling mode (GHM):** During the ground handling process this mode will make sure the refuelling and loading of the aircraft is done safe.
- **System reboot mode (SRM):** Control room is warned. The A/C starts loitering while system is rebooted.
- **Loitering mode (LoitM):** Control room and ATC are warned. The aircraft starts loitering and warns aircraft in its proximity.

These modes are used in Table 6.1 to make sure that the aircraft is safe. The failure modes are split in aviatational, navigational, communication and mitigation failures. Note that for the preliminary design only single failures are mitigated. For the detailed design, common combinations of failures should be assessed as well.

Even with a lot of sensors in the subsystems of the aircraft to detect failures, it is still possible that undetected failures occur. The undetected failures are difficult to mitigate. That is why the unmanned control system should be designed in such a way that failures can be detected. This can be done by simulating the response of the aircraft to different inputs it can give to its subsystems. If the response does not match the response of the simulation, the aircraft 'detects' the undetected failure. In this case the aircraft should assess if it can 'learn' to control itself again by monitoring its response to inputs it is giving to its subsystems. If this is possible, the aircraft should go in forced landing mode. If the aircraft becomes uncontrollable it should go in emergency landing mode. If the aircraft crashes, research on the black boxes and the aircraft itself should show what caused the crash. The cause of the crash should be assessed and a solution should be implemented in all other aircraft, if possible.

Table 6.1: Unmanned control safety design.

Function	Failure	Consequence	Mitigation
<u>AVIATE</u>			
Control flight path (FP)			
Determine FP state	Detected loss of function of sensors	Without FP info such as attitude continued safe flight cannot be assumed.	ERM is activated, if alternate solution is not found after 10 min ELM is activated.
Determine guidance command	Detected loss of function to create command autonomously	A/C is unable to create command and is autonomously uncontrollable.	ERM is activated, system rebooted, if this does not work Control Room enters FP command manually
Produce guidance command	Detected loss of function to give FP command	Nor A/C or control room can change FP. The aircraft is autonomous and manually uncontrollable however last given command can be used as prediction for crash site.	ERM is activated, if no solution is found ELM is activated
Execute guidance command	Detected loss of function of actuators	A/C is uncontrollable because no guidance commands changes are possible. For example aileron failure or loss of propulsion.	ERM is activated, if solution using alternate actuators is not found after 10 min ELM is activated.
Landing control			
Determine FP state	Detected loss of function of sensors	Without FP info such as attitude continued safe flight cannot be assumed.	Abort landing, LoitM and ERM are activated, if solution is not found EML is activated.
Determine landing command	Detected loss of function to create landing command autonomously	A/C is unable to create command and cannot land autonomously controllable.	Abort Landing, activate ERM, system rebooted, if this does not work Control Room enters FP command manually

Produce landing command	Detected loss of function to give landing command	Nor A/C or control room can change FP. The aircraft is uncontrollable however last given command can be used as prediction for crash site.	ERM is activated, if no solution is found activate ELM
Execute landing command	Detected loss of function of actuators	A normal controllable landing is not possible because landing gear fails to deploy or due to Aileron failure or loss of propulsion.	Abort landing, activate LoitM and ERM, if solution is not found EML is activated.
Take-off control			
Departure command	Detected failure of subsystems	A normal take-off is not possible	Abort take-off, activate ERM.
Execute TO command	Detected loss of function of sensors or actuators	A normal controllable take off and flight is not possible	Before V1 abort TO, after V1 continue TO and start EML
Monitor and record UAS data	Detected loss of function	UAS is not able to reproduce state data in case of incident	ERM is activated, if needed system reboot, FL is activated
<u>NAVIGATE</u>			
Convey navigation state	Detected loss of function	A/C loses awareness of location and environmental conditions concerning FP	ERM is activated, system reboot, control room/UAS rely on ATC for guidance
Determine FP	Incorrect FP	Potential conflict with other A/C, environmental conditions, terrain or obstacles.	Sensors will detect conflicts plus monitoring by ATC and control room provide safety back up, manually adjust FP from control room
Determine next way-point	Detected loss of function	A/C unable to continue FP	Work with ATC and Control Room to plan next part of flight, if necessary abort mission
Determine right-of-way rules	Incorrect right-of-way rules are determined	A/C can create dangerous situations	ATC will monitor right-of-way violations, Control Room will contact ATC and update system if needed FLM is activated
<u>COMMUNICATE</u>			
Broadcast communication	Detected loss of communication	A/C detects loss of Voice Communication to ATC and other aircraft	ERM is activated to search for alternate way to communicate, if not control room uses alternate communication (land line) to keep contact with ATC

Broadcast Transponder data	Detected loss of communication	A/C more likely to collide with another aircraft and its transponder is not detected by ATC	A/C has its own UAV detect & avoid anti-collision system. ATC uses secondary radar to detect transponders and will know A/C has lost transponder function with primary radar. Control room communicates with ATC for guidance.
C2 Link	Detected loss of command and control link	Control room is not able to send commands or control the aircraft, it is now fully autonomous	Activate ERM
Receive communication	Detected loss of communication	No incoming communication possible with ATC or other aircraft. For example due to failure of antenna. Command and control is still intact.	Activate ERM, if alternate communication with ATC (e.g. via control room through land line) is not found, activate FLM
Receive transponder data	Detected loss of function	A/C does not receive data from other A/C and changes on collisions increase	Use detect & avoid as collision avoidance and contact ATC for assistance.
MITIGATE			
Detect air traffic	Detected total loss of function	Possibility of conflict with another A/C. This can be due to failure of detect & avoid anti-collision system	ATC provides separation under assumption of being in class A airspace under IFR.
Avoid vertical ground obstacles	Loss of function	Increased probability for collision. E.G. due to failure of TAWS	Activate ERM to restore TAWS, if not successful, warn control room and ask ATC for guidance
Avoid obstacles while taxiing	Loss of function	Increased probability for collision.	Activate ERM to restore camera function. If camera function cannot be restored, abort taxiing.
Avoid adverse environmental conditions	Detected loss of function	A/C might enter unforeseen environmental conditions and lose control if weather radar has failed	ATC warns A/C and will give new weather avoidance directions and clearance for detour. In case of loss of control activate ELM.
Protect against hacks	Detected hack	Command over aircraft can be taken over	C2 link is disconnected, emergency signal broadcasted, EMR is activated, if hack is not resolved FLM is activated

6.2 Operations and logistic concept

Since one of the top level requirements is to speed up the ground operations it is important to get an overview of the chain of events during ground operations. Two chains will be examined in detail, firstly the chain of events during the the cargo loading events chain and secondly the turn around time (TAT) chain.

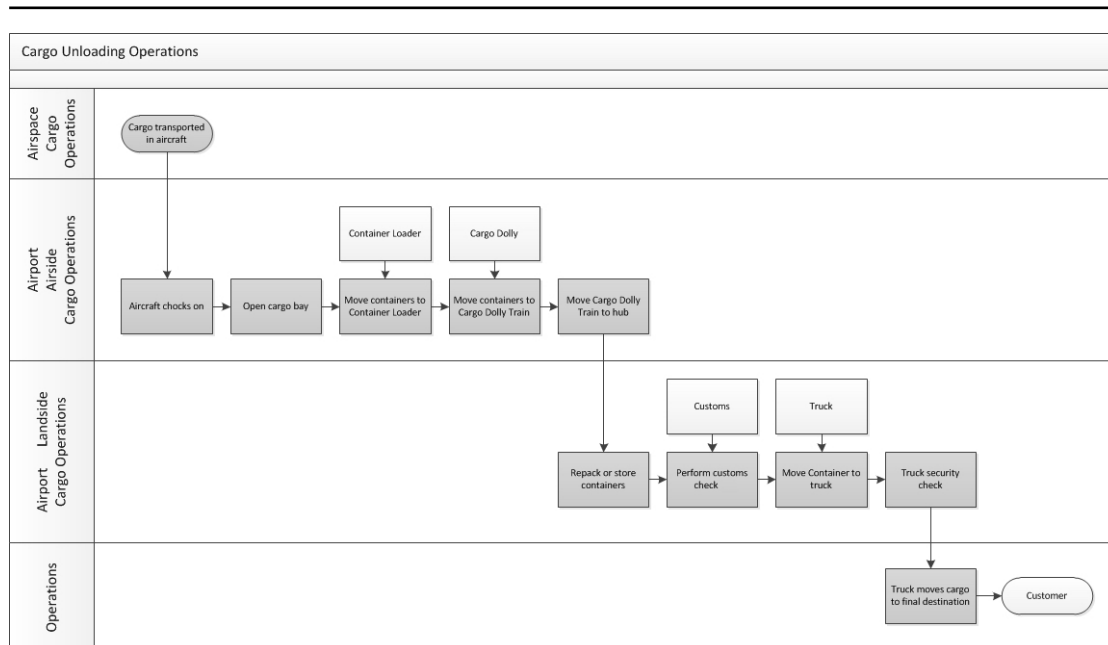


Figure 6.7: Cargo operations as sub-chain in the entire cargo transport chain.

6.2.1 Cargo logistics

From the beginning of the design of ATLAS its purpose was clear: air cargo transportation. The ATLAS design team was represented during the PUCA meeting of June 2015 where it became clear that it is important to analyse the *air* cargo part in the whole transport chain of a certain good. In order to fit the market it is important that it connects with the other forms of transport. ATLAS is designed to be as compatible as possible with all systems involved. It meets this requirement by having four 20 feet containers which fit on standardised trucks and in standardised sea containers. Also standardised ULDs are able to be transported in the cargo bay. The sub-chain of the whole transport chain can be seen in Figure 6.7. This cargo chain starts with opening the cargo bay door and ends with the goods delivered at the final destination. The events in between are chronologically dependent and therefore this whole chain is a critical chain shown by the grey boxes.

In this flow chart it is clear that the whole chain is a critical path: a delay in one task will immediately result in the delay of the whole project. Using theory of constraints it is clear that there are a lot of constraints limiting the minimum time spend on this whole path. The theory of constraints is about finding the bottleneck of a process. Normally the bottleneck for a conventional passenger aircraft are cabin operations and catering [72]. The bottlenecks of this chain are 'repack container' and 'truck moves goods'. Constraints during these operations are reduced by ATLAS' large truck-compatible container design, for which, if the transport airliner decides to do so, it is possible to leave the airport via other modes.

Turn around time

The turn around time (TAT) is a way to define the time spent on ground operations between flights. The TAT of an aircraft is defined from the moment when the wheel chocks are placed around the landing gear until all the ground operations are done and the chocks are removed [73][74]. A decrease in Turn Around Time offers economic benefit and will lead to a more efficient utilisation of the fleet of an airliner. According to a new study of Boeing a 10 min decrease in turn-time can increase the utilisation by 8 percent and lower the operating cost by 2 percent for a typical single-aisle aircraft. [72]

The ground operations consist of multiple parallel tasks which can be seen in the flow chart in Figure 6.8. In order to reduce the time that these events will take first the critical events are

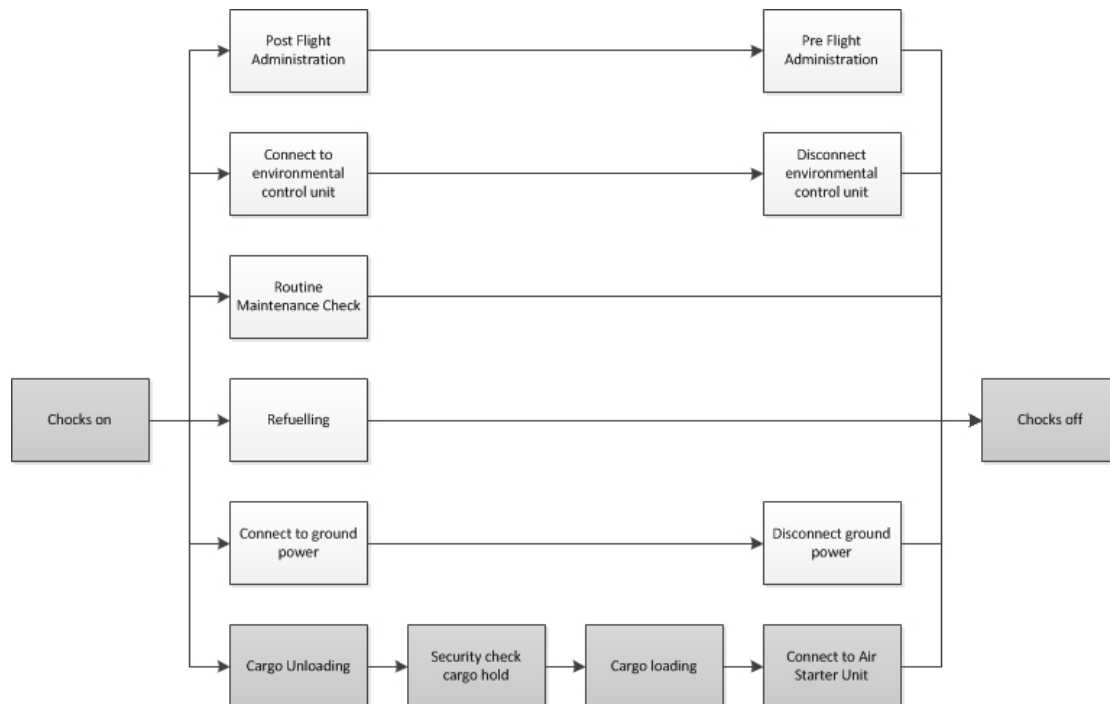


Figure 6.8: Turn around time operations.

found. The critical chain is the sequence of events which determines the minimum time spent on the whole process. The events in this path are the grey boxes in the flow chart. In order to reduce the total time spent on these operations, these critical events will have to be reduced.

The time spent on the ground operations described in the flow charts above can be improved using multiple strategies. Optimising the critical chain in a process can be done using Project Evaluation and Review Technique (PERT) and critical chain analysis [75] [73]. In Figure 6.9 the result of these project management techniques are visible. PERT is a method to analyse the tasks within a certain project from start to finish. The order of activities and the inter-dependencies are visible in the predecessor column. The time spent on each activity together with the order determines the critical path: the chain of events that determine the end time of the whole project. In order to make ATLAS as efficient as possible these activities have to be reduced. Critical paths can be decreased using three types of solutions: increasing the efficiency of tasks, eliminating tasks or scheduling tasks parallel. Because ATLAS is an unmanned freighter a lot of tasks can be eliminated and scheduled parallel. In the following section the time noted for each task is explained and how this time relates to this specific aircraft.

Refuelling operations

The benefits of unmanned aviation are noticed clearly; due to the fact that no people are on board of the ATLAS the refuelling can be performed simultaneous with cargo loading and unloading, something that normally is not allowed due to safety. This parallel scheduling of tasks benefits the TAT. For a typical range with a typical payload the ATLAS needs 13,439 litres of fuel. When refuelling at a pressure of 200 *kPa* and a fuel flow of 3500 L/min [76] this aircraft will need 3.8 minutes for this task. Both connecting and disconnecting will take 30 seconds [77] which adds up to a refuelling time of 4.8 minutes.

Loading operations

In order to meet the loading requirement of 30 minutes a design is chosen, which has 4 large 20 feet containers and a slide through loading system. It is assumed that loading can be performed with a rate of 1.7 minutes/container and unloading at a rate of 1.4 minutes/container [77]. This means that within 1.7 minute a container is transported from a cargo dollie to the

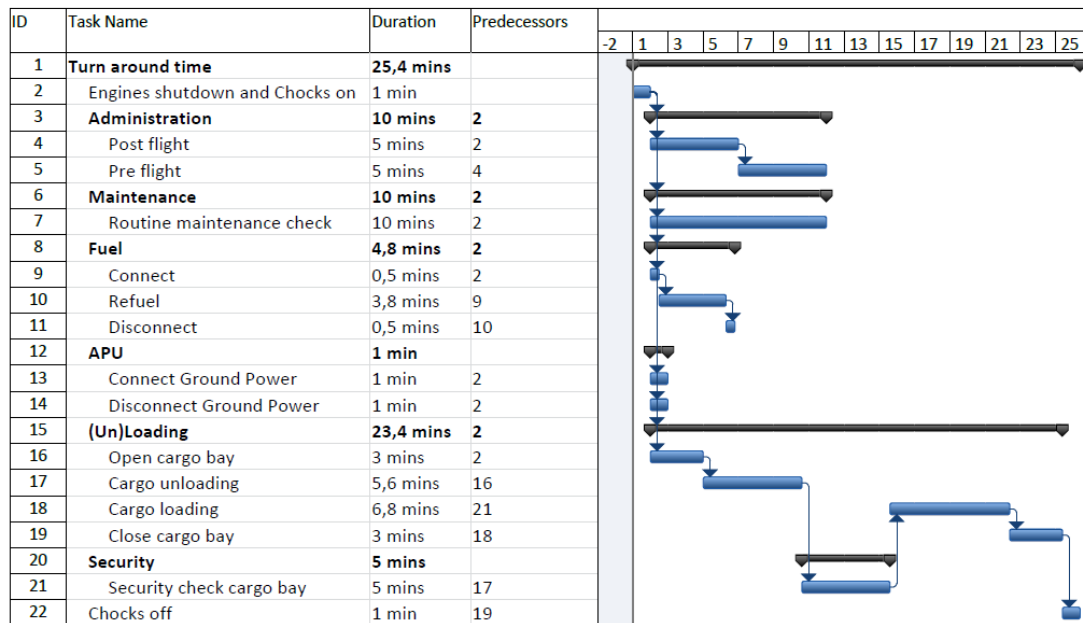


Figure 6.9: Turn around time PERT analysis.

cargo bay using a cargo loader. For four containers this adds up to 5.6 minutes for unloading and 6.8 minutes for unloading. Note that this assumption only holds if the ground crew knows how to work with the ATLAS. For safety 5 minutes are added to check the cargo bay for any problems with fasteners or other loading systems. A safety factor is put on the cargo bay door opening because the ATLAS has unconventional loading procedures, which might be mitigated by extra safety measurements taken by the ground handlers. It is common that opening takes only 30 seconds [72] which is now increased to 3 minutes. Also for this analysis the simultaneous loading is assumed not to be possible. This is decided on to mitigate the risk that a certain airport does not yet have the trained ground handlers to perform this new way of loading.

Maintenance

This routine maintenance check is part of the complete maintenance program further explained in section 6.4. An important part of this is de-icing, checking for any obvious signs of damage or malfunction, checking emergency equipment, and inspection of instruments such as pitot tube and antennae. This daily check is the simplest inspection that an aircraft regularly undergoes.

Environmental unit

This routine service will provide the aircraft with all necessary supplies to provide the environmental control. This tasks also involves checking the systems which protect the valuable cargo from any damage in terms of temperature, pressure and humidity.

Other operations

Due to the fact that ATLAS is unmanned certain tasks are eliminated with respect to conventional aircraft. All passenger, lavatory, air condition, catering, cleaning, cabin and cockpit services such as cleaning and catering are eliminated. The TAT of a cargo aircraft is faster than passenger aircraft due to the fact that catering and cabin services usually are a part of the critical chain. ATLAS has a quicker TAT than most cargo aircraft due to the fact that it is unmanned. The amount of ground handling services is even more reduced; attaching crew stairs for the pilot and cockpit lavatory and cabin services is not necessary. The elimination of these tasks benefits the TAT of ATLAS greatly. However, in order to mitigate particular risks for this innovative unmanned systems a safety factor is added for post and pre-flight administration and regular maintenance check.

Results: total TAT

Using these assumptions and values a TAT of 24.4 minutes is reached. If loading is performed simultaneously a turn around time of 12.6 minutes can be achieved. This is a significant increase compared to current freighters which average 30-50 min [72].

6.2.2 Container management & operations

The logistic process behind the cargo process in terms of container operations is a significant part of a lean transportation process. The paragraphs below describe how the ATLAS fits within this framework.

Container management

Four containers are necessary in every ATLAS. At every airport it operates, another four containers should be available. If the airliner decides to let the container leave the airport this number should be increased, in order to make sure enough containers are available at each airport. As mentioned before, ATLAS is able to take standardized ULDs in its cargo bay.

Minimum container loading configuration policy

For container management a minimum container loading configuration policy should be developed by the airliner. For container management it is preferable to fill an aircraft with empty containers. This the best configuration to reduce the imbalances of containers in an airline network. [78]. It is recommended that the airliner trades this problem off with the extra fuel cost of the weight of the empty containers.

Container safety

The container is secured with fasteners on rails to the floor of the cargo bay. This is important because during flight the containers are not allowed to move to make sure the aircraft is balanced. For this standardised fittings are used to make ATLAS and its containers compatible with other aircraft. In order to protect the cargo a fire control system is implemented and an environmental control system.

Intelligent cargo container

By integrating technology and intelligence into cargo the efficiency of the cargo chain can be improved and emissions can be reduced. Also it can help with regulatory compliance. Control over entire cargo chain is possible by implementing smart sensors and GPS: smart sensors will constantly measure temperature to make sure perishable goods are protected, whereas GPS will provide track and trace, which provides real-time asset management by all parties involved. Collecting all this data, a clear image can be made on the amount of emissions that are released per unit payload, to ensure that ATLAS is as sustainable as possible. Furthermore, using this data optimisation of the entire chain will be possible to increase efficiency between different modes of transport.

Production

The container designed for ATLAS can be seen in Figure 6.10 and is made from high strength 7000 series aluminium alloy which is highly resistant to racking.¹ The benefit of metal is that it is strong yet lightweight, recyclable and it has proved itself as a ULD material having an average lifetime of 10-15 years.² Composite was taken into account as an option, however the

¹<http://www.nordisk-aviation.com/main/en/ld-containers/nordisk-lite-family/nordisk-alulite-ake/> [accessed on 19/06/2015]

²<http://www.people.hofstra.edu/geotrans/eng/ch3en/conc3en/containerlifespan.html> [accessed on 19/06/2015]

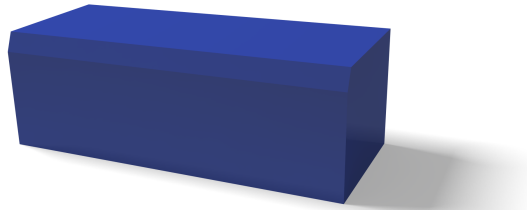


Figure 6.10: ATLAS container.

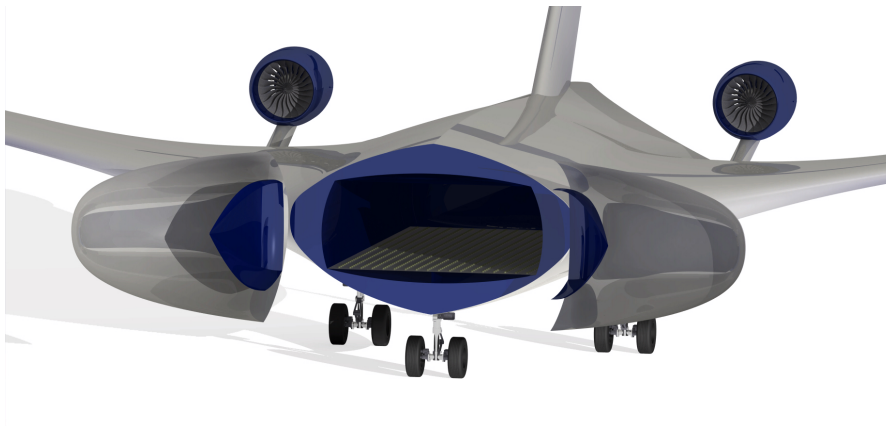


Figure 6.11: Front nose loading.

environmental degradation of composite is unknown and it is not as recyclable as aluminium. Recycling scrap aluminium requires only 5 percent of the energy used to make new aluminium.³ Comparing this with the high price of composite, aluminium is considered the best option.

6.2.3 Loading operations

The following subsection describes the process of loading and unloading the cargo in the ATLAS. Effort has been put into decreasing the TAT, which influences the method of loading and unloading. Also, the way of moving containers within the cargo bay is described.

Cargo slide loading

A significant part of the air cargo transport process are the loading operations. ATLAS is designed to have simultaneous loading and unloading, which will be implemented using the cargo-slide concept [79]. Loading will be performed via an upward nose door while unloading will happen via doors in the back as can be seen in Figure 6.11 and Figure 6.12. This means that at the same time one 20 feet cargo loader will be in the front and one in the back. Since only four containers will have to be replaced a total loading time of 6.8 minutes is achieved as can be seen in subsection 6.2.1. In order to support this a simultaneous loading safety system is implemented to make sure the cargo is never pushed through without a cargo loader being ready in the back, since no visual guidance is possible.

After the cargo loader provides vertical transport the container is placed on a cargo dolly in the case of unloading.⁴ A cargo dolly moves containers horizontally across the airport, usually connected to each other in a dolly train. The containers are 20 feet which are already stan-

³<http://www.hydro.com/en/About-aluminium/How-its-made/> [accessed on 19/06/2015]

⁴<http://ialcargo.com/specs/b747.pdf> [accessed on 18/06/2015]



Figure 6.12: Back loading.

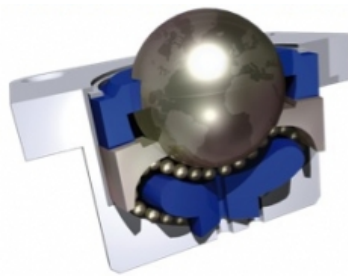


Figure 6.13: Ball transfer units.

standardised sizes for ground handling agents. If ground handlers redesign their loaders as a future development, two 40 feet containers can also be transported.

Interior cargo bay

To move the containers as safe and fast as possible inside the aircraft ball transfer units will be implemented throughout the whole cargo bay. These small balls can be seen in Figure 6.13 and implemented in the floor they will horizontally translate the containers smoothly. Due to the low friction of 0.5% even heavy containers can be moved by ground handlers.⁵ Using this system also other containers, pallets or ULDs can be moved inside the cargo bay.

To protect the valuable cargo and the balance of the aircraft a fastening system is implemented in the floor and the walls of the cargo bay. This system will consist of standardised fasteners, straps and fittings to make sure that the aircraft is compatible with other forms of transportation. The standard ATLAS container will lock itself in the floor using locks and fittings. The standard strap locks can also be used to secure the container inside a truck or a sea container.

6.3 Manufacturing, assembly, integration plan

This chapter will explain the suggested production plan for the design. It will describe the lean six sigma methodology with which a lean manufacturing and assembly process can be made. The value stream mapping part of lean six sigma will be used to find an efficient process to assemble the aircraft.

⁵http://www.airport-suppliers.com/supplier/Omnitrack_Ltd/ [accessed on 20/06/15]

6.3.1 Production plan

The production plan of the design mainly focuses on the assembly process, which is shown in Figure 6.14. The assembly process exists of one large assembly line, to which separate assembled parts of the design are added. This large assembly line can be seen as the main value stream. In order to design a dynamic, knowledge-driven and customer-focused assembly process, this line should continuously be moving [80]. Therefore separate assembly lines, or small value streams, are added at specific moments to the main value stream. The assembly processes of these smaller assembly line can be performed simultaneously, in order to continuously add value to the product. [81]

The customer-focused approach is also visualised in the value stream map in Figure 6.14, based on the six sigma tool 'SIPOC' (Supplier, Input, Process, Output and Customer)⁶. As explained in chapter 2, the customers require five aircraft per month which equals the required output. The five aircraft required per month will go through the assembly process. Since a lean assembly process is essential, the input needed for five aircraft has to be determined. As a last step the input needed can be communicated to each of the suppliers.

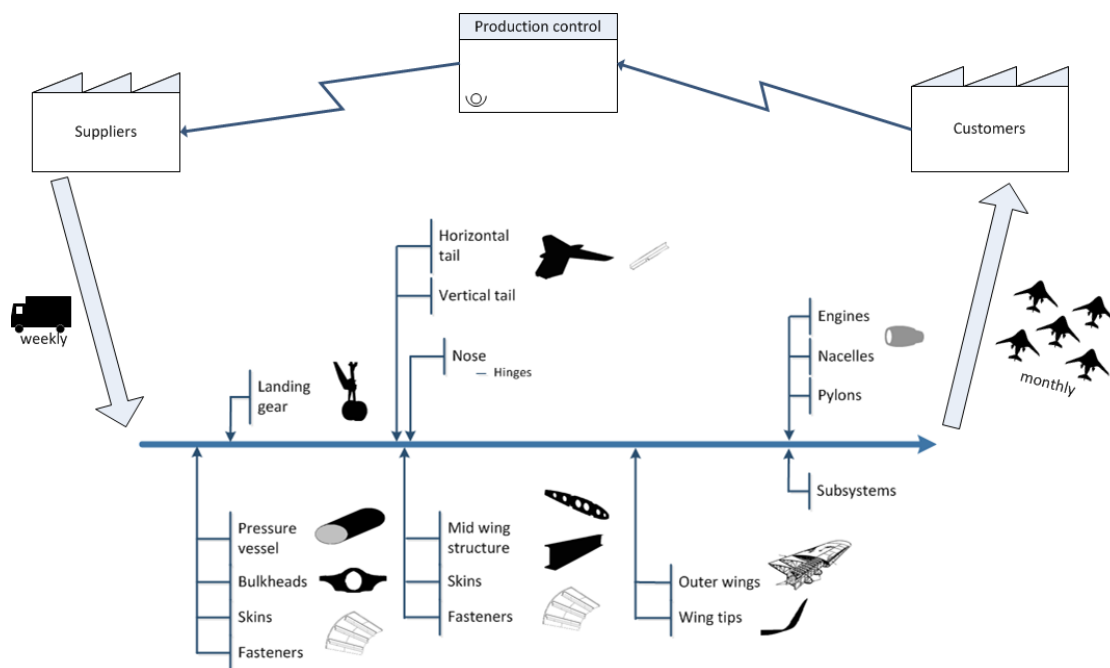


Figure 6.14: Graphic representation of the assembly line.

As can be seen in Figure 6.14 the first three parts that are assembled are the pressure vessel, the centre body and the landing gear. Parallel to this assembly, the sub-assembly of the tail and the mid wing is conducted. The start of this parallel process is planned in such a way, that once the pressure vessel, the centre body and the landing gear are assembled, the tail, mid wing and nose of the aircraft can be added to the main assembly line. In the same manner, the sub-assembly of the outer wings is performed parallel to the main assembly, planned to be added to the main assembly line when the assembly of the tail, mid wing and nose is finished. The last parallel processes are the sub-assembly of the engines and subsystems, planned in the same manner as the previous sub-assemblies.

The parts needed for the sub-assembly, such as the bulkheads, skin panels and landing gear will be manufactured by subcontractors. Examples of subcontractors are provided in Table 6.2.

⁶<http://www.isixsigma.com/tools-templates/sipoc-copis/sipoc-diagram/>, [accessed on 19/06/15]

Table 6.2: Examples of subcontractors.

<i>Part</i>	<i>Subcontractor</i>
Skin panels	Airborne composites ⁷
Bulkheads	Airborne composites
Pressure vessel	Airborne composites
Landing gear	Fokker (Landing Gear) ⁸
Tail	Fokker Aerostructures ⁹
Mid wing structure	Fokker Aerostructures
Outer wing structure	Fokker Aerostructures
Engines	SFM Aero Engines
Subsystems	Fokker ELMO ¹⁰

6.3.2 Impact on sustainability

Next to the economical and time benefits of implementing a lean production process, there are several advantages that can be identified in terms of sustainability. A number of these are presented below [80].

- Overproduction can be prevented. Due to this there is less plant space and labour required to accommodate storage. Also, transportation to and from storage is prevented.
- Minimise transportation waste. By incorporating a logical factory assembly line flow transportation in between work stations is minimised. This again prevents excess transportation and labour costs.
- Large sub-assemblies are manufactured at once. This decreases the transportation effort required by subcontractors.
- Having to reproduce an entire wing section due to production mistakes is a costly process and has a direct environmental impact. Adequate employee education and instructions will minimise rework.
- By preventing poor hiring practises employees will be used to maximum efficiency. This reduces the total amount of workers needed and hence reduces the environmental footprint.
- Universal tools will be used where possible. Therefore, fewer new tools have to be developed and produced, and employees do not require additional education.

6.3.3 Safety assurance

Assuring a safe work environment is of great importance. Apart from adhering to the present regulations, preventing accidents and abnormalities on the factory floor is essential to maintain a viable company image. The entire production process will be designed to concur with the Occupational Safety and Health Standards¹¹. Some of the implementations include:

- Safety training of work forces.
- Mandatory personal protective equipment for each worker in areas where there is increased risk of injuries due to work related activities.
- Proper implementation of emergency evacuation plans.

6.4 Reliability, availability, maintainability (RAM) characteristics

The availability of an aircraft is influenced by the scheduled maintenance and unscheduled maintenance. Unscheduled maintenance depends on the reliability of the aircraft's main systems and subsystems. In order to give an approximation of the expected reliability and availability a list of critical subsystems will first be provided. This list is called the master minimum equipment

¹¹https://www.osha.gov/pls/oshaweb/owastand.display_standard_group?p_toc_level=1&p_part_number=1910 [accessed on 19/06/15]

Table 6.3: Master minimum equipment list for ATLAS.

<i>Subparts of system</i>	<i>Number installed</i>	<i>Number required for dispatch</i>
Auto Flight	3	3
Communications	3	3
Fire Protection	4	3
Flight Controls	3	2
Fuel System	2	2
Electrical Power	2	2
Ice and Rain Protection	2	1
Landing Gear	4	3
Lights	4	2
Navigation	3	3
Environmental control	2	0
Auxiliary Power	1	0
Engine Fuel and Control	2	2

list (MMEL). The last section of this chapter will describe the safety management system of the design.

Master minimum equipment list (MMEL)

In order to enhance safety a master minimum equipment list (MMEL) is provided. This list identifies items which individually may be unserviceable at the commencement of a flight. In Table 6.3 the subsystems that are included in the MMEL are stated. For each subsystem the number installed in the aircraft and the number required for dispatch is given.¹²

Individual items from Table 6.3 may be unserviceable, but it must be noted that a combination of some items unserviceable can not be allowed. For example, a combination of flight control failure and engine control failure can not be accepted.

Due to the unmanned characteristic of the ATLAS, failures of the auto flight, communications, electrical power system and navigation are critical. Therefore the number of these systems required for dispatch is higher than for conventional aircraft.

Expected reliability

The reliability of the ATLAS is indicated by the product of the reliability of its systems and subsystems or, according to Lusser's Law, the so-called weakest link concept. [82]. In order to quantify the expected reliability of the total system, first the expected reliability of the subsystems has to be quantified. Since the reliability of the subsystems is hard to approximate at this stage of the design, an approximation for the reliability of groups of subsystems is provided in Table 6.4. The expected reliability is based on reference aircraft and estimations. [83] The percentage is stated at the bottom row of Table 6.4 and represents the percentage of serviceable subsystems per aircraft per operational year.¹³ The percentage should be seen as a goal to achieve, since it can not be verified at this stage of the design. The expected reliability can be achieved by performing scheduled maintenance.

Maintainability

Thorough, planned and predefined maintenance is needed for the aircraft to ensure a safe flight, keep the reliability and availability high and to ensure a safe flight. Also maintenance management is required to ensure the airworthiness of the aircraft. In order to be certified for airworthiness a scheduled maintenance guideline is generated. With scheduled maintenance the

¹²[http://www.skybrary.aero/index.php/Minimum_Equipment_List_\(MEL\)](http://www.skybrary.aero/index.php/Minimum_Equipment_List_(MEL)) [accessed on 18/06/15]

¹³<https://blog.globalair.com/post/Reliability-and-Availability.aspx>, [accessed on 18/06/2015]

Table 6.4: Reliability of the subsystems divided in reliability groups.

<i>Flight Operations</i>	<i>Flight Controls</i>	<i>Flight and cargo safety</i>
Auto flight Communications Navigation Auxiliary power	Flight controls Fuel system Electrical power Landing Gear Engine fuel and control	Fire protection Ice and rain protection Lights Environmental control
90 %	90%	95%



Figure 6.15: Lockheed C-130J Hercules maintenance platform.

performance of the aircraft can be kept as high as possible, which also results in a more sustainable performance.

Adapting maintenance to the ATLAS design

Certain characteristics of the design can be pointed out that change the maintenance process compared to current aircraft. First of all, since the ATLAS is unmanned there are no windows, also not around the cockpit. These are critical areas for cracks to appear at conventional aircraft. This gives a maintenance advantage for the ATLAS, reducing the possibility of cracks to occur. The blended shape of the design influences the maintenance process, since the upper surfaces are difficult to reach. Also the engines on top of the wings are less convenient for current maintenance processes. Airliners have the possibility to use lifters to reach this kind of surfaces, but another solution is also provided for the ATLAS. This solution is based on the Lockheed C-130J Hercules maintenance platform¹⁴. In Figure 6.15 the maintenance platform of the Hercules is depicted. The high lift devices used also have an impact on the maintainability of the aircraft. As explained in subsection 4.5.5 control surfaces have been chosen for the ATLAS that consist of simple mechanisms and are therefore easy to maintain.

For the composite skin and structure should not affect the current maintenance processes to a large extend. When a part of the skin or structure needs to be replaced, a new laminated piece of composite can be provided and used to replace the old part.

¹⁴<http://www.fall-arrest.com/industries/aircraft-fall-protection/maintenance-platforms/c-130/> [accessed on 18/06/15]

Table 6.5: Scheduled maintenance guideline.

<i>Check</i>	<i>When</i>	<i>Tasks (examples)</i>	<i>Man hours required</i>
Daily checks	Daily	Visual inspection of aircraft at airport	0.5
A	Aprox. 250 flight hours	Visual inspection of aircraft structure Lubricate nose gear retract actuator Test Flap/Slat Electronics Unit	20 - 50
B	6 months	Detailed check of components and system	120 - 150
C	20 - 24 months	A and B check tasks Inspect engine inlet for cracks Visually check condition of door seals	6000
D	Every 6 years	A, B and C check tasks Inspect floor beams Detailed inspection of wing box structure Inspect stabiliser attach bolts	50000

Scheduled maintenance

The scheduled maintenance of the ATLAS is based on current maintenance processes. The guideline for the scheduled maintenance is provided in Table 6.5. [84] The tasks listed in Table 6.5 are examples of the tasks included in that type of check to give a general idea of the purpose of the check.

Unscheduled maintenance

Unscheduled maintenance is needed when unexpected failures or damages occur to the aircraft. These repairs are often done within the turnaround process or during overnight stops [85]. Since the ATLAS is unmanned, overnight stops are not necessary and therefore unscheduled maintenance should be fitted in the turnaround process.

6.4.1 Expected availability

Availability is defined as a percentage of days an aircraft is available for flight in an operating year. When an aircraft is in for maintenance, it is not available for flight. The more time the aircraft spends in or waiting for maintenance, the less time the aircraft is available to be scheduled for flights.¹⁵ The unmanned characteristic of the ATLAS has a beneficial impact on the availability of the aircraft, since the operation is not dependent on the availability of pilots and crew.

6.5 Data and electrical block diagrams

This chapter describes both the data as well as the electrical block diagrams. Firstly, the data block diagram is discussed. Secondly, the electrical block diagram is depicted.

¹⁵<https://blog.globalair.com/post/Reliability-and-Availability.aspx> [accessed on 18/06/15]

6.5.1 Data block diagram

The data block diagram of the ATLAS is shown in Figure 6.16. The hardware of the main systems is also depicted in the diagram. Software has to be developed in the detail design phase to make the hardware work together.

The data block diagram consists of six main subsystems: sensor, computer, communications, electrical power, aircraft control and the environmental subsystem. They interact as shown with the connections in the flow diagram. Two computers are used, so one backup system is available if a computer failure occurs. All the sensors and subsystems are described in section 6.1.

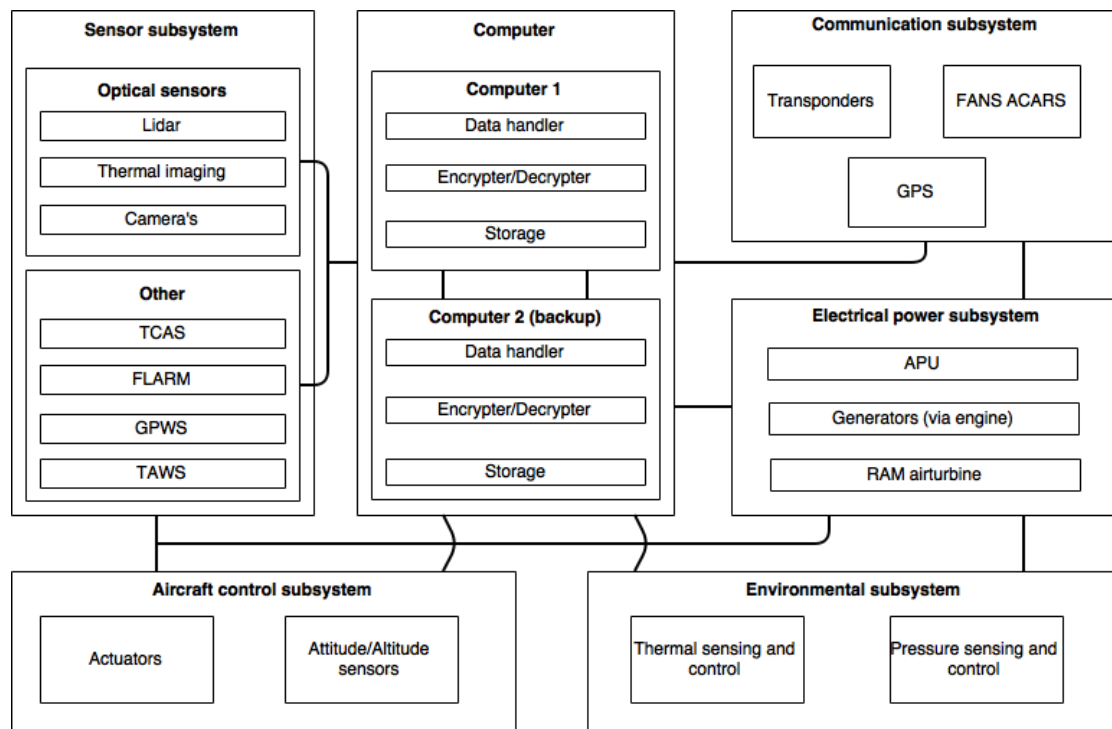


Figure 6.16: Data handling block diagram.

6.5.2 Electrical block diagram

The electrical block diagram of the aircraft is shown in Figure 6.17. The electrical system provides the required power to all subsystems of the aircraft. The lithium-ion battery is used to start the APU generator which starts the auxiliary power unit (APU). The APU is used to start the engine starter generator which starts the engines and can also be used to start up the electrical system of the aircraft while on the ground like air conditioning, lightning and other electrical systems. While cruising the engines can provide power to the power processing unit. The power processor and converter will manage the income of electricity and convert to required voltages and can also be used to recharge the battery.¹⁶ The main bus provides all subsystem with available power at their required voltages. In case of emergencies the ram air turbine (RAT) can be deployed and also the APU can be started to provide a second source of power. The RAT provides power to the emergency hub which will provide power to most important subsystems of the aircraft: flight control computer, control surfaces and sensors. A detailed analysis of the power allocation can be seen in subsection 4.7.2.[38]

¹⁶http://www.skybrary.aero/index.php/Aircraft_Electrical_Systems [accessed on 17/06/15]

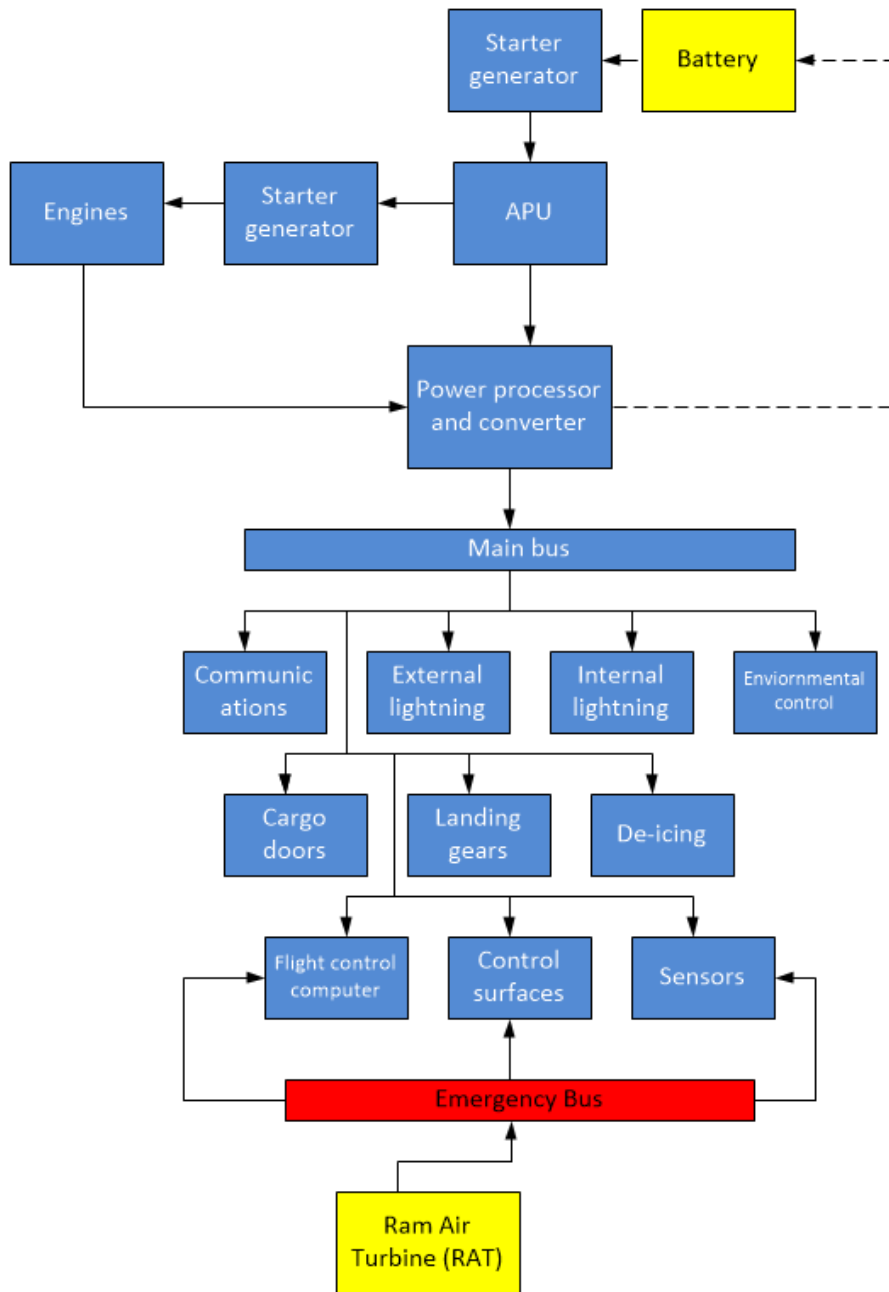


Figure 6.17: Electrical block diagram.

7 Requirement compliance matrix

The requirements compliance matrix (Table 7.1) contains all requirements and indicates with a tick mark, when a requirement is met. When the requirement is not met the actual value is given in the comment section. In the comment section additional information can also be found regarding the elaboration on the state of the requirement. In the reference column the chapters containing the elaboration on these requirements are given and can be consulted for more details.

Table 7.1: Requirements compliance matrix.

Req. ID	Requirement	✓/X	Comments	Reference
UCCF-Cons-Dsgn-01	The take-off runway required shall be less than 3000 meters at maximum take-off weight at 0 meter for standard ISA conditions.	✓		section 4.4
UCCF-Cons-Dsgn-02	The landing runway required shall be less than 2000 meters at maximum landing weight at 0 meter for standard ISA conditions.	✓		section 4.4
UCCF-Cons-Dsgn-03	The maximum payload range shall be 3000 nautical miles.	✓		subsection 5.1.1
UCCF-Cons-Dsgn-04	The maximum payload volume shall be larger than 50 m^3 .	✓		subsection 5.1.1
UCCF-Cons-Dsgn-05	The maximum payload weight shall be larger than 20 metric tons.	✓		section 4.6
UCCF-Cons-Dsgn-06	The wing span shall be less than 80 meters.	✓		subsection 4.5.1
UCCF-Cons-Cost-01	The unit production cost shall be lower than 50 million euros.	✓		subsection 5.5.2
UCCF-Cons-Regu-01	The system shall comply with CS25.	✓	While designing the aircraft, CS25 requirements are used as initial requirements. Hence, throughout the whole report CS25 is complied with.	

UCCF-Cons-Regu-02	The aircraft shall provide the same level of control as described in CS25 for manned aircraft.	✓		section 6.1
UCCF-Cons-Regu-03	The aircraft shall not increase the risk to people or property on the ground compared with manned aircraft of equivalent category.	✓		section 6.1
UCCF-Cons-Regu-04	The aircraft shall provide fire extinguishing options for a class C cargo compartment as specified in CS25	✓		subsection 4.5.9
UCCF-Cons-Regu-05	The aircraft shall have a climb gradient as specified in CS25.	✓		subsection 5.1.2
UCCF-Cons-Regu-06	The aircraft shall be certifiable according to environmental regulations of CS25.	✓		subsection 6.5.1 and 4.5.8
UCCF-Cons-Regu-07	The aircraft shall be certifiable according to maintenance regulations of CS25.	✓		subsection 6.1.2
UCCF-Cons-Regu-08	The aircraft shall be certifiable according to emergency regulations of CS25.	✓		sec:regulations
UCCF-Cons-Regu-09	The aircraft shall be able to communicate with air traffic control according to communication regulations of CS25.	✓		subsection 6.1.2 / Figure 6.1.2
UCCF-Cons-Sust-01	The noise shall have a 50% smaller SEL contour than the 55 dB SEL contour of an A320 [km^2].	✓		subsection 5.1.8

UCCF-Cons-Sust-02	The fuel consumption shall be smaller than 25% of the fuel consumption per tonne of payload of a 747-400F freighter.	X	The fuel consumption of the ATLAS is $7.47 \frac{L}{10^{-5} kg \cdot km}$. This is 54% of the fuel consumption of the 747-400F per 100 tonne payload, per kilometre. This requirement is therefore not met. This is discussed in subsection 5.1.9	subsection 5.1.9
UCCF-Cons-Sust-03	The CO_2 production shall be smaller than 25% of the CO_2 production per tonne of payload of a 747-400 freighter.	X	The production of CO_2 production per tonne of payload for the ATLAS is $4.11 \cdot 10^{-4} \frac{kg}{kg \cdot nmi}$. This is 54% of the CO_2 produced by the 747-400 freighter. Since the fuel requirement is not met, it is only logical that the CO_2 production requirement also falls short. By decreasing the fuel usage the CO_2 production can also be reduced.	subsection 5.1.10
UCCF-Cons-Oper-01	The direct operational costs shall be smaller than 25% of the direct operational costs per tonne of payload of a 747-400 freighter.	✓		subsection 5.5.1
UCCF-Cons-Oper-02	It shall be possible to shift the total load from the aircraft to a road capable truck in less than 30 minutes.	✓		subsection 6.2.1
UCCF-Tech-Perf-FD-01	The aircraft shall be able to be trimmed at all times.	✓		section 5.4 subsection 4.5.5
UCCF-Tech-Perf-FD-02	The aircraft shall be laterally stable.	✓		subsection 5.4.2
UCCF-Tech-Perf-FD-03	The aircraft shall be longitudinally statically stable.	✓		subsection 5.4.1
UCCF-Tech-Syst-Oper-01	The aircraft shall be able to taxi.	✓		subsection 4.5.6
UCCF-Tech-Syst-Oper-02	The aircraft shall be able to take-off.	✓		subsection 5.1.7
UCCF-Tech-Syst-Oper-03	The aircraft shall be able to cruise.	✓		section 5.1
UCCF-Tech-Syst-Oper-04	The aircraft shall be able to land.	✓		subsection 4.5.6/ subsection 5.1.7

UCCF-Tech-Syst-Oper-05	The aircraft shall provide cargo loading.	✓		subsection 6.2.1
UCCF-Tech-Syst-Oper-06	The aircraft shall provide cargo unloading.	✓		subsection 6.2.1
UCCF-Tech-Syst-Oper-07	The aircraft shall be able to refuel.	✓		subsection 6.2.1
UCCF-Tech-Syst-Power-01	The aircraft shall be able to provide 40 KW power for all subsystems.	✓		subsection 4.5.11
UCCF-Tech-Syst-Prop-01	The aircraft shall be able to provide 95429 N thrust.	✓		subsection 4.5.7
UCCF-Tech-Cargo-Cont-01	The aircraft shall be able to transport the container.	✓		subsection 4.5.3
UCCF-Tech-Cargo-Cont-02	The container shall be transportable by truck.	✓		subsection 4.5.3
UCCF-Tech-Cargo-Envi-01	The temperature in the container shall be controllable.	✓		subsection 4.5.8
UCCF-Tech-Cargo-Envi-02	The pressure in the container shall be controllable.	✓		subsection 4.5.8
UCCF-Tech-Struct-01	The aircraft shall be able to sustain the specified aerodynamic loads.	✓		section 5.3
UCCF-Tech-Struct-02	The aircraft shall be able to sustain the specified gust loads.	✓	The structure of the aircraft is designed for the maximum load factor. Since the gust loads are lower than this, the requirement is fulfilled.	section 5.3
UCCF-Tech-Struct-03	The aircraft shall be able to sustain the specified cargo loads.	✓	The weight of structure is taken into account for the design of the fuselage.	section 5.3
UCCF-Tech-Struct-04	The aircraft shall be able to sustain the specified take-off loads.	✓		section 5.3
UCCF-Tech-Struct-05	The aircraft shall be able to sustain the specified landing loads.	✓		section 5.3
UCCF-Tech-UAS-01	The aircraft shall be designed to perform the flight unmanned.	✓		section 6.1

UCCF-Tech-UAS-02	The aircraft shall be able to communicate with Air Traffic Control.	✓		subsection 6.1.2
UCCF-Tech-UAS-03	Air Traffic Control shall be able to communicate with the aircraft.	✓		subsection 6.1.2
UCCF-Tech-UAS-04	The aircraft shall be able to navigate using a navigation system.	✓		subsection 6.1.2
UCCF-Tech-UAS-05	The unmanned control system shall be fail-safe.	✓		subsection 6.1.3
UCCF-Tech-UAS-06	The unmanned control system shall navigate the unmanned aircraft to pre-selected emergency sites to make a safe landing or a controlled crash, when an unrecoverable failure occurs.	✓		subsection 6.1.2
UCCF-Tech-UAS-07	The unmanned control system shall be able to control the aircraft in all its operations.	✓		subsection 6.1.2

8 Project design and future development strategy

In this chapter the future project design & development logic of ATLAS is discussed. A detailed Gantt chart is also presented that maps the future activities on a timescale.

8.1 Project design & development logic

The Project Design Development (PD&D) logic, visualised in figure Figure 8.1, shows the logical order of activities to be executed in the post-DSE phases of the project. It contains a number of blocks connected by arrows. The blocks contain the activities needed to be taken to complete the development of ATLAS and to have a commercially viable aircraft flying. It consists of three major phases; the detailed, development and post-development phase. The grey boxes indicate specific milestones which the project has reached. Some activities are performed in parallel during the PD&D.

8.2 Gantt chart post DSE

The post DSE Gantt chart shows the future development and different phases to be completed by 2035. The chart divides the post DSE into different phases: detail design phase, development phase manufacturing, testing phase, certification phase and post development phase.

Each phase is then divided into two different sections. The detailed design phase includes an analysis of the system by computational fluid dynamics (CFD). Various other activities also take place in it such as optimisation of the design and planning maintenance procedures. After finalising the design the aircraft goes through the development phase manufacturing. In this phase all required parts are ordered and manufactured. At the end of this phase a prototype is assembled.

After manufacturing the prototype the testing phase takes place which includes system and subsystem tests of the aircraft. After successful completion of the testing phase, the aircraft has to be certified before production can be launched. The last development phase consists of launching the ATLAS into market. This consists primarily of demonstrating the aircraft in front of the public and doing the sales. After completion of everything the ATLAS can be flown. For more details the Gantt chart and its phases it can be seen in Figure 8.2.

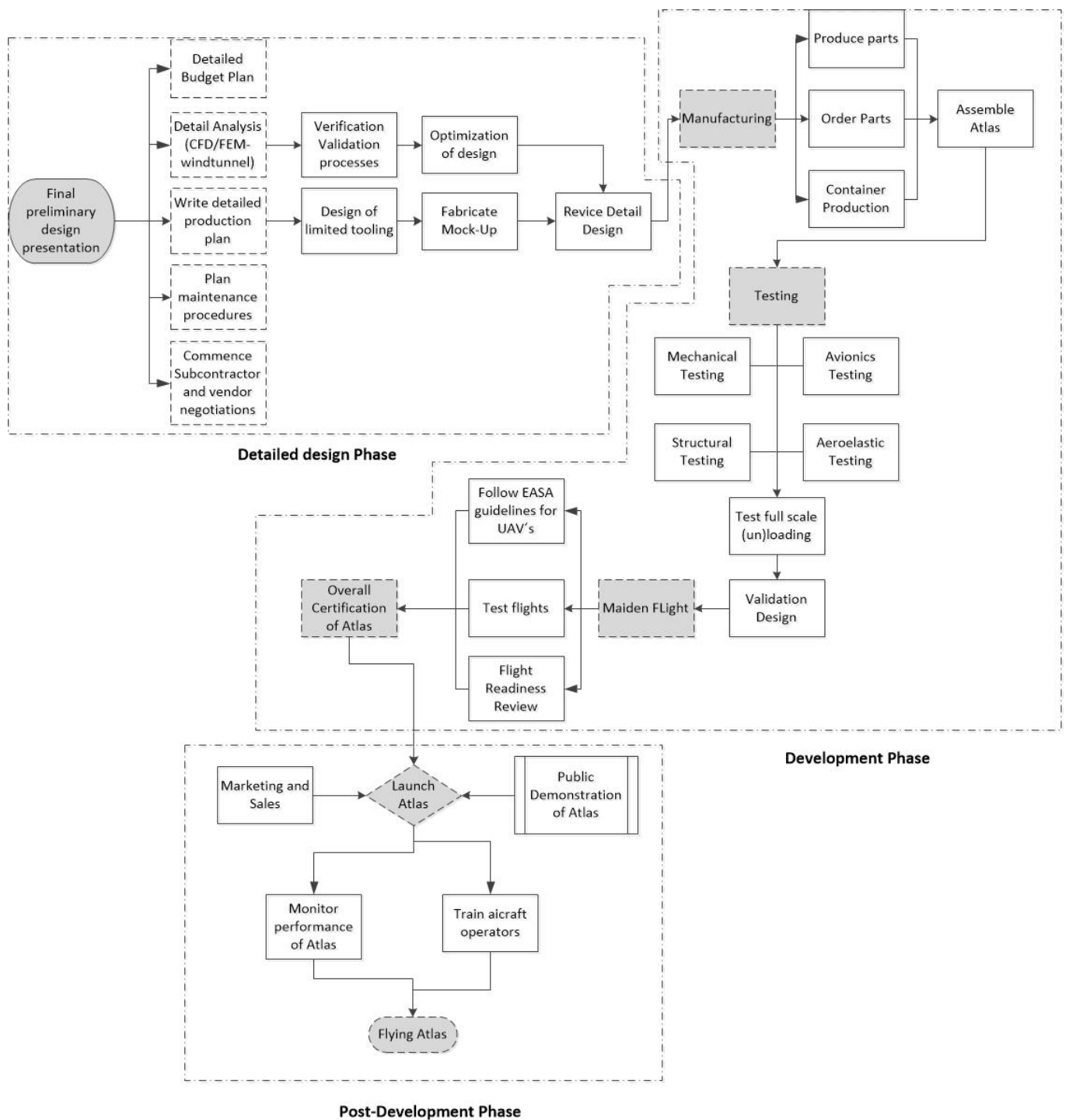


Figure 8.1: Project design and development logic.

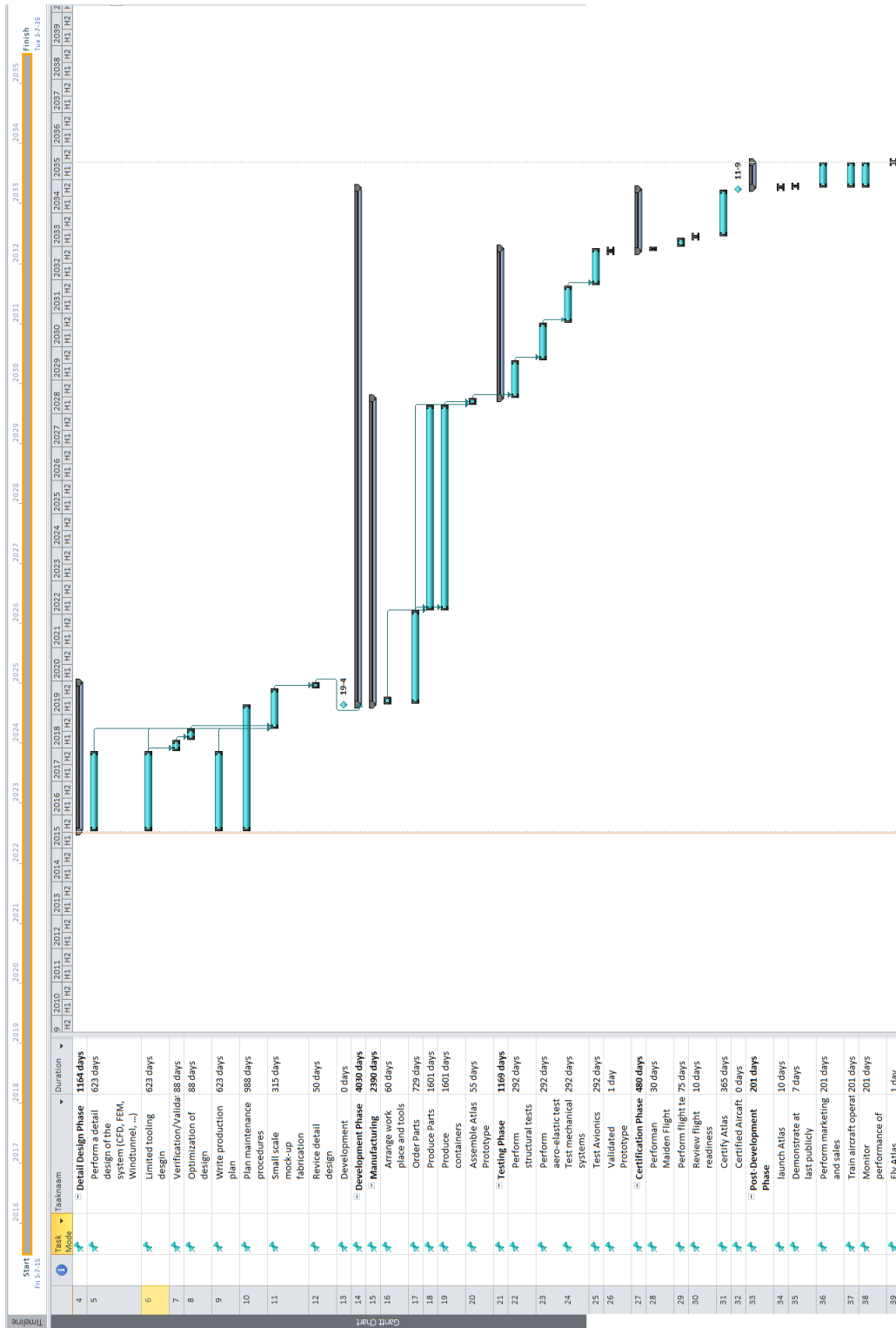


Figure 8.2: Gantt chart post DSE.

9 Conclusion

This final report provides the reasoning of the conceptual phase and the selection of the final concept. Furthermore the report presents the design, the performance analysis and the operations of ATLAS.

The preliminary design was based on a market analysis with multiple concepts. The best performing design according to the trade-off was a blended wing body. The high aerodynamic efficiency and inherent stability due to the tail resulted in a exceptional combination for the operating cost and sustainability. The design is profitable and has a relatively small environmental footprint.

To attain a more detailed design, the subsystems of the aircraft were designed. The subsystem design was done in an iterative process, where new information provided more accurate results than previous estimates. The internal subsystems of the aircraft focus on the environmental control of the cargo bay, which has to function without direct human intervention. Several computer controllable protection systems have been designed to ensure the safety and preservation of cargo. The operational design of ATLAS concentrates on the aircraft being unmanned, considering primarily safety for people on ground. Different failure modes have been considered along with appropriate responses.

Several important requirements were driving this design. These requirements steered the design to a high level of performance for multiple categories. The direct operation cost, fuel consumption and produced emissions compared to a Boeing 747-400 have been reduced with 75%, 50% and 46% respectively. Also, the noise production has been reduced with 78.5% compared to an Airbus A320. However the fuel and emissions requirement could not be fulfilled. It did however push the design towards a significantly lowered fuel consumption.

In summary, ATLAS satisfies almost all requirements and it also performs significantly better than any aircraft flying today. In the context of increasing fuel prices and high consideration for the environment, ATLAS is a sustainable choice due to its low fuel use and low noise contour. The compatibility with other transport modes makes delivery times shorter and the low operating cost makes it very profitable.

10 Recommendations

Some recommendations can be made to further improve the initial design of ATLAS. For the weight estimations it is recommended to select actual subsystems where possible, and get the weight from the manufacturers website. Also if a third class weight estimation will be performed, more accurate values of the weight of the aircraft could be obtained. It is also recommended to place all subsystems in CATIA, so the centre of gravity positions of these subsystems can be estimated more accurately. This also gives the opportunity to estimate the z-location of the subsystems, since the z-location is now assumed to be in the middle of the centre body for most of the systems. For the moment of inertia it is recommended not to neglect higher order terms, and also use the moment of inertia of the subsystem around its own axis.

For the propulsion system it is highly recommended to work closely with the manufacturer of the engine and other related systems. This enables the designers to get more accurate values for the inlet design. Also, using CFD is recommended for calculating the flows in and around the engines. Moreover, more accurate models for scaling the engines are recommended to use. In that way internal systems can be scaled as well, and more accurate values can be obtained of the actual engine used.

To investigate the aerodynamic properties of the aircraft more accurately, it is recommended to use CFD. This will model the viscous flow effects better, which results in more accurate and realistic aerodynamic values. Next to that, it is recommended to investigate the usage of a morphing wing. A morphing wing can show great advantages in terms of fuel efficiency during different mission segments. For the aerodynamic properties, it is recommended to perform real-life tests of ATLAS to see what the actual aerodynamic properties are, for example in a wind tunnel.

For tail sizing it is recommended to put more effort in finding the optimum ratio between the fuselage length and tail size in terms of drag and weight. This is part of an iterative process, and would require some more time. Next to that, it is also recommended to revise the used NACA0015 airfoil. This airfoil could probably be made thinner, and solve the created controllability problem with control surfaces.

For the structural analysis of the aircraft, most of the assumptions that are taken into account can be incorporated in the program with additional resources. For example, by not neglecting deformations, the stress computations can be done more accurately. Also this makes it possible to perform a vibrational analysis. The major drawback of the used program is that it only analyses the pressure vessel and the spars and skins in the wing. Any other structural members, i.e. the tail, engine reinforcements, wing ribs, fuselage longerons, stiffener and rivets have not been taken into account. If one wants to fully analyse the aircraft's structure, a detailed FEM analysis should be performed. For the structural analysis it is also recommended to perform real-life tests, for example a wing bending test.

For investigating the noise, a more accurate value of the airframe noise could be obtained using Fink method. In this method, every system is analysed separately, instead of the aircraft as a whole.

For stability it is recommended to design the ailerons and to get a more accurate design of the elevator. This would not change whether the aircraft is stable or not, but it will affect the response of the aircraft to certain motions.

For the power budget it is recommended to look into more detail what the actual power of different subsystems is. This goes together with selecting actual subsystems (as described above), since then the actual power usage of the subsystems is known as well.

For the cost analysis it is recommended to use a different cost estimation method. Now, Roskam is used since this theory was easily accessible and is good enough to give a first impression about the cost. However, this is a relatively old method, so some techniques used in Roskam are not applicable to current aircraft design. For example maintenance cost are reduced greatly compared to the days when Roskam was written. This is because nowadays sensors are present in the engines, which warn the operator when something should be replaced soon.

For the unmanned part, it is recommended to design the actual software program that will be used to link for example the sensors to the actuators. Also it is highly recommended to talk with the regulators, to make sure regulations allow unmanned flying, and that changes are being made on CS-25 for unmanned aircraft. For the unmanned part it is also recommended to evaluate double failures. For now, only single failures have been evaluated, and not two failures at the same time.

It is also recommended to investigate the wake of the airflow at high angles of attack. Since the engines are placed on top of the wing, and ATLAS has a T-tail configuration, there might be a risk for deep stall in which the aircraft stalls and both the engines and the horizontal tail are become ineffective due to the wake of the airflow.

It is also recommended to do more research about how airports and people will adapt to this new design. For example if many people working on an airport need to have additional knowledge and how airports will change their current way of operations when more and more airplanes fly unmanned would be interesting research topics before unmanned aircraft come on the market. Also it is recommended to do more research about whether unmanned flying will be accepted by people, and what it will do to the acceptance if the aircraft only transport cargo.

To conclude, it is recommended to investigate the possibility to fly even higher than the current cruising altitude of 12,500m. This would be beneficial for the fuel use and operating cost, but would make it harder to have stable eigenmotions.

Bibliography

- [1] European Commission. EU Transport In Figures, Statistical Pocketbook 2014. Technical report, European Commission, February 2015.
- [2] The World Bank Group. Air Freight: A Market Study with Implications for Landlocked Countries. Technical report, The World Bank Group, Washington, D.C., February 2009.
- [3] J. Roskam. *Airplane Design Part I: Preliminary Sizing of Airplanes*. Roskam Aviation and Engineering Corporation, January 1997.
- [4] J. Roskam. *Preliminary Configuration Design and Integration of the Propulsion System*. Roskam Aviation and Engineering Corporation, 1997.
- [5] S. Gudmundsson. *General Aviation Aircraft Design: Applied Methods and Procedures*. Butterworth-Heinemann, September 2013.
- [6] A. Wick J. Hooker. Design of the Hybrid Wing Body for Fuel Efficient Air Mobility Operations. Technical report, Lockheed Martin Aeronautics Company, 2014.
- [7] P. Lempereur L. Lylekian, M. Lebrun. Overview of aircraft noise reduction technologies. Technical report, Aeroacoustics, 2014.
- [8] Informal South Pacific Air Traffic Services Coordinating Group. FANS-1/A Datalink Communications Environment. Technical report, ISPACG, March 2008.
- [9] M. Amato. Air Cargo Technology Roadmap. Technical report, European Commission, April 2013.
- [10] E. Gaier J. Johnson. Air Cargo Operations Cost Database. Technical report, NASA, April 1998.
- [11] European Aviation Safety Agency. *Certification Specifications for Large Aeroplanes CS-25*. Amendment 16, consolidated edition.
- [12] DSE Group 12. Baseline report. Technical report, Delft University of Technology, May 2015.
- [13] M. Wouters J. van de Reyd. Air Cargo Density Research. Technical report, Delft University of Technology, May 2005.
- [14] E. Roux. *Turbofan and Turbojet Engines: Database Handbook*. LuLu Press, Inc., 2007.
- [15] The Boeing Company. Boeing 747-100/-200/-300/-400 freighters. Powerpoint Presentation, 2003.
- [16] DSE Group 12. Mid-term report. Technical report, Delft University of Technology, May 2015.
- [17] W. Verhagen R. Curran. *Concurrent Engineering Design for Lifecycle, Lecture 9*. AE3211-I: Systems Engineering and Aerospace Design (Delft University of Technology). March 2015.
- [18] E. Schoep R. Martinez-Val. Flying Wing Versus Conventional Transport Airplane: The 300 Seat Case. Technical report, ETSI Aeronuticos, Universidad Politecnica de Madrid, 2000.
- [19] L. McCullers C. Nickol. Hybrid Wing Body Configuration System Studies. Technical report, NASA Langley Research Center, ATK, 2009.
- [20] B. Zandbergen R. Vos, J. Melkert. *Aerospace Design Systems Engineering Elements I, Lecture 3*. AE1222-II: Aerospace Design Systems Engineering Elements I (Delft University of Technology). 2011.

-
- [21] B. Zandbergen R. Vos. *Aerospace Design System Engineering Elements I, Lectures 4 and 5*. AE1222-II: Aerospace Design System Engineering Elements I (Delft University of Technology). 2012.
- [22] International Organization for Standardization. Standard Atmosphere, 1975.
- [23] D. Raymer. *Aircraft Design, A Conceptual Approach*. American Institute of Aeronautics and Astronautics, Inc., 1992.
- [24] D. Steenhuizen. *Wing Design Part 2*. AE2101: Aerospace Design and Systems Engineering Elements II (Delft University of Technology). 2013.
- [25] O. Bergsma A. Beukers F. Geuskens, S. Koussois. Non-Cylindrical pressure fuselages for future aircraft. Technical report, Delft University of Technology, April 2008.
- [26] O. Bergsma A. Beukers F. Geuskens, S Koussois. Analysis of Conformable Pressure Vessels: Introducing the Multibubble. *American Institute of Aeronautics and Astronautics*, 49(8):1683–1692, 2011.
- [27] H. Westergaard. Moments and Stresses in Slabs. *Proceedings of the American Concrete Institute*, 17(32):1–124, 1921.
- [28] M. Sadraey. *Aircraft Design: A Systems Engineering Approach*. Wiley Publications, 2012.
- [29] A. Young. The Aerodynamic Characteristics of Flaps. Technical report, Aeronautical Research Council Reports and Yemoranda, February 1947.
- [30] D Steenhuizen A.Cervone. *Aerospace Design Systems Engineering Elements II, Lecture 3*. AE2111-II: Aerospace Design Systems Engineering Elements II (Delft University of Technology). 2011.
- [31] J. Grasmeyer. Stability and Control Derivative Estimation and Engine-Out Analysis. Technical report, Virginia Polytechnic Institute and State University, January 1998.
- [32] E. Torenbeek. *Synthesis of Subsonic Airplane Design*. Springer, 1982.
- [33] M. Sadraey. *Aircraft Design: A Systems Engineering Approach*. Wiley Publications, 2012.
- [34] J. Roskam. *Airplane Design Part IV: Layout of Landing Gear and Systems*. Roskam Aviation and Engineering Corporation, 2000.
- [35] C. Lan J. Roskam. *Airplane Aerodynamics and Performance*. Roskam Aviation and Engineering Corporation, July 1998.
- [36] P. Weed K. Gould. *The Aircraft Engine Design Project- Engine Cycles Design Problem Overview*. March 2009.
- [37] K. Ajoy Kumar. *Aircraft Design*. Cambridge University Press, April 2010.
- [38] M. Sinnett. 787 No-Bleed Systems: Saving Fuel and Enhancing Operational Efficiencies. Technical report, The Boeing Company, April 2007.
- [39] J. Roskam. *Airplane Design Part V: Component Weight Estimation*. Roskam Aviation and Engineering Corporation, 1999.
- [40] A. Elham. Weight Indexing for Multidisciplinary Design Optimization of Lifting Surfaces. Technical report, Delft University of Technology, February 2013.
- [41] A. Trani. Fundamentals of Aircraft Performance (2). Powerpoint Presentation, 2013.
- [42] M. Kamgarpour J. Robinson. Benefits of Continuous Descent Operations in High-Density Terminal Airspace Under Scheduling Constraints. Technical report, American Institute of Aeronautics and Astronautics, September 2010.

-
- [43] Landrum & Brown, Inc. Runway Length Requirements Analysis. Powerpoint Presentation, 2005.
- [44] J. Dons. Optimization of Departure and Arrival Routing for Amsterdam Airport Schiphol. Master's thesis, Delft University of Technology, June 2012.
- [45] Office of Environment and Energy. INM Technical Manual. Technical report, Federal Aviation Administration, January 2008.
- [46] E. Olson R. Thomas, C. Burley. Hybrid Wing Body Aircraft System Noise Assessment With Propulsion Airframe Aeroacoustic Experiments. *International Journal of Aeroacoustics*, 11(3):369–410, 2012.
- [47] R. Shevell I. Kroo. *Aircraft Design: Synthesis and Analysis*. Unpublished, 2001.
- [48] J.D. Anderson. *Introduction to Flight*. McGraw-Hill, Inc., 1989.
- [49] W. Sutherland. The Viscosity of Gases and Molecular Force. *Philosophical Magazine*, 5(36):507–531, 1893.
- [50] E. Torenbeek. *Advanced Aircraft Design: Conceptual Design, Analysis and Optimization of Subsonic Civil Airplanes*. Wiley Publications, 2013.
- [51] J. Roskam. *Airplane Design Part VI: Preliminary Calculation of Aerodynamic Thrust and Power Characteristics*. Roskam Aviation and Engineering Corporation, 1990.
- [52] W. Mason. *Transonic Aerodynamics of Airfoils and Wings, Lecture 7*. AOE 4124: Configuration Aerodynamics (Virginia Tech). March 2006.
- [53] D. Steenhuisen. *Wing Design Part 1*. AE2101: Aerospace Design and Systems Engineering Elements II (Delft University of Technology). 2013.
- [54] D. Steenhuisen. *Wing Design Part 3*. AE2101: Aerospace Design and Systems Engineering Elements II (Delft University of Technology). 2013.
- [55] J. Peraire C. Sequira, D. Willis. Comparing Aerodynamic Models for Numerical Simulation of Dynamics and Control of Aircraft. Technical report, AIAA paper 2006-1254.
- [56] J. Mariens. Wing Shape Multidisciplinary Design Optimization. Master's thesis, Delft University of Technology.
- [57] R. Whitcomb. A Design Approach and Selected Wind Tunnel Results at High Subsonic Speeds for Wing-tip Mounted Winglets. Technical report, July 1976.
- [58] M. Winter R. Faye, R. Laprete. Blended Winglets for Improved Airplane Performance. Technical report, The Boeing Company, January 2002.
- [59] A. von Doenhoff H. Abbott. *Theory of Wing Sections*. Dover Publications, Inc, New York, 1959.
- [60] B. Manes. Extending USAF F-16 Force Structure. Technical report, USAF, April 2001.
- [61] T. Megson. *Aircraft Structures for Engineering Students*. Elsevier Ltd., 2007.
- [62] C. Kassapoglou. *Buckling of beams, Lecture 4*. AE2135-I: Structural Analysis Design (Delft University of Technology). November 2014.
- [63] United States of America Department of Defence. *Composite Materials Handbook*. Unpublished, 2002.
- [64] R. Benedictus F. Morniere, R. Alderliesten. Energy Distribution in Glare and 2024-T3 Aluminium During Low-velocity Impact. Technical report, Delft University of Technology, September 2012.

-
- [65] F. Wypych K. Satyanarayana, G. Arizaga. Biodegradable composites based on lignocellulosic fibers - An overview. *Progress in Polymer Science*, 34(9):982–1021, 2009.
- [66] M. Salkind. Fatigue of composites. *Composite Materials: Testing and Design Conference*, 497(2):143–169, 1972.
- [67] E. Gill. *Systems Engineering Methods, Lectures 3, 4 and 5*. AE3211-I: Systems Engineering and Aerospace Design (Delft University of Technology). February 2015.
- [68] A. in 't Veld and T.J. Mulder. *Flight Dynamics Lecture Notes*. Delft University of Technology, 2015.
- [69] J. Roskam. *Airplane Design Part VIII: Airplane Cost Estimation: Design, Development, Manufacturing and Operating*. Roskam Aviation and Engineering Corporation, January 2002.
- [70] A. Barthe. Sustainable Aviation. Technical report, Airbus, April 2013.
- [71] European Aviation Safety Agency. E.Y013-01 - Airworthiness Certification of Unmanned Aircraft Systems (UAS). Technical report, EASA Europe, 2009.
- [72] T. Barnett M. Mirza. Aeromagazine Economic Impact of Airplane TurnTimes Improving Airplane Turn Time Operations. Technical report, The Boeing Company, October 2008.
- [73] S. Hartjes. *Airport and Ground Operations, Lecture 11*. AE4443: Airline Operations (Delft University of Technology). 2014/2015.
- [74] T. Barnett. Improving Ramp/Terminal Operations for Shorter Turn Around Times. Technical report, Boeing Aeromagazine, April 2008.
- [75] C. Wu. *Airline Operations and Delay Management*. Ashgate, 2010.
- [76] DSE Group 10. Quick turnaround aircraft. Technical report, Delft University of Technology, February 2012.
- [77] R. Stahls S. Santema W. Beelaerts van Blokland, R. Huijser. Future Airport Turnaround Ground Handling Processes. Technical report, TRAIL Research School, Delft University of Technology, October 2008.
- [78] B. Huff C. Roongrat, J. Rosenberger. Simulation of Unit Loading Device Inventory in Airline Operations. Technical report, University of Texas, 2008.
- [79] W. Heinze M. Hepperle. Future Global Range Transport Aircraft. Technical report, Technical University of Brunswick & German Aerospace Center, 2003.
- [80] J. Sinke. *Lean Manufacturing, Chapter 10*. AE3211-II: Production of Aerospace Systems (Delft University of Technology). May 2014.
- [81] J. Shook M. Rother. *Learning to See: Value-stream Mapping to Create Value and Eliminate MUDA*. Cambridge: Lean Enterprise Institute, 1999.
- [82] C. Ebeling. *An Introduction to Reliability and Maintainability Engineering*. McGraw-Hill, 2009.
- [83] Transportation Research Board. Defining and Measuring Aircraft Delay and Airport Capacity Thresholds. Technical report, Aircraft Cooperative Research Program, January 2014.
- [84] Federal Aviation Administration. *Aviation Maintenance Technician Handbook*. US Department of Transportation, 2008.
- [85] M. Fricke M. Wagner. Estimation of Daily Unscheduled Line Maintenance Events In Civil Aviation. Technical report, Berlin University of Technology, September 2006.

A Aircraft dimensions, planform details and characteristics

Table A.1: Empennage details.

Empennage			
Horizontal Tail		Vertical Tail	
Airfoil	NACA 0012	Airfoil	NACA 0015
CG location (x/y/z)	26.07/04.53/06.06 [m]	CG location (x/y/z)	22.52/0.00/3.35 [m]
Volume Coefficient	0.800	Volume Coefficient	0.013
Surface Area	66.45 [m ²]	Surface Area	19.16 [m ²]
Span	21.57 [m]	Span	4.80 [m]
MAC	3.08 [m]	MAC	4.00 [m]
Root Chord	4.24 [m]	Root Chord	4.77 [m]
Tip Chord	1.48 [m]	Tip Chord	3.10 [m]
Taper Ratio	0.350	Taper Ratio	0.650
Aspect Ratio	7.0	Aspect Ratio	1.2
Sweep Angle	35 [deg]	Sweep Angle	50 [deg]
Dihedral	0.0 [deg]	Dihedral	0.0 [deg]
Incidence	-2.1 [deg]	Incidence	0.0 [deg]
Root Twist	0.0 [deg]	Root Twist	0.0 [deg]
Tip Twist	0.0 [deg]	Tip Twist	0.0 [deg]

Table A.2: Rudder dimensions.

Maximum rudder deflection angle (δ_R)	30.5	[deg]
Rudder root chord (C_{rR})	1.89	[m]
Rudder span (b_R)	4.77	[m]
Rudder Hinge Angle (λ_R)	50	[deg]

Table A.3: Container details.

Container	
Height (max)	1.95 [m]
Height (min)	1.64 [m]
Width	2.35 [m]
Length	5.7 [m]
Volume	25.5 [m ³]

Table A.4: Cargo bay details.

Cargo bay	
Height	1.97 [m]
Width	2.37 [m]
Length	11.4 [m]
Volume	102 [m ³]

Table A.5: Main wing details.

Parameters	Value [Unit]
Airfoil	Whitcomb Supercritical
Span	49.9 [m]
Surface Area	221 [m ²]
Aspect Ratio	11.3 [-]
Root Chord	24.5 [m]
Tip Chord	1.49 [m]
Taper Ratio	0.0608 [-]
Body Span	10.5 [m]
Body Sweep Leading edge	51.0 [°]
Outer Wing Sweep Leading Edge	31.0 [°]
Body Dihedral	1.00 [°]
Outer Wing Dihedral	8.50 [°]
Body Thickness over Chord	0.17 [-]
Outer Wing Thickness over Chord	0.11 [-]
Body MAC	17.1 [m]
Outer Wing MAC	4.00 [m]
Twist	0.0 [°]
Incidence	0.326 [°]
$S_{w,flaps}$	45.8 [m ²]
$S_{w,slats}$	52.0 [m ²]
b_{flaps}	8.8 [m]
b_{slats}	10.1 [m]

Table A.6: Financial analysis summary.

Parameters	Value [Unit]
Development cost per aircraft	1.916 [M USD]
Production cost per aircraft	32.5 [M USD]
Maintenance cost	1.83 [USD/nmi]
Direct operating cost	0.1363 [USD/tkm]
Aircraft unit cost	30.2 [M EUR]
Aircraft unit price	33.2 [M EUR]
Best RoI	1.806 [-]
Worst RoI	0.374 [-]
Best BEP	0.492 [years]
Worst BEP	2.380 [years]

Table A.7: Aircraft performance.

Aircraft Performance			
Climb		Descent	
Time to climb	1459 [s]	Time to descent	1309 [s]
Ground distance during climb	133 [km]	Ground distance descent	172 [km]
Climb velocity	91 [m/s]	Descent velocity	131 [m/s]
max. Rate of Climb MTOW sea	26 [m/s]	Mean descent angle	-4.15 [deg]
max. Rate of Climb MTOW cruise	2.1 [m/s]	Max descent angle	-5.71 [deg]
max. Rate of Climb OEW sea	85 [m/s]		
max. Rate of Climb OEW cruise	18 [m/s]		
Stall Speed [mach]		Manoeuvring	
OEW sea level	0.081	Maximum load factor	2.5g
MTOW sea level	0.145		
OEW cruise altitude	0.130		
MTOW cruise altitude	0.230		
OEW sea level HLD	0.065		
MTOW sea level HLD	0.119		
OEW cruise altitude HLD	0.115		
MTOW cruise altitude HLD	0.205		
Turning		Noise	
Minimum turn radius	462 [m]	55dB SEL - Approach	210.5 [km ²]
Minimum turn time	28.5 [s]	55dB SEL - Departure	102 [km ²]
Fuel		Emissions	
		CO ₂	$4.11 \cdot 10^{-4} \left[\frac{kg}{kg \cdot nmi} \right]$
	Range [nmi]		
	Range max payload	2188	
	Range typical payload	3000	
	Ferry Range	9500	